

PHD

Agile legged robot locomotion

Ding, Beichen

Award date:
2019

Awarding institution:
University of Bath

[Link to publication](#)

General rights

Copyright and moral rights for the publications made accessible in the public portal are retained by the authors and/or other copyright owners and it is a condition of accessing publications that users recognise and abide by the legal requirements associated with these rights.

- Users may download and print one copy of any publication from the public portal for the purpose of private study or research.
- You may not further distribute the material or use it for any profit-making activity or commercial gain
- You may freely distribute the URL identifying the publication in the public portal ?

Take down policy

If you believe that this document breaches copyright please contact us providing details, and we will remove access to the work immediately and investigate your claim.

PHD

Agile legged robot locomotion

Ding, Beichen

Award date:
2019

Awarding institution:
University of Bath

[Link to publication](#)

General rights

Copyright and moral rights for the publications made accessible in the public portal are retained by the authors and/or other copyright owners and it is a condition of accessing publications that users recognise and abide by the legal requirements associated with these rights.

- Users may download and print one copy of any publication from the public portal for the purpose of private study or research.
- You may not further distribute the material or use it for any profit-making activity or commercial gain
- You may freely distribute the URL identifying the publication in the public portal ?

Take down policy

If you believe that this document breaches copyright please contact us providing details, and we will remove access to the work immediately and investigate your claim.

Agile Legged Robot Locomotion

Beichen Ding

A thesis submitted for the degree of Doctor of Philosophy

University of Bath

Department of Mechanical Engineering

April 2019

COPYRIGHT

Attention is drawn to the fact that the copyright of this thesis rests with the author. A copy of this thesis has been supplied on condition that anyone who consults it is understood to recognise that its copyright rests with the author and that they must not copy it or use material from it except as permitted by law or with the consent of the author.

This thesis may be made available for consultation within the University Library and may be photocopied or lent to other libraries for the purpose of consultation.

Abstract

Running robots are legged machines with a dynamic capability, i.e. with sensing, actuation and control systems which enable operation outside the constraints of static balance. They also require passive dynamics which are carefully tuned to the required running motion. Such robots have the potential to reach many parts of the planet which are inaccessible by wheeled or tracked vehicles, and to venture into unstructured environments which are dangerous for humans. Hopping is particularly useful to study since it leads to a fundamental understanding of legged locomotion, which can be extended to multi-legged platforms. A springy leg interacts with body mass to give a natural hopping or running frequency. Servo hydraulics is highly suitable for robot leg actuation due to the high power density and quick response.

This thesis concerns several aspects of dynamics and control for hydraulically actuated bipedal hopping robots. The development of a hydraulically actuated bipedal hopping robot, named BBH1, is presented, including the design of a compliant leg to provide desirable passive characteristics. Using a hydraulic accumulator is a promising approach to provide the required compliance in a hydraulically-actuated leg. However, there is friction from the sealing around the piston, especially at a high working pressure, and this has a significantly negative effect on the actuator's position tracking performance. In order to quantify this friction effect, a novel factor called the '*error-time integral*' is introduced to link the friction effect with the system compliance and aids component selection for this application.

As a consequence of the friction investigation, the BBH2 was developed with a mechanical extension coil spring to provide leg compliance instead of an accumulator. Most hopping height controllers require explicit detection of the ground contact, plus several state variables usually need to be measured. A novel self-excited hopping controller is developed to address these challenges. This controller is composed of a positive force feedback loop plus a saturation limit dictating the hopping height, a conventional proportional-integral position feedback loop, and command velocity feedforward is used to improve the system

response. A criterion for guaranteed self-excited hopping is theoretically derived using the describing function technique, and experimentally verified on the BBH2. A nonlinear simulation model is used to explain the main findings from the experimental results and provide a better understanding of the effects of practical nonlinearities.

A modified double inverted pendulum model is used to study the balancing control while the BBH2 is standing on the ground with point foot contact. The balancing controller is developed using the pole-placement method and investigated via simulation. The results indicate that high order motion derivatives need to be sensed or estimated, and the corresponding noise issue plays an important role in the performance of this controller.

A controller is developed to maintain balance while the BBH2 is hopping. It follows the well-established structure of the ‘Three-part Controller’. The three controlled parts are: hopping height control; longitudinal control by changing the leg angle during the flight phase to place the foot in the desired position; and body attitude correction during the stance phase. Simulation results from a detailed nonlinear model indicate that this controller can successfully balance the hydraulic robot while hopping with different longitudinal velocities.

Acknowledgements

I would like to express my sincere gratitude to my supervisors Prof. Andrew Plummer and Dr. Pejman Iravani for their guidance, encouragement and valuable advice. Thanks are also given to the technical staffs of the 4E and 8E laboratories for assisting in experiments.

I also obliged to the staffs in Centre for Power Transmission and Motion Control for the assistance along with this project.

Many thanks to my friends in Bath, for their accompanying and understanding.

I am deeply grateful to my beloved parents for their endless love, support, understanding and tolerance. It is never too many appreciations to what they gave me. Special thanks to my wife for staying by my side, trusting me and making my life colourful.

Contents

Abstract.....	I
Acknowledgements.....	III
Contents	V
List of figures.....	IX
List of tables	XIII
Notation	XV
1 Introduction	1
1.1 Motivation	1
1.2 Aims and objectives	2
1.3 Novel research contribution	2
1.4 Thesis outline	3
1.5 Note on format.....	4
2 Literature review	5
2.1 A brief history of legged robots	5
2.2 Compliant robot leg design	11
2.2.1 Compliant leg using coil springs.....	11
2.2.2 Compliant leg using compressed air	14
2.2.3 Compliant leg solutions from hydraulic domain	15
2.3 Balancing control while walking and running	15
2.3.1 Zero moment point (ZMP) control	16
2.3.2 Virtual model control.....	17
2.3.3 Controlled passive dynamic walking	17
2.3.4 ‘Three-Part’ control	18
2.4 Hopping height control.....	20
2.5 Control of hydraulic actuators	22
2.6 Conclusions	23
3 BBH1 robot	25
3.1 Mechanical design.....	25

3.1.1 System overview	27
3.1.2 Actuation system	28
3.1.3 Sensory system	33
3.1.4 Control system.....	36
3.2 Modelling of the BBH1 robot	38
3.2.1 Hydraulic models	38
3.2.2 Mechanical models	42
3.3 Bench test results and analysis.....	42
3.3.1 Bench test results.....	42
3.3.2 Evaluation of the friction effect.....	46
3.4 Conclusions.....	48
4 BBH2 robot	51
4.1 Mechanical design	51
4.2 Modelling of the BBH2 robot	56
4.2.1 Hydraulic models	56
4.2.2 Mechanical model	57
4.2.3 3D visualised model	59
4.3 Bench test results and analysis.....	60
4.3.1 Leg actuator position tracking performance.....	60
4.3.2 Sinusoid excited hopping	62
4.4 Conclusions.....	65
5 Motion control.....	67
5.1 Balancing control while standing	67
5.1.1 Introduction	67
5.1.2 Modelling	67
5.1.3 Controller design	68
5.1.4 Evaluation of the controller	71
5.1.5 Summary	75
5.2 Vertical hopping height control	76
5.2.1 Introduction	76
5.2.2 Control concept	76
5.2.3 Results and discussion.....	85
5.2.4 Summary	86

5.3 Balancing control while hopping	87
5.3.1 Introduction.....	87
5.3.2 Controller implementation	87
5.3.3 Simulation results.....	90
5.3.4 Summary	91
6 Conclusions and further work	93
6.1 Conclusions	93
6.2 Further work	95
Bibliography	97
Appendix 1.....	103
Statement of Authorship.....	103
PAPER 1: A study of a compliant hydraulic actuator for running robots	
104	
Appendix 2.....	121
Statement of Authorship.....	121
PAPER 2: Investigating balancing control of a standing bipedal robot with	
point foot contact.....	122
Appendix 3.....	139
Statement of Authorship.....	139
PAPER 3: A novel self-excited hopping controller for legged robots	140
Appendix 4.....	169
Statement of Authorship.....	169
PAPER 4: Investigating balance control of a hopping bipedal robot.....	170

List of figures

Figure 2.1. Phoney Pony	5
Figure 2.2. General Electric ‘CAM’ Walking Truck.....	6
Figure 2.3. Ohio State University’s ASV	7
Figure 2.4. The first generation of Big Dog	8
Figure 2.5. Alpha Dog	8
Figure 2.6. PETMAN.....	9
Figure 2.7. Cheetah.....	9
Figure 2.8. Asimo	10
Figure 2.9. Atlas.....	11
Figure 2.10 Monopod II	12
Figure 2.11 Kenken.....	12
Figure 2.12 Uniroo, Zeglin’s first one-legged hopping robot.....	13
Figure 2.13 A 3D one-legged hopping machine from MIT.....	13
Figure 2.14 Mowgli, a pneumatic driven frog-like hopping robot	14
Figure 2.15 One working cycle of a hydraulic accumulator, diaphragm type.....	15
Figure 2.16. Silo4.....	16
Figure 2.17. Virtual model control	17
Figure 2.18. IHMC Fast-Runner: a DARPA funded project	18
Figure 2.19 The SLIP model (showing the stance phase)	19
Figure 2.20 Raibert’s 2D planar hopper	21
Figure 2.21 Hopping leg with a springy foot.....	21
Figure 3.1 The BBH1 robot (showing the front view)	26
Figure 3.2 The BBH1 robot (mainly showing the spring accumulators, with a side view showing the body actuator).....	26
Figure 3.3 The BBH1 robot (showing with a mechanical constraint)	27
Figure 3.4 System schematic	28
Figure 3.5 Hydraulic circuit of the BBH1 robot (showing one of the three valve-actuator pairs)	29

Figure 3.6 Moog E242 proportional valve	30
Figure 3.7 Hoerbiger LB6 hydraulic actuator	31
Figure 3.8 HYDAC diaphragm accumulator	31
Figure 3.9 Maxon/Escon 24/2 motor controller	32
Figure 3.10 Motor controllers (showing the assembly with the motherboard)	33
Figure 3.11 Active Sensors position sensors (showing with rod end mountings)	33
Figure 3.12 Hengstler incremental encoder	34
Figure 3.13 Hydraulic pressure sensor	35
Figure 3.14 Yost Labs inertial measurement unit	36
Figure 3.15 Target PC: Terasoft MicroBox 2000	37
Figure 3.16 Valve hysteresis	40
Figure 3.17 Hydraulic models of the BBH1 robot in Simulink®	41
Figure 3.18 One robot leg model of the BBH1	42
Figure 3.19 Closed loop position control of the leg actuator, using square wave demand	44
Figure 3.20 Cylinder pressure of the leg actuator, using square wave demand ...	44
Figure 3.21 Closed loop position control of the leg actuator, using sinusoid wave demand	45
Figure 3.22 Cylinder pressure of the leg actuator, using sinusoid wave demand	45
Figure 3.23 Rearranged system block diagram	47
Figure 3.24 Investigating the value of <i>error-time factor</i> using sinusoid demand	47
Figure 4.1 Sketch of the BBH2 robot.....	52
Figure 4.2 Hydraulic circuit of the BBH2 robot (showing one of the three valve- actuator pairs).....	53
Figure 4.3 The BBH2 robot (showing with a mechanical constraint)	54
Figure 4.4 The BBH2 robot (showing a close-up view)	54
Figure 4.5 Simplified sketch of the robot leg.....	55
Figure 4.6 Top-level of the mechanical model	58
Figure 4.7 Spring and damper model	58
Figure 4.8 3D visualisation of BBH2.....	59
Figure 4.9 Closed loop position control of the leg actuator, using square wave demand (BBH2)	60
Figure 4.10 Closed loop position control of the leg actuator, using square wave demand, with dither (BBH2).....	61

Figure 4.11 Structure of the ‘Coordinated Controller’	62
Figure 4.12 Closed loop position control of the leg actuators, using ‘Coordinated Controller’ (BBH2).....	62
Figure 4.13 1 Hz sinusoid signal excitation.....	63
Figure 4.14 2 Hz sinusoid signal excitation.....	64
Figure 4.15 3 Hz sinusoid signal excitation.....	64
Figure 5.1 The modified double inverted pendulum model	68
Figure 5.2 Block diagram of pole placement controller	69
Figure 5.3 Step response with closed-loop poles for cut-off frequencies of 7 rad/s, 5 rad/s, 3 rad/s and 1 rad/s.....	71
Figure 5.4 Closed-loop block diagram with $H(s)$ filter	73
Figure 5.5 Frequency response of output angle (y) over noise (e) for different cut-off frequency of $H(s)$, as 0.7 rad/s, 1 rad/s, 3 rad/s, 5 rad/s, 7 rad/s and 10 rad/s	74
Figure 5.6 Frequency response of control signal (u) over noise (e) for different cut-off frequency of $H(s)$, as 0.7 rad/s, 1 rad/s, 3 rad/s, 5 rad/s, 7 rad/s and 10 rad/s.....	75
Figure 5.7 Modified SLIP model.....	76
Figure 5.8 Controller structure.....	78
Figure 5.9 Nyquist diagram of the OLTF and $-1/DF$	80
Figure 5.10 Using DF to predict amplitude A	81
Figure 5.11 Simulation results of using saturation limit to dictate body position	82
Figure 5.12 Simulation model considering foot lift off the ground.....	82
Figure 5.13 The threshold of spring displacement	83
Figure 5.14 Simulation results of $S=0.01$, $S=0.02$ and $S=0.03$	84
Figure 5.15 Simulation results of $S=0.0133$. The close-up figure shows a small difference between ‘fixed foot’ and ‘free foot’ cases, which indicate the foot leaves the ground momentarily.....	85
Figure 5.16 Results comparison.....	85
Figure 5.17 Results comparison.....	86
Figure 5.18 Simplified diagram of one hopping cycle	87
Figure 5.19 Simulation results	91

List of tables

Table 3.1 Main dimensional specifications of the BBH1 robot	27
Table 3.2 Main specifications of the hydraulic valve	30
Table 3.3 Main specifications of the hydraulic actuator.....	31
Table 3.4 Main specifications of the hydraulic accumulator.....	32
Table 3.5 Main specifications of the motor controller.....	32
Table 3.6 Main specifications of the position potentiometer.....	34
Table 3.7 Main specifications of the incremental encoder	34
Table 3.8 Main specifications of the pressure sensor	35
Table 3.9 Main specifications of the IMU	36
Table 3.10 Main specifications of the MicroBox 2000	37
Table 3.11 Parameter values of the hydraulic models	41
Table 4.1 Main dimensional specifications of BBH2.....	52
Table 5.1 Physical parameters	71
Table 5.2 Parameter values	79
Table 5.3 Controller and feedback gains	90

Notation

Variables

A_a	Annulus area of the hydraulic actuator
A_p	Full piston area of the hydraulic actuator
B	Oil bulk modulus
b_y	The ground vertical damping coefficient
b_z	The ground tangential damping coefficient
e	Position error
F_c	Coulomb friction
F_f	Friction force
F_h	Hydraulic force
F_s	Velocity-dependent friction at low velocity
f_v	Friction coefficient
F_y	The ground vertical reaction force
F_z	The ground horizontal friction force
K_h	Pressure loss factor
K_i	Integral gain
K_{mc}	Calibration gain of the motor driver
K_p	Proportional gain
k_y	Ground vertical spring stiffness
k_z	Ground tangential spring stiffness

l_{AB}	Length of the <i>thigh</i>
l_{AD}	The length between the <i>hip</i> and cylinder rear rod end mounting
l_{BC}	The length between the <i>knee</i> and piston rod end mounting
$l_{BC'}$	The length between the <i>knee</i> and piston rod end mounting, after deformation
l_{BE}	Length of the <i>shank</i>
$l_{BE'}$	Length of the <i>shank</i> , after deformation
l_{BG}	The length between the <i>knee</i> and spring end mounting
l_{DC}	Length of the leg actuator
$l_{DC'}$	Length of the leg actuator, after deformation
l_{EF}	The length between the <i>heel</i> and spring end mounting
$l_{EF'}$	The length between the <i>heel</i> and spring end mounting, after deformation
l_{GF}	Length of the spring
$l_{GF'}$	Length of the spring, after deformation
l_s	Spring displacement
M	Mass of the load
n	Adiabatic index
P_0	Gas pre-charge pressure
P_a	Accumulator output pressure
P_c	Full piston side pressure of the actuator
P_m	Mean working pressure
P_r	Return pressure
P_s	Supply pressure
Q_a	Piston side flow rate

Q_v	Valve output flow rate
u_c	The output signal of the motor controller
\tilde{u}_c	Actual valve spool driving signal
u_w	The dead-band width of the backlash
V	Gas volume
V_0	Initial gas volume
V_m	Gas volume at the mean working pressure
V_t	Trapped oil volume in the full piston chamber
X	Nominalised valve spool displacement
y_a	Average (vertical) position
y_n	Vertical foot tip coordinate
y_r	Roll position
z_t	Horizontal foot tip coordinate

Greek

α	The output signal of the incremental encoder
β	Auxiliary angle assists in calculating spring displacement
ε	The output signal of the position potentiometer
ζ_v	Valve spool damping coefficient
θ	<i>Knee</i> angle, after deformation
ω_v	Valve spool natural frequency

Acronyms

ASV	Adaptive Suspension Vehicle
-----	-----------------------------

BBH	Bath Bipedal Hopper
BBH1	Bath Bipedal Hopper 1
BBH2	Bath Bipedal Hopper 2
CAM	Cybernetic Anthropomorphous Machine
CoM	Centre of Mass
DoF	Degree of Freedom
SLIP	Spring Loaded Inverted Pendulum

1 Introduction

Inspired by legged animals in the natural world, research on legged locomotion has been going on for a few decades. The legged moving machines are capable of traversing through rough terrain since the foot placement does not require continuous supporting surface, in which the wheeled or tracked vehicles cannot, and to venture into unstructured environments which are dangerous for humans. Therefore, further in-depth study of legged locomotion is necessary.

1.1 Motivation

Historical records indicate that most of the earliest legged moving machines consist of the simple cam and linkage-based mechanisms and were driven by operators, manually (Bahtti et al., 2015). In the past few decades, more advanced legged robots have been designed making use of the rapid development of multidisciplinary technologies, especially computer science. In the 1980s, Raibert and his co-workers made great contributions to developing control algorithms for legged robots, especially in solving the dynamic balancing issues (Raibert, 1986). In 2005, with the creation of BigDog, the research into legged robots stepped into a new era (Raibert et al., 2008). Although there are very few publications about this famous mobile robot, it stimulated researchers' interest to create different multi-legged robots and develop the corresponding motion control strategies. As a result, other multi-legged robots were successfully developed, such as the Spot (Boston Dynamics, 2017) and HyQ (Semini, 2011).

The study of mono-legged or bipedal hopping robot is a sustained interest that is motivated by human's desire to have a comprehensive understanding of this locomotion, which can also be expanded and applied to multi-legged robots since there is only one type of gait, namely, hopping. Zhou (2012) summarised some exist single-legged hopping robots, which mainly focus on the mechanical design aspect. The highly non-linear system dynamics of legged robots bring control challenges. For example, the significant load change between the stance phase and flight phase require high adaptiveness for controllers. Therefore, this thesis will

look into several aspects of bipedal hopping robots, both mechanical design and motion control strategies.

1.2 Aims and objectives

The aim of this research is to develop or investigate control techniques and algorithms for a bipedal hopping robot, which are intended to address the control objectives from the following aspects:

- Vertical hopping control. Develop a hopping controller which significantly reduce the complexity of running robots, from mechanical design and/or sensor measurement perspectives.
- Static balancing control. Develop a controller which can allow the robot to maintain balance while standing with a point foot contact, for which a small foot supporting area can increase the capability of traversing rough terrain.
- Dynamic balancing control. Investigate the balancing control method while the robot is hopping, not only hopping on a spot but also moving with different longitudinal velocities.

In order to achieve these objectives, the following tasks are also undertaken:

- Develop a bipedal hopping robot for experimental validation. Particularly, the robot foot contact area will be very small, i.e. it is a point foot contact.
- Develop detailed nonlinear simulation models to explain the main findings from the experiments and improve understanding of the system behaviours.
- Refine the hardware to improve the prototype's performance.

1.3 Novel research contribution

In this research, novel contributions have been made in several aspects. A rigorous study of the compliant hydraulic actuator is undertaken. Particularly, a novel factor, called the *error-time integral*, is introduced to provide a quantified analysis of the

friction effect linked with the system compliance, which aids components selection for this actuator design in future research.

A novel hopping controller is successfully developed and validated through simulation and experiments, which significantly reduces the number of measured variables without the need to explicitly detect the ground contact. In other words, this controller can reduce the complexity of running robots, from mechanical design and/or sensor measurement perspectives.

Investigations into balancing control while standing and hopping give new insights into possible design methods and challenges for bipedal legged robots with either telescopic or articulated types of robot leg.

Two small-sized hydraulically actuated bipedal hopping robots, the BBH1 (telescopic type of leg) and BBH2 (articulated type of leg), are successfully designed and built to be the experimental basis to validate the proposed compliant hydraulic actuator design and to demonstrate the efficacy of the hopping controller. These experimental systems are modelled in detail, and the simulation results provide a better understanding of the main findings from experiments.

1.4 Thesis outline

This thesis is comprised of research papers accompanied by traditional chapters relate to several aspects of hydraulically actuated bipedal hopping robots.

Chapter 2 presents a literature review of the legged robot field focusing on motion control and compliant robot leg design. Several insightful examples are described to present up-to-date research achievements in this area. The research potentials for this thesis are summarised and discussed.

Chapter 3 describes the first prototype of a bipedal hopping robot, namely the BBH1. It starts with a general introduction of the robots and followed by detailed descriptions of the hardware and signal processing. A detailed nonlinear simulation model is developed aims to explain the main findings from the bench test, plus the corresponding results analysis is provided.

Chapter 4 describes the second prototype of a bipedal hopping robot, namely the BBH2. This chapter is organised similar to Chapter 3 accompanied by some essential changes due to the different type of robot leg. This robot platform is used to be the simulation and experimental basis for controller development.

Chapter 5 presents the research of motion control for bipedal hopping robot, which is summarised from three research papers, including investigation of static and dynamic balancing control, and vertical hopping height control.

Chapter 6 presents the conclusions and recommendations for further research.

1.5 Note on format

Chapter 3 and 5 contains summarised content from research papers, which are presented in Appendix. These papers are reformatted from their published form for consistency. A *Statement of Authorship* is attached to each research paper to clarify the candidate's contribution to the published research. The references for each paper are self-contained plus a full bibliography in alphabetical order is given. The *list of figures*, *list of tables* and *notations* only include those within the chapter based contents. The recorded video is provided on a CD disk as supplementary material for visualised demonstration. In Chapter 5, sections are arranged in a sequence following the published/submitted year of the papers, from 2016 to 2019.

2 Literature review

This chapter reviews the literature which is relevant to the research topics within this thesis. Note that the content is the expansion of a published research paper in 2015, entitled '*A survey of dynamic robot legged locomotion*', which is a collaborative work done by the thesis author and other colleagues. Some up-to-date research achievements of legged locomotion are added and other relevant literature is reviewed, e.g. control of hydraulic actuators.

2.1 A brief history of legged robots

According to historical records, human's activities of creating 'automatons' started from ancient China and Greece. Around 480 BCE the Chinese master carpenter Lu Ban invented a mechanical horse as an entertainment facility. The four legged wooden horse and carriage would move in the downhill direction as a result of gravity when it stands on a slope (Chen and Hsu, 2007). The earliest walking machines consisted of cam and linkage-based mechanisms (Silva and Tenreiro, 2007), which restricted them to walk with a fixed gait.

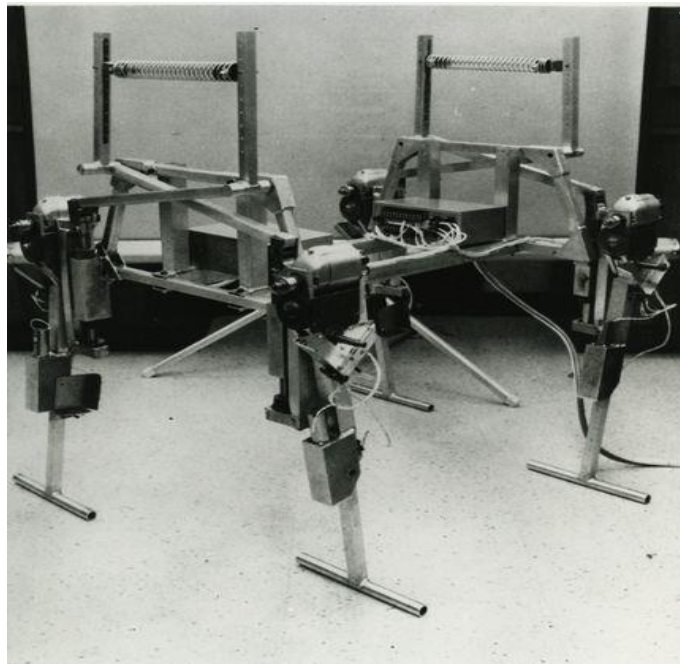


Figure 2.1. Phoney Pony (Bekey, 2005).

In 1968, Andrew Frank built the ‘Phoney Pony’ (see Figure 2.1), a quadruped robot, which was capable of moving very slowly with the stable crawl, walk and trot gaits (Li et al., 2011). Phoney Pony employed computer control before the appearance of microprocessors. Joint states were used in state-machine feedback control with the computer sitting in an adjacent building (Bekey, 2005).

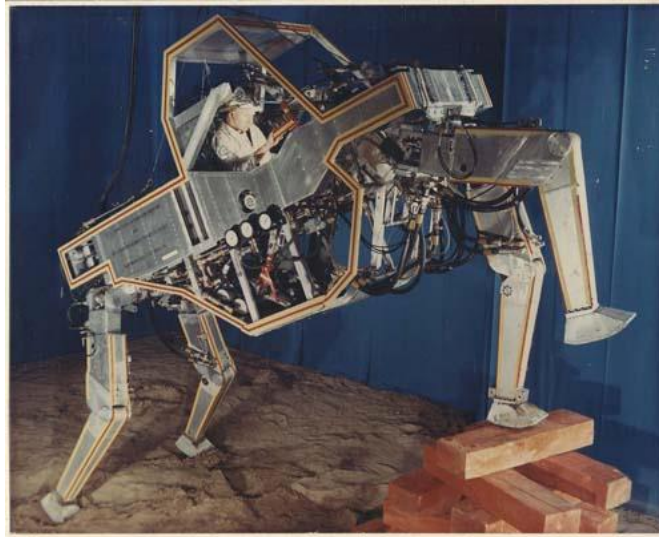


Figure 2.2. General Electric ‘CAM’ Walking Truck (Mosher, 1969).

In the same year, General Electric made a walking truck, named the ‘Cybernetic Anthropomorphous Machine’ (see Figure 2.2). This was a hydraulically actuated quadruped vehicle, which was intended to travel through rough terrain to meet the requirements of the US army. The CAM weight 1,360kg and could achieve 2.2 m/s. A human operator was involved in coordinating with the movement and force-feedback control of the machine (Mosher, 1969). Although the walking task would cause operator fatigue, a legged vehicle capable of variable gait had been built.

A hexapedal vehicle (see Figure 2.3) was developed by Ohio State University, called the ‘Adaptive Suspension Vehicle’ (ASV), in 1985 (Waldron and McGhee, 1986). It applied computer technology to implement a controller so that the whole system could achieve position, velocity and pressure feedback control. Moreover, a human operator could switch the locomotion type between basic and advanced mode. In the advanced mode, the foot placement was determined by a scanning rangefinder. The ASV had onboard power from a 50 kW internal combustion engine and had a maximum speed of 3.6 m/s. Comparing with CAM, ASV incorporated more intelligent control, reducing operator workload.

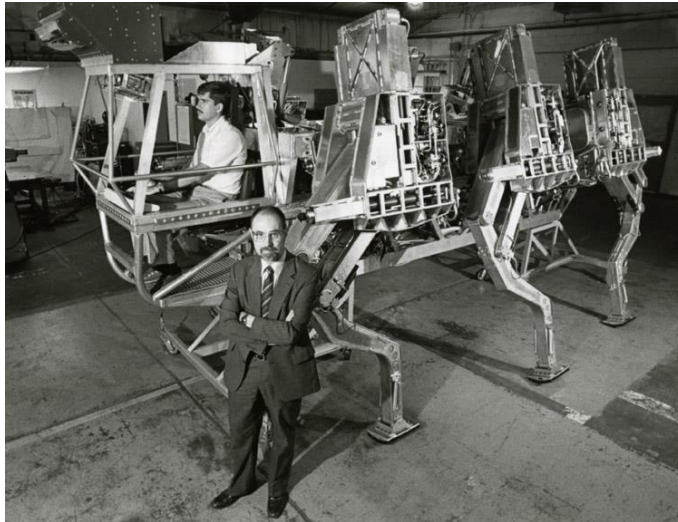


Figure 2.3. Ohio State University's ASV (Waldron and McGhee, 1986).

These are examples of robots or walking trucks that could maintain static stability and low speed. In the 1980s and early 1990s, Marc Raibert made great contributions to the design of mechanical structures and control algorithms of robots in order to increase the movement speed and maintain kinetic stability. In Raibert's early published papers, he discussed the locomotion principles of legged animals (Raibert and Ivan, 1983). Moreover, he demonstrated the influence of mechanical structure when considering balance issues. He developed the 'Three-Part' control algorithm to maintain dynamic balance while the robot is moving. For a one-legged hopping robot, this method controls the forward velocity, hopping height and body attitude, respectively. This basic control technique was extended successfully from one to two and four-legged running robots (Raibert, 1986). During this period, Raibert's Leg Lab at MIT created several dynamic running robot platforms. Some of these robots will be presented in the following sections.

Additionally, Raibert founded the company Boston Dynamics in 1992. In 2005, Boston Dynamics working with Foster-Miller, NASA's Jet Propulsion Lab and Harvard University, developed a famous mobile robot, BigDog (see Figure 2.4). This is a four-legged robot with a dynamically balancing gait able to traverse a variety of outdoor terrain and recover from disturbances. BigDog actively balances and reacts to disturbances to maintain a dynamic balance in a way that looks uncannily similar to quadruped mammals (Raibert et al., 2008). Though there are many nuances and details as to how this is achieved, the underlying concepts are

those developed at the MIT Leg Lab in the 1980s. BigDog weighs about 109 kg and is about 1 m tall. It is hydraulically actuated and powered by an onboard 11 kW internal combustion engine. Each actuator is fitted with a load-cell and position sensor. Each leg has four actuated and one passively compliant degrees of freedom. Alongside proprioception and an internal measurement unit (IMU), BigDog also has lidar, stereo vision and GPS to allow autonomous navigation and obstacle avoidance.

Boston Dynamics successor to BigDog is the AlphaDog (see Figure 2.5), also called the Legged Squad Support System (Raibert, 2012). AlphaDog is a more rugged version of BigDog currently being field tested for military use. It is quieter, able to carry a greater payload, has greater range and able to self-right after falling over.



Figure 2.4. The first generation of Big Dog (Raibert et al., 2008).



Figure 2.5. Alpha Dog (Raibert, 2012).

Another two advanced and dynamic mammal-like legged machines are Boston Dynamics' PETMAN (Nelson et al., 2012) and Cheetah (Michael, 2012). PETMAN (see Figure 2.6) is an anthropomorphic robot that walks and performs movements in order to stress test clothing designed to protect against hazardous chemical exposure. PETMAN balances itself and simulates the temperature, humidity and sweating of a person. The Cheetah (see Figure 2.7) is a plane-dimensional, tethered robot that can achieve 13 m/s running speed on a treadmill. Its successor, the Wildcat, aims to achieve high speed running outdoors without a tether.

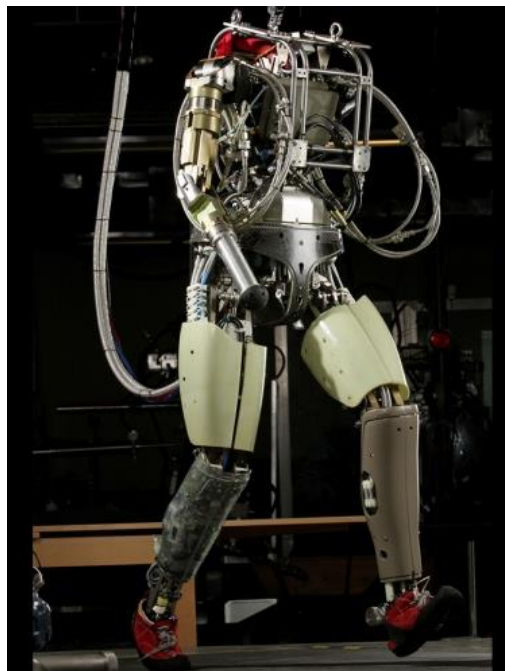


Figure 2.6. PETMAN (Nelson et al., 2012).

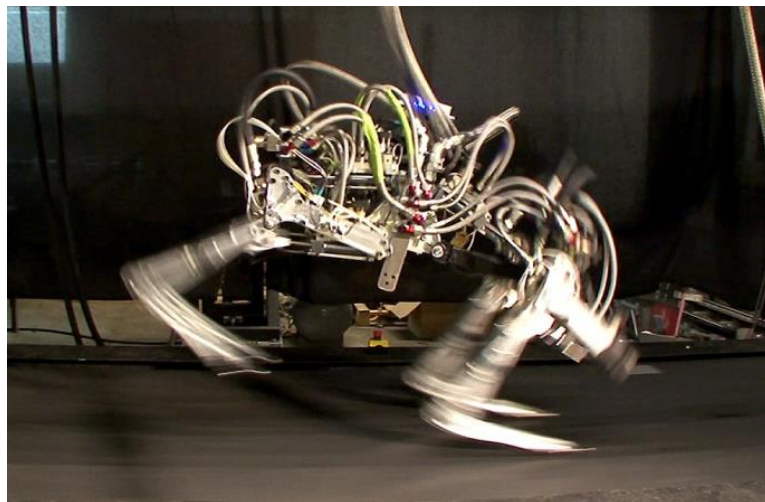


Figure 2.7. Cheetah (Michael, 2012).



Figure 2.8. Asimo (Sakagami et al., 2002).

Among animals, bipedal locomotion is relatively rare but attracts researchers' attention, because it is a window into intelligence in general. One motivation behind research into humanoid robots is that they can function as generalists in human environments. They could use tools and negotiate environments designed for humans, working alongside people and freeing them from menial labour. For a bipedal walking robot, the high centre of gravity and a small base of support on the ground are the main issues, which means it will tip over very easily. In order to study these issues, since the 1970s, the researchers from Honda, have developed a well-known bipedal walking robot, Asimo (see Figure 2.8) uses the Zero Moment Point Control (ZMP) method to keep itself staying balanced while walking or climbing (Sakagami et al., 2002).

In 2016, Boston Dynamics released a new generation of Atlas (see Figure 2.9), which is the world's most dynamic humanoid robot. It is 1.5 m in height, 75 kg in weight with 11 kg payload capability. The Atlas is powered by battery accompanied by hydraulic actuation. The hardware takes advantage of 3D printing to save weight and space (Boston Dynamics, 2016). In their latest videos, the Atlas can even accomplish manoeuvres which are difficult for normal human beings, e.g. maintain balance after a backward flip from a stage. Moreover, the running speed in the field is increased dramatically, compared with their earlier generations.



Figure 2.9. Atlas (Boston Dynamics, 2016).

2.2 Compliant robot leg design

From biomechanical studies, the springy elements, e.g. tendons, fascia lata and aponeurosis ligaments, distributed in legs of running animals provide significant advantages to achieve efficient running or hopping (Zhou and Bi, 2012). For legged robots, the development is a systems design problem requiring the selection of an appropriate actuation approach and leg compliance solution, and the development of a motion control method. The elastic element, e.g. coil spring or compressed air, is widely used to provide this leg compliance. This section reviews some existing compliant robot leg designs.

2.2.1 Compliant leg using coil springs

Monopod II (see Figure 2.10) uses a compression coil spring placed in series with a telescopic leg driven by an electrical actuator (Ahmadi and Buehler, 1999). The actuator drives the spring to be further compressed during the stance phase so that the energy loss caused by friction is compensated to achieve the desired hopping height. However, this simple prismatic mechanism exposes the leg actuator to a bending moment due to the side force at each touchdown.

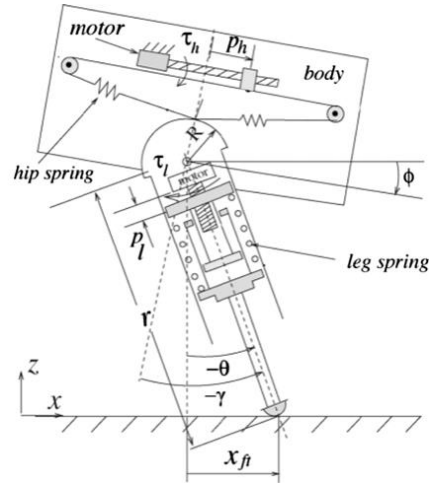
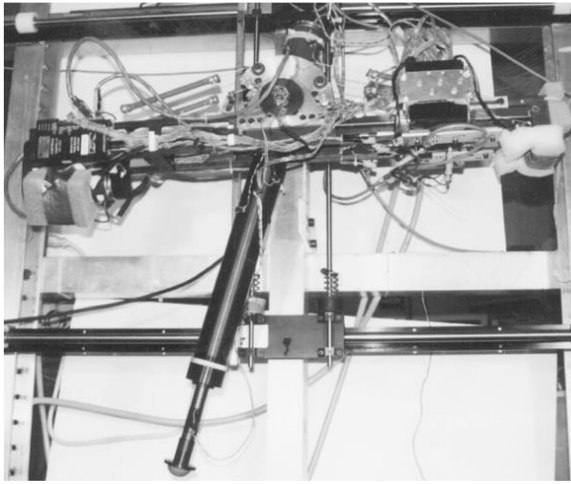


Figure 2.10 Monopod II (Ahmadi and Buehler, 1999).

Kenken (see Figure 2.11), another one-legged hopping robot designed to mimic the hind limb of a dog, uses an extension spring instead of compression type (Hyon and Mita, 2002). The articulated type of leg is composed of three links. A hydraulic actuator is placed in parallel with the *thigh* to provide the main actuation force; an extension coil spring is mounted in parallel with the ‘*shank*’ to provide the leg compliance; a *foot* is used to connect the heel to the *ankle*. Due to the parallelogram structure, the spring can be passively extended to absorb the impact energy. A significant improvement of this robot leg is to insulate the hydraulic actuator from the side force. However, complex leg kinematics brings control challenges. In practice, it is difficult to align the body’s CoM perfectly vertically above the *toe*. To maintain balance, tuning of the hip actuator is consistently needed for correct foot placement.

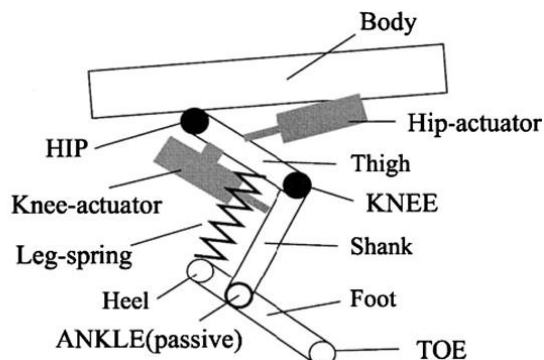
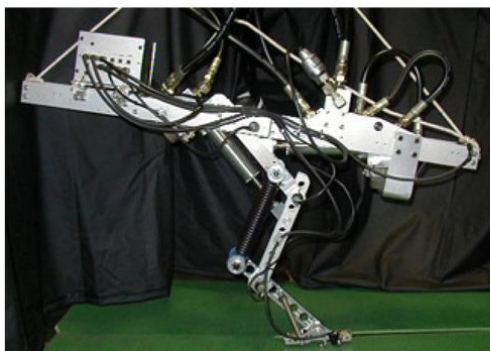


Figure 2.11 Kenken (Hyon and Mita, 2002).

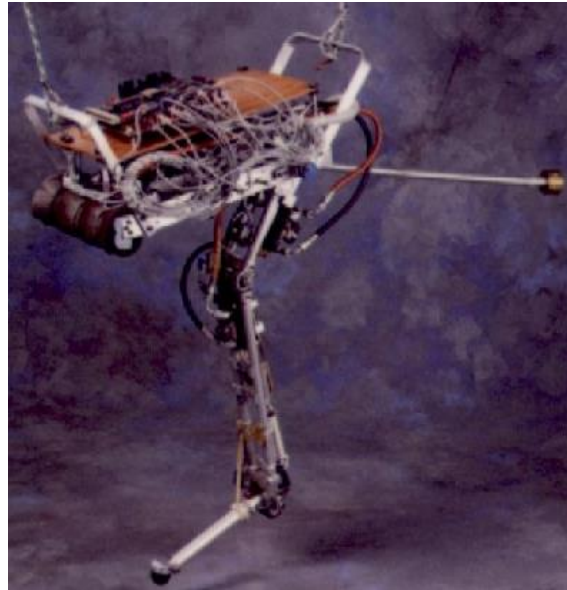


Figure 2.12 Uniuroo, Zeglin's first one-legged hopping robot (Zeglin, 1991).

Inspired by kangaroos, the 'Uniuroo' (see Figure 2.12) is developed by MIT Leg Lab in 1991. Unlike Kenken, Uniuroo uses the hydraulic actuator in series with the spring and a tail is added for balancing purpose (Zeglin, 1991). This design takes advantage of the actuation force directly acting on the elastic element, which is an energy efficient solution for the articulated type of leg. Moreover, a 'virtual leg' concept is applied to design the balancing controllers. This approach was successfully expanded to apply on the quadruped robots, Spot (Boston Dynamics, 2015) and Spot mini (Boston Dynamics, 2017).

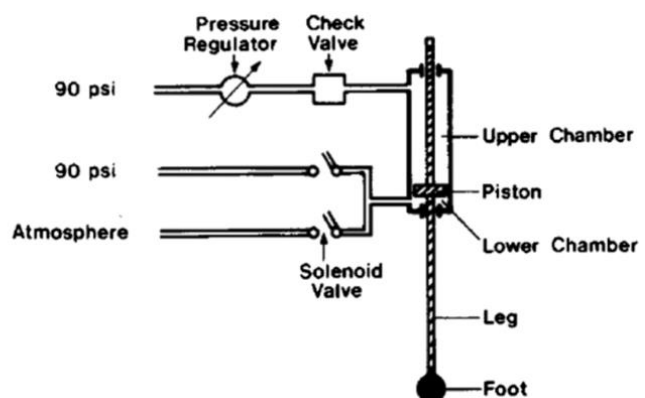
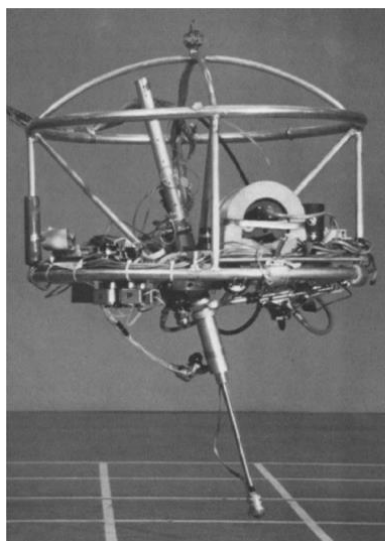


Figure 2.13 A 3D one-legged hopping machine from MIT (Raibert et al., 1984).

2.2.2 Compliant leg using compressed air

It is known that air/gas has significant compressibility, which is widely used in the automotive industry to design suspension systems. Raibert developed the first 3D one-legged hopping machine (see Figure 2.13) using a double acting pneumatic cylinder as the telescopic leg. A rubbery foot is attached at one end of the piston rod (Raibert et al., 1984). During the stance phase, the air in the upper chamber is compressed to absorb the energy, and further compression is given by regulating the pressure in the lower chamber. The upper chamber is connected to the supply pressure permanently, a check valve is able to stop the air flow into the supply line since the air pressure in this upper chamber may be larger than the supply during the stance phase. The leg stiffness is determined by the compressed air pressure, resulting in the linearity not being as good as the coil spring.

‘Mowgli’ (see Figure 2.14) is another bio-inspired bipedal hopping robot design based on the biological musculoskeletal structures (Niiyama et al., 2007). The two articulated legs are driven by pneumatic artificial muscles (PAM). It is able to jump up to 0.5 m with a soft landing. The experimental results have shown that with compliant pneumatic actuation, the robot has the most animal-like motion.

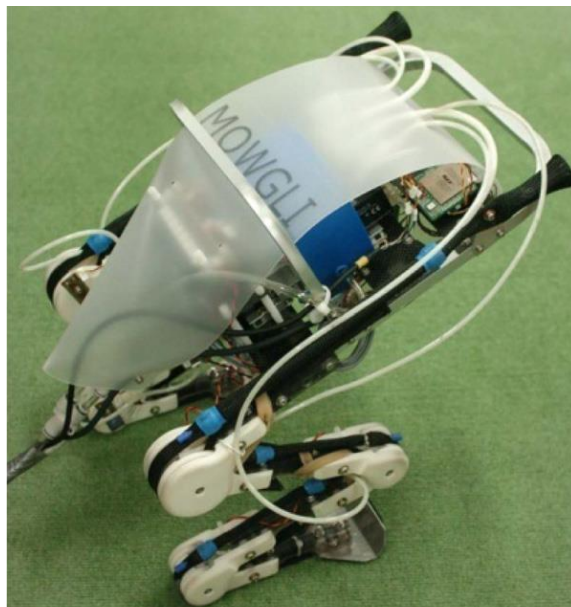


Figure 2.14 Mowgli, a pneumatic driven frog-like hopping robot (Niiyama et al., 2007).

2.2.3 Compliant leg solutions from hydraulic domain

In the hydraulics research area, hydraulic accumulator is a promising solution to provide leg compliance. As Figure 2.15 shows, the pressurised fluid delivered into the oil chamber pushes the diaphragm to compress the gas volume, resulting in an increase of the gas pressure. Therefore, a nonlinear spring characteristic is generated. A well-tuned pre-charge pressure and carefully sized gas volume are able to give a reasonable natural bouncing/hopping frequency.

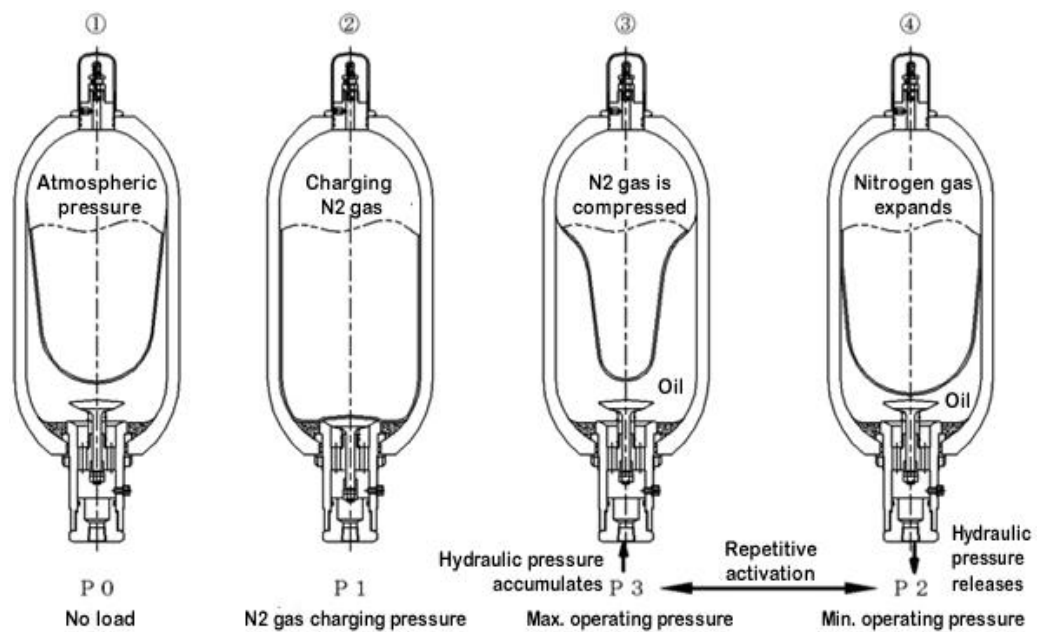


Figure 2.15 One working cycle of a hydraulic accumulator, diaphragm type.

2.3 Balancing control while walking and running

Maintaining balance is the main objective for dynamic robots while walking or running. The main issue of keeping balance while walking and running is that as the speed increases, inertial forces become significant, and actuators need to respond rapidly. There are a few different ways to simplify the control concept so that the controller can be designed in a logical manner.

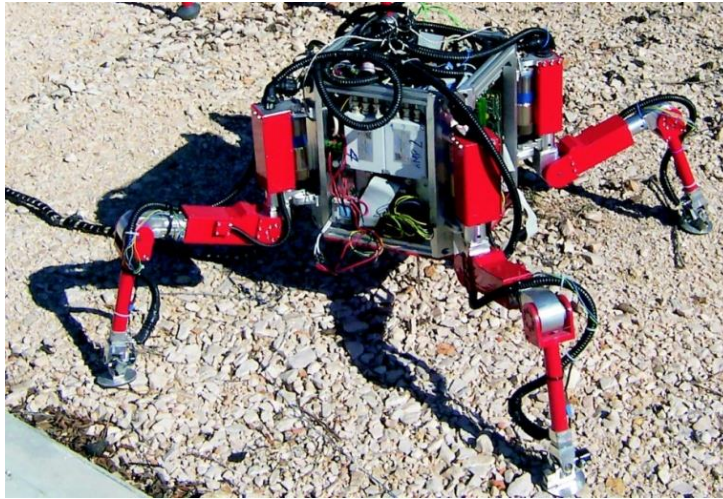


Figure 2.16. Silo4 (De Santos et al., 2003).

2.3.1 Zero moment point (ZMP) control

ZMP control is an approach to maintain legged machines balance by keeping the centre of mass (CoM) directly above a support region (Bretl and Lall, 2004). The SILO4 robot (see Figure 2.16) is an example of applying this kind of method. As long as the robot moves slowly enough so that inertial forces can be ignored, kinematic control to maintain static balance will be sufficient to prevent tipping over. However, the small support region between the feet and ground is a challenge when extending this method to bipedal robots. So the small base and high CoM of bipeds restrict them to a very slow walking speed if control is implemented with a view to maintaining static balance.

Since 1986, Honda started to build the E-series bipeds using the ZMP control concept, which could only walk in a straight line and take a step every 30 seconds (Hirose and Ogawa, 2006). In 1991, Honda's E4 robot approached a higher speed of 1.3 m/s by using the extended control method, called ZMP-CoP. CoP means the centre of pressure, which is the point where the resultant ground reaction force intersects the plane of support. If the robot trajectory is designed to maintain the calculated ZMP-CoP within the support envelope, tipping is avoided. The ZMP-CoP concept allows the latest Honda Asimo robot to negotiate stairs, turn or run at 2.5 m/s, and even walk over slightly uneven terrain and maintain balance against some external disturbances. However, it cannot negotiate rough terrain.

2.3.2 Virtual model control

The concept of ‘Virtual Model Control’ (VMC) was applied by Jerry Pratt on the Spring Flamingo and Spring Turkey bipedal, planar walking robots (Pratt et al., 2001). In VMC, control laws for walking and balancing are conceptualised as virtual mechanical components which act to keep the robot balanced. For example, Figure 2.17 shows how a virtual walking trolley keeps the robot balanced in the sagittal plane. The joints of the robot are series elastically actuated so they can operate in a force control loop which is necessary in order to emulate the virtual components. Moving the robot forwards was similarly conceptualised using virtual components.

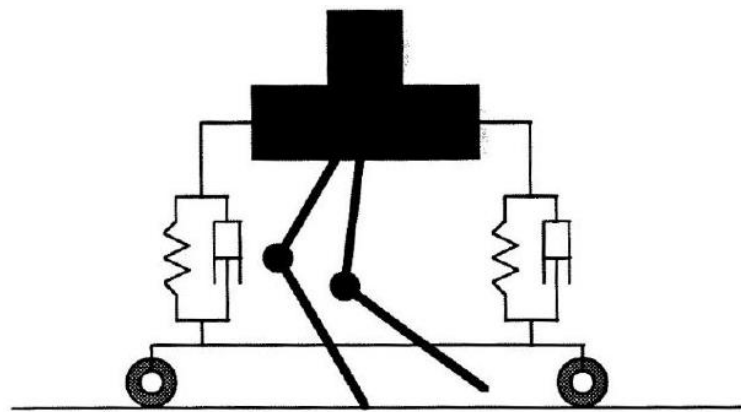


Figure 2.17. Virtual model control.

2.3.3 Controlled passive dynamic walking

In a passive walker, the mechanisms are simply non-actuated, but the link and joint parameters are carefully selected through analysis, simulation and tuning so that the device can stably walk down slopes with a gait that resembles human walking. They were studied by McGeer (McGeer, 1990). Since there are no actuators or control electronics, the behaviour is reliant on mechanical design. However, this kind of walker cannot walk on level ground and has very limited ability to remain stable on varying terrain. A number of researchers have added actuators to passive dynamic walkers to build walking robots. The controlled passive dynamic walkers (CPD) are not merely passive walkers with the ability to traverse flat terrain, they provide an opportunity for researchers to develop very energy efficient robots.

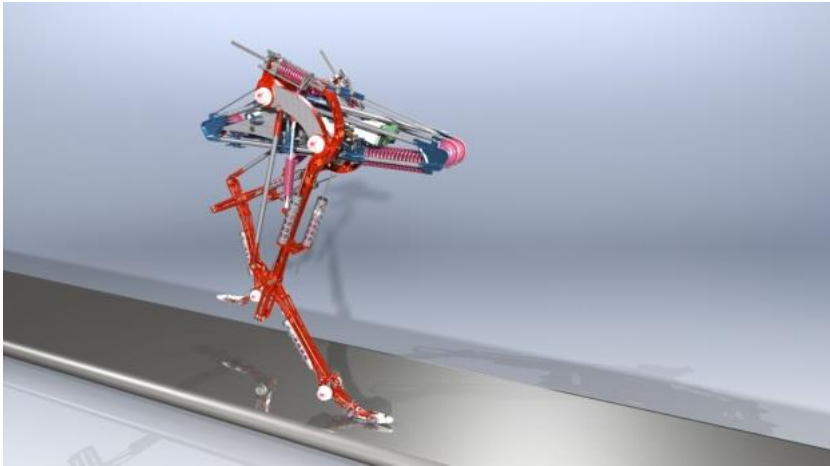


Figure 2.18. IHMC Fast-Runner: a DARPA funded project (Cotton, 2012).

2.3.4 ‘Three-Part’ control

In 1986, Raibert and his co-workers built several one legged machines to study running locomotion and found a simple set of algorithms could be used to design the controller. Raibert’s ‘Three-Part’ control method has made a remarkable contribution to the research of robot running (Raibert, 1986). For a one-legged robot, hopping and running are the same, and the running cycle is separated into two parts, stance and flight phase.

During the stance phase, the basic model of a one-legged robot is an inverted pendulum with the foot fixed on the ground. This particular model leads to the discussion of self-stabilization. In order to achieve self-stabilization, the control could be simplified by improving the mechanical design, as for example in the FastRunner (see Figure 2.18), which was developed by Institute for Human and Machine Cognition (IHMC). The FastRunner applies passive dynamic and elastic components to allow the actuator power used to excite the running motion and not lost working against limb inertia (Cotton, 2012). Although this robot is only self-stabilizing around its operating speed of 9 m/s, it shows the importance of mechanical design.

The other phase is called the flight phase when the foot loses contact with the ground and need to be positioned to make the robot ready for the next step. In the ‘Three-Part’ controller, the control system is considered as three parts respectively, the hopping motion, forward travel and posture of the body.

- Control of the hopping height: hopping can be achieved by exciting a leg spring in series with a telescopic leg actuator. By applying the appropriate vertical thrust or displacement during the stance phase, it is possible to input energy vertically and thus control the hopping height.
- Control of the horizontal velocity: the horizontal velocity of the robot after a hop is affected by the angle of the leg before impact. A control loop can be set up which adjusts the leg angle during flight in order to increase or decrease the horizontal velocity and maintain balance.
- Control of the body orientation: during stance phase, by applying a hip torque, it is possible to control body orientation and remove angular momentum.

During the 1980s and 1990s, the Leg Lab built increasingly sophisticated dynamic running machines by implementing the ‘Three-Part’ control algorithm (MIT Leg Laboratory, 1986). Moreover, this control strategy was successfully extended to multi-legged running robots. An additional concept of the ‘virtual leg’ was developed in order to achieve running with a quadruped (Raibert et al., 1986). In gaits such as the trot, pace and bound, where sets of legs enter stance simultaneously and different sets do not overlap in their stance phase, the sets can be treated as though they were one ‘virtual leg’. In this way, quadruped locomotion can effectively be achieved by using the one-leg ‘Three-part’ controller with some extensions in order to control body pitching and rolling.

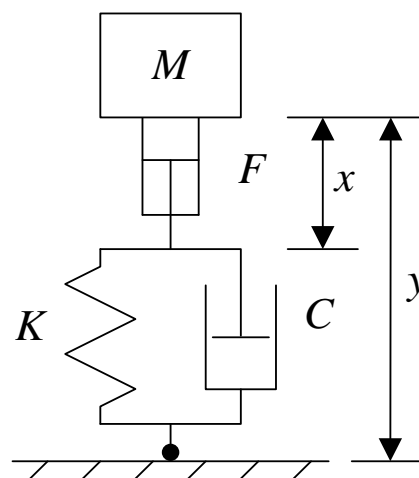


Figure 2.19 The SLIP model (showing the stance phase).

2.4 Hopping height control

Among the research on legged locomotion, mono-legged or bipedal hopping is a sustained interest. The study of hopping aims to provide an understanding of running dynamics as the results can be extended for multi-leg platforms. A springy leg interacting with the body mass is able to give a natural hopping frequency.

The main control actions for hopping height are required to be accomplished within the stance phase. The spring-loaded inverted pendulum model (see Figure 2.19) with the foot fixed on the ground (assuming the ground friction is sufficient) can be used to analyse the motion (see equation 2-1). The equation of motion for this model is:

$$M\ddot{y} = -Mg - C(\dot{y} - \dot{x}) - K(y - x) \quad (2-1)$$

where x is the actuator displacement, y is the mass displacement, K is the spring stiffness, C is damping coefficient, M is the mass and g is the gravitational acceleration.

Using the first planar hopper (see Figure 2.20), Raibert's vertical hopping control approach was tested (Raibert, 1984). The controlled variable, i.e. the actuator position, is derived from the energy conversion equation, which is given by:

$$E_{\text{stance}} = PE_e + PE_g + KE + E_{\text{loss}} \quad (2-2)$$

where E_{stance} is total energy during the stance phase, PE_e is the elastic potential energy stored in the spring, PE_g is the gravitational potential energy, KE is the kinetic energy and E_{loss} is the energy loss due to friction.

During stance, if the energy stored in the spring is sufficient for the robot to lift off the ground, hopping happens. The energy loss due to friction can be compensated by moving the piston to the desired position so that the spring will be compressed further. This position based controller has been successfully implemented on other legged hopping robots (Raibert, 1986).

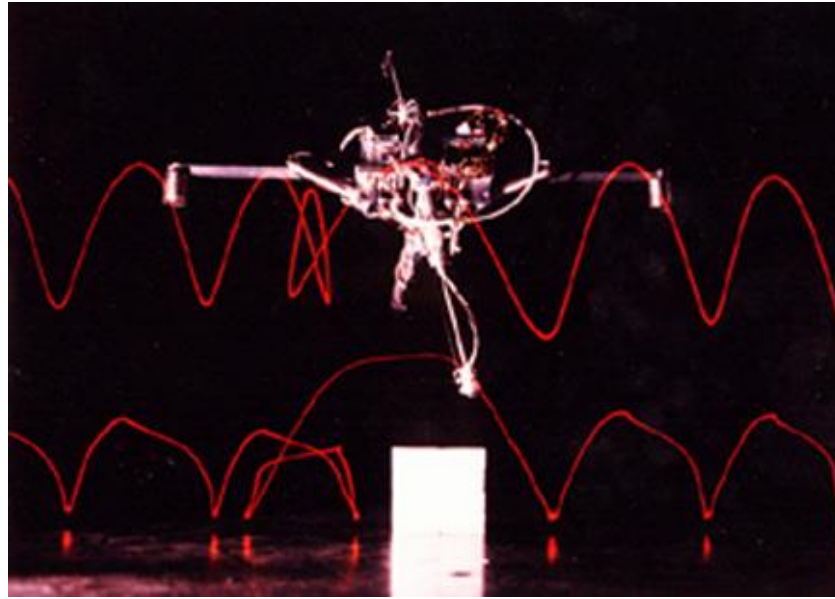


Figure 2.20 Raibert's 2D planar hopper (Raibert, 1984).

Hyon and Mita (2002) described an empirical hopping controller based on a comprehensive understanding of the dynamics of the SLIP model and tested this controller on Kenken. The controller generates the control signal according to the required lift-off velocity. The displacement of the leg actuator is determined by the need for the leg spring to be further deflected to provide the required energy for sustained hopping.

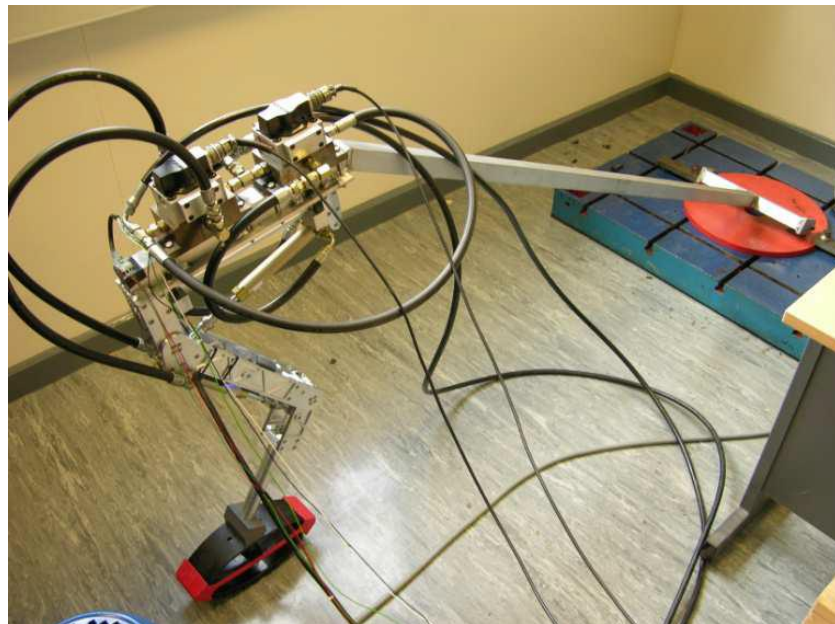


Figure 2.21 Hopping leg with a springy foot (Bhatti et al., 2012).

Bhatti et al. (2012) developed a simple adaptive algorithm for hopping that allows rapid changes of height even when the ground properties change. An adaptive actuator velocity demand signal is calculated using the previous hopping height and the demand hopping height for the next cycle. It is also found that this adaptive velocity signal has the potential to be replaced by other control parameters, such as the valve's driving voltage. This controller is successfully tested on a two-link robot leg with a springy foot, which is driven by a hydraulic valve-controlled actuator system, as shown in Figure 2.21.

2.5 Control of hydraulic actuators

The motion control of legged robots is closely related to the actuation approach. Servo-hydraulics is highly suitable for robot leg actuation due to the high power density and quick response. A hydraulic valve-controlled actuator system is a simple and reliable way to obtain motion control of a robot leg. Jelali and Kroll (2012) summarised some well-studied closed-loop position control approaches for hydraulic actuators. However, the nonlinearities of this actuation system may cause a significant negative effect on the control performance, e.g. due to the friction effect (Ding et al., 2018). Therefore, some nonlinear adaptive control approaches have been proposed (Yao et al., 2000).

Closed-loop force control is particularly difficult for hydraulic actuators. Unlike an electrical motor, the actuator output force/torque is not proportional to the control input. For example, a closed-loop error leads to an opening of valve orifice, which allows a certain amount of flow to be delivered into a trapped volume, and taking the fluid compressibility into account, the pressure is an integration of this rate of change of oil volume. Negative force, pressure or acceleration feedback are well-known methods for increasing damping in servohydraulic position control systems. When driving large inertia loads, the force feedback gain can be adjusted to provide damping to attenuate the system resonance associated with actuator compliance. Positive force feedback performs in the opposite way, tending to reduce or eliminate the stability margins. This is not desirable for common control systems, but a consistent hopping motion can be achieved by creating a marginally stable system. From biomechanical studies, Geyer et al. (2003) described a

possible bouncing gait is achievable using positive force feedback approach. However, this has not been discussed further in depth or demonstrated using legged robots.

2.6 Conclusions

Legged locomotion is a fascinating topic that attracts research to design and develop more powerful and more agile legged moving machines. The rapid development of multidiscipline technologies aids the study of legged locomotion which has now reached an unprecedented level. Since the 1980s, research about control strategies and mechanical structure have made remarkable contributions to increase the running speed and solve the balance issues while the robot is moving. Most of the previous paradigms and platforms demonstrated specific control strategies to solve particular balancing issues. A kangaroo-like, hydraulically actuated bipedal hopping robot, called the Bath Bipedal Hopper (BBH), has been developed as part of this research and provides another platform to test the performance of different controllers.

According to the reviewed literature in this chapter, motion control strategies for legged robots are closely related to the mechanical design and components selection. Particularly, most hopping height controllers require detection of ground contact to enable different control actions to handle the rapid change of system characteristics between the flight and stance phases. This transition can be provided either mechanically or electrically. Moreover, several state variables usually need to be measured, e.g. the actual body position, and the corresponding velocity or acceleration. Therefore, sensor selection and signal processing should be considered carefully to provide sufficiently accurate low-noise measurements. Thus, a novel hopping height controller will be developed to address these challenges.

The balancing issues should be considered either statically or dynamically. A static balance is simple to achieve as long as the robot has a sufficient foot supporting area. A smaller foot contact area can increase the capability of traversing rough or uneven terrain, however, it makes the motion control to be challenging. It is

difficult to perfectly align the body centre of mass above the foot contact point, vertically, in practice. Therefore, the static balancing controller needs to be carefully designed. The dynamic balancing control for a bipedal hopping robot should concentrate on not only hopping on a spot but also moving with different longitudinal velocities. Raibert's 'Three-part' control algorithm is a well-established structure to be followed.

3 BBH1 robot

This chapter describes the first prototype of the bipedal hopping robot, namely, the BBH1. The chapter starts with a general introduction to the mechanical design of the BBH1 including an overview presenting the system schematic; a detailed description of the actuation systems, the sensory system and the real-time control system used for controller implementation. Particularly, a compliant hydraulic actuator is designed to be used for robot leg actuation. The next section describes the dynamic modelling of the robot focusses on the hydraulic domain and mechanical domain, and aims to explain the main findings from the experiments, which have been under taken to examine the efficacy of the mechanical design of the robot. The last section presents a detailed discussion and analysis of the bench test results.

3.1 Mechanical design

Inspired by kangaroos, the largest animals using bipedal hopping mechanism on the planet, the BBH1 is designed to be small-sized, hydraulically actuated bipedal hopping robots. As shown in Figure 3.1, the robot body is an aluminium frame for mounting the manifold, valves and PC-104 controller, giving a compact size with reasonable mass. The upper body and the legs are connected by a revolute joint, named the hip joint. Figure 3.2 shows that the two legs are rigidly connected in parallel using a metal rod so that the body actuator can sway the legs front and back around the hip joint to place the feet in the desired position; the leg actuator with a rubbery foot, mounted at the end of the piston rod, directly interacts with the ground to perform as a telescopic type of robot leg; the leg compliance is provided by connecting an accumulator to the full piston chamber of the cylinder. Due to the compressibility of the pre-charged gas in the accumulator, the actuator compliance is much higher than a conventional valve controlled actuator system. This type of arrangement is named a compliant hydraulic actuator.

Figure 3.3 shows that in the bench test stage, the upper body is constrained using a connection beam with a pivot joint on the ground. This test rig is driven by a

hydraulic power pack placed in the adjacent area, which eventually can be replaced by pressurised accumulators to allow untethered operation. The main dimensional specifications of BBH1 are summarized in Table 3.1.

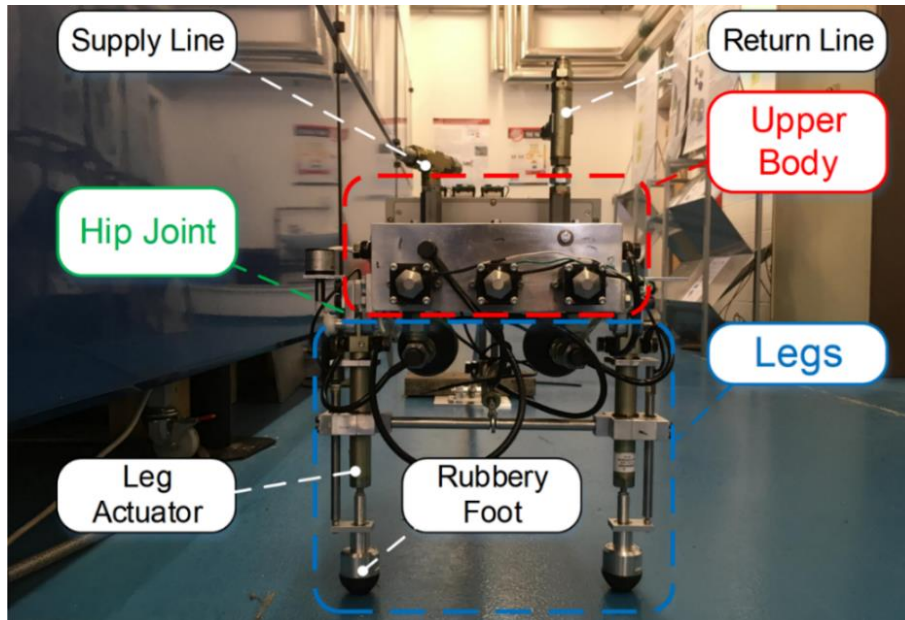


Figure 3.1 The BBH1 robot (showing the front view).

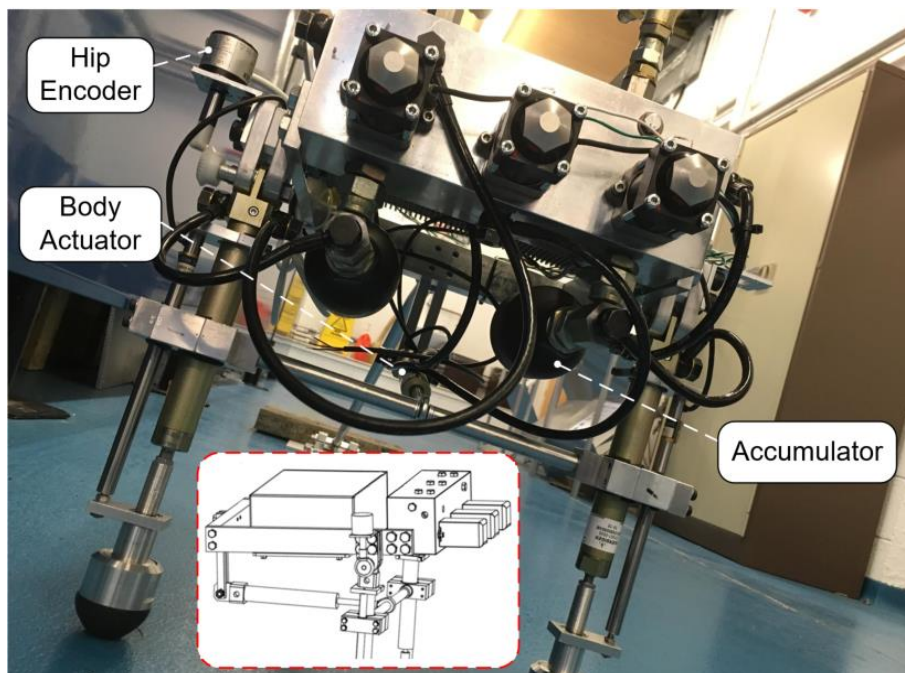


Figure 3.2 The BBH1 robot (mainly showing the spring accumulators, with a side view showing the body actuator).

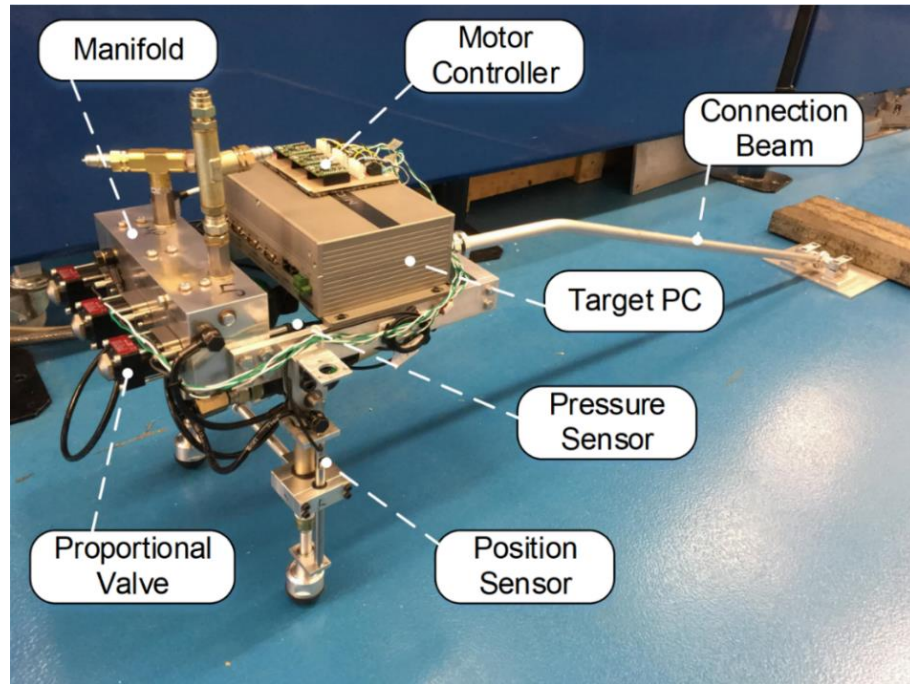


Figure 3.3 The BBH1 robot (showing with a mechanical constraint).

Table 3.1 Main dimensional specifications of the BBH1 robot.

Height:	394 mm
Length (without connection beam):	414 mm
Width:	275 mm
Weight:	15.2 kg

3.1.1 System overview

The experimental system can be described as three sections: the actuation system, the sensory system and the control system, which is shown in Figure 3.4. The hydraulic actuation system consists of valve-controlled actuators powered by a constant pressure supply. The linear force motor in each direct drive spool valve is driven by a motor controller. The sensory system consists of two leg position potentiometers, hip and ankle incremental encoders, and hydraulic cylinder pressure sensors. All electrical signals are acquired by a compact target PC with a built-in data acquisition board. The controller implementation is achieved using a real-time control system running on the target PC.

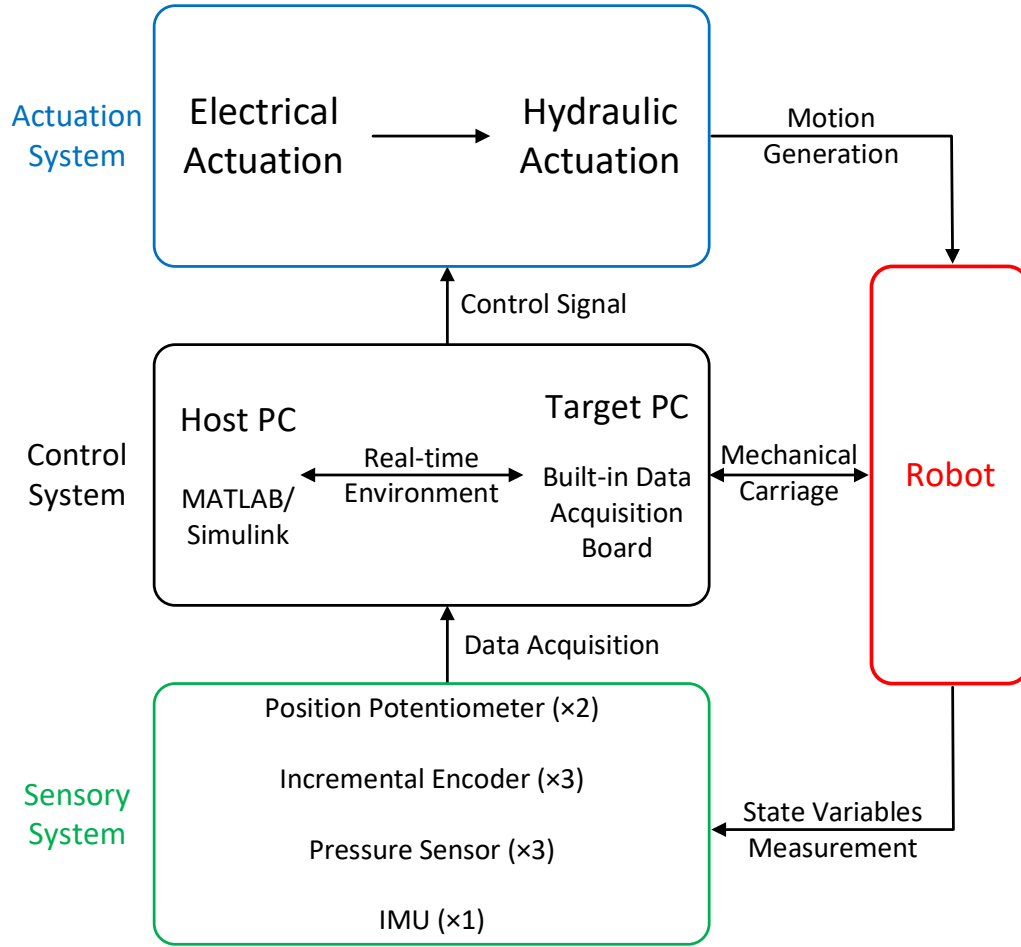


Figure 3.4 System schematic.

3.1.2 Actuation system

The actuation system includes hydraulic and electrical parts. Hydraulic actuators provide the main power transmission to generate the robot motion, and electrical linear force motors are used to move the spools in the valves which control the hydraulic actuators.

3.1.2.1 Hydraulic circuit

The hydraulic system has a fixed displacement pump supplying the 3 valve-controlled actuators via a regenerative arrangement, i.e. the supply pressure is permanently connected to the rod-end of the single-ended cylinder. The hydraulic circuit of one of three valve-actuator pairs of BBH1 is shown in Figure 3.5.

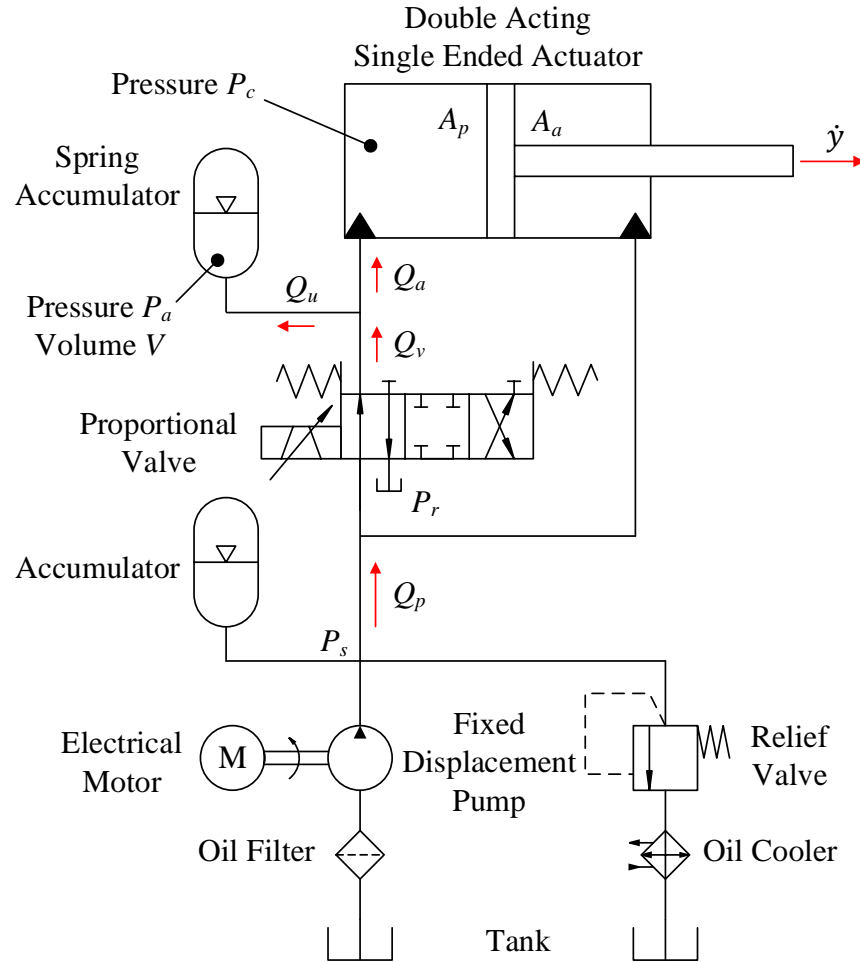


Figure 3.5 Hydraulic circuit of the BBH1 robot (showing one of the three valve-actuator pairs).

3.1.2.2 Valve

The Moog E242 hydraulic valve is used to control the fluid direction as shown in Figure 3.6. It is a 4 way/3 position proportional valve using the Moog Direct Drive technology which is developed according to the established Moog D633-7 design (Moog Inc, 2009). A linear force motor directly actuates the valve spool to a position which is proportional to the input driving current signal. The centring spring is used to keep the spool in the middle position when there is no input control signal. The main specifications are summarized in Table 3.2.



Figure 3.6 Moog E242 proportional valve (Moog Inc, 2009).

Table 3.2 Main specifications of the hydraulic valve (Moog Inc, 2009).

Maximum supply pressure:	210 bar
Rated flow:	5 L/min
@ 70 bar valve pressure drop	
Electrical input signal:	+/- 1.0 A into a 5.2 ohm load
Dynamic performance:	90° phase lag >150 Hz
25% signal @ 210 bar & 40 °C	-3 dB attenuation >150 Hz
Accuracy of flow control:	Full amplitude hysteresis
	< 120 mA
Weight:	380 g

3.1.2.3 Actuator

The hydraulic cylinders are from the Hoerbiger LB6 series as shown in Figure 3.7. This double acting differential cylinder is designed according to the twin-tube principle with rear connections (A and B). The area ratio between the full piston side and the annulus side is about 1.6. Mechanical buffers or stops are located at 1 mm offset from each end of the full stroke (Hoerbiger, 2008). The main specifications are summarized in Table 3.3.



Figure 3.7 Hoerbiger LB6 hydraulic actuator (Hoerbiger, 2008).

Table 3.3 Main specifications of the hydraulic actuator (Hoerbiger, 2008).

Operating pressure range:	5 – 160 bar
Piston / rod diameter:	12 mm / 8mm
Stroke:	80 mm
Maximum piston moving speed:	4 m/s

3.1.2.4 Accumulator

To provide leg compliance in BBH1, a diaphragm accumulator is used, as shown in Figure 3.8, which comes from HYDAC Technology Ltd (HYDAC Technology, 2015). The 0.075 L nominal volume and 40 bar pre-charge gas pressure are determined due to the system compliance requirement, plus the compact series is selected to suit the application on a small size robot. The main specifications are summarized in Table 3.4.



Figure 3.8 HYDAC diaphragm accumulator (HYDAC Technology, 2015).

Table 3.4 Main specifications of the hydraulic accumulator
(HYDAC Technology, 2015).

Nominal volume:	0.075 L
Pressure ratio:	8:1
Permit / pre-charge pressure:	250 bar / 40 bar
Weight:	0.7 kg

3.1.2.5 Valve spool actuation

The Maxon/Escon motor controller 24/2 module, which is shown in Figure 3.9, is used to convert the control voltage to the driving current of the linear force motor in the valve. The module output is controlled by the built-in current feedback controller (Maxon motor, 2014). The controller parameters are set up using the OEM manufacturing software before implementing on the test rig. The main specifications are summarized in Table 3.5. Moreover, three motor controllers are mounted on a motherboard, as shown in Figure 3.10, to make a compact electrical actuation box.



Figure 3.9 Maxon/Escon 24/2 motor controller (Maxon motor, 2014).

Table 3.5 Main specifications of the motor controller (Maxon motor, 2014).

Nominal operating voltage:	10 – 24 VDC
Output current (continuous/peak):	2 A / 6A
Analog input voltage:	+/- 10 V
Weight:	7 g

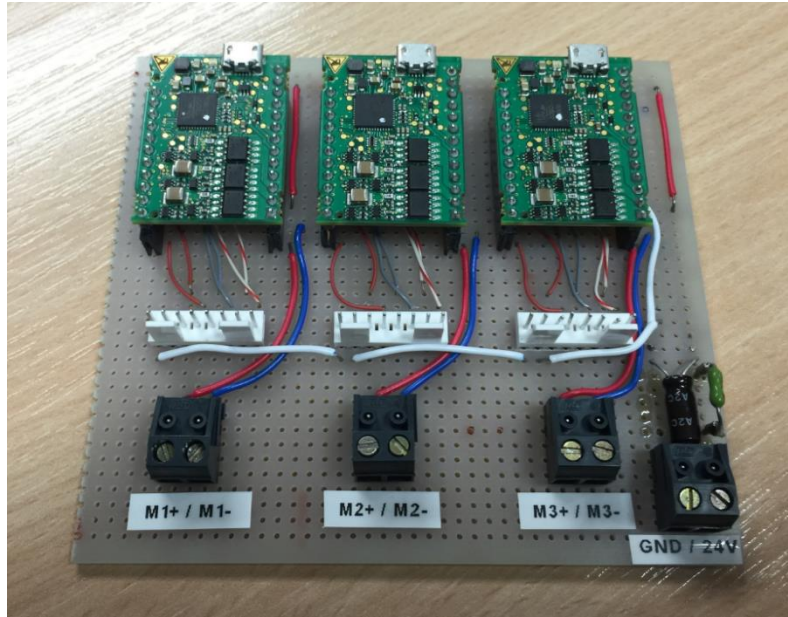


Figure 3.10 Motor controllers (showing the assembly with the motherboard).

3.1.3 Sensory system

This section gives a detailed description of the sensors, plus some useful settings and calibration information in used practice.

3.1.3.1 Position potentiometer

The linear potentiometers for leg actuator displacement measurement come from the Active Sensors Ltd., the CLS1320 compact series as shown in Figure 3.11. They are constructed from aluminium alloy for a lightweight design (Active Sensors Ltd, 2015). A 5V voltage is applied across the potentiometer and the output signal is calibrated to give 0V when the piston is at the middle stroke. The main specifications are summarized in Table 3.6.



Figure 3.11 Active Sensors position sensors (showing with rod end mountings)
(Active Sensors Ltd, 2015).

Table 3.6 Main specifications of the position potentiometer
(Active Sensors Ltd, 2015).

Measurement range:	100 mm
Applied voltage:	5 V
Rod end bore size:	Ø5 mm
Weight:	78 g

3.1.3.2 Incremental encoder

The incremental encoder used for hip and ankle angle measurement, which is shown in Figure 3.12, is the Hengstler RI32 type with 1000 pulses per revolution (Hengstler, 2014). It is an economical compact encoder with low friction achieved by means of ball bearings. Combined with the data acquisition board in MicroBox 2000, the collected data is the number of pulses corresponding to the encoder shaft rotation angle. Each encoder is driven by its corresponding joint through a 1:2 ratio bevel gear, giving 8000 pulses for each 360-degree rotation. Therefore, the resolution is 0.045 degree per pulse. The main specifications are summarized in Table 3.7.



Figure 3.12 Hengstler incremental encoder (Hengstler, 2014).

Table 3.7 Main specifications of the incremental encoder (Hengstler, 2014).

Shaft maximum speed:	6000 rpm
Nominal operating voltage:	5 V
Maximum output pulse counts:	4000
Weight:	50 g

3.1.3.3 Pressure sensor

The three hydraulic pressure sensors are of the EPT1200 type as shown in Figure 3.13 (Variohm, 2014). The output voltage signal ranging from 0 to 5V corresponding to the pressure change between 0 and 160 bar, therefore, the calibration gain is 32 bar/V. The main specifications are summarized in Table 3.8.



Figure 3.13 Hydraulic pressure sensor (Variohm, 2014).

Table 3.8 Main specifications of the pressure sensor (Variohm, 2014).

Measurement range:	0 – 160 bar
Excitation:	24 V
Output voltage:	0 – 5 V
Mechanical connection:	M8×1 male thread
Weight:	25 g

3.1.3.4 Inertial measurement unit

An inertial measurement unit (IMU), as shown in Figure 3.14, from the Yost Labs is used to measure the robot body posture in three axes to the global coordinate system, e.g. the body orientation angle and the corresponding angular velocity. The IMU is attached to the robot upper body. Serial communication is built between the RS232 port on the MicroBox and the 4-poles stereo port on the IMU using ASCII code-based protocols (Yost Labs, 2016). The main specifications are summarized in Table 3.9.



Figure 3.14 Yost Labs inertial measurement unit (Yost Labs, 2016).

Table 3.9 Main specifications of the IMU (Yost Labs, 2016).

Supply voltage (external jack):	5 V
Serial baud rates:	1,200~921,600
Orientation accuracy:	$\pm 2^\circ$ for dynamic conditions
Orientation resolution:	$< 0.08^\circ$
Dimensions:	35mm×50mm×15mm
Weight:	17 g

3.1.4 Control system

The controller implementation is achieved using the xPC Target in Simulink[®], which is a real-time target system product established on the real-time workshop (RTW) framework developed by MathWorks. In this project, the target PC is the MicroBox 2000 from Terasoft Ltd., shown in Figure 3.15, which is a rugged, high performance x86-based industrial PC, in PC-104 format. It supports TCP/IP communication interfaces and various PC-104 based AD/DA, DIO and Encoder modules (Terasoft Ltd., 2014). The host PC is a laptop with an Ethernet card.

Additionally, the Windows operating system is required to run MATLAB[®]/Simulink[®], C language compiler and RTW. The main specifications of the MicroBox 2000 are summarized in Table 3.10.

Table 3.10 Main specifications of the MicroBox 2000 (Terasoft Ltd., 2014).

CPU:	Celeron® M 1GHz, 256MB DDR2 RAM
Flash memory:	64MB flash card
Power input:	19 VDC / 3.42 A
Weight:	2 kg
ADC – built-in I/O:	Sensoray 526, 8-ch single-ended, 16-bit A/D converter (± 10 V)
DAC – built-in I/O:	Sensoray 526, 4-ch single-ended, 16-bit A/D converter (± 10 V)
Digital I/O – built-in I/O:	Sensoray 526, 8-bit digital I/O
Encoder – built-in I/O:	Sensoray 526, 4-ch 24-bit incremental encoder (1×, 2× or 4×)
Signal sampling frequency:	1 kHz

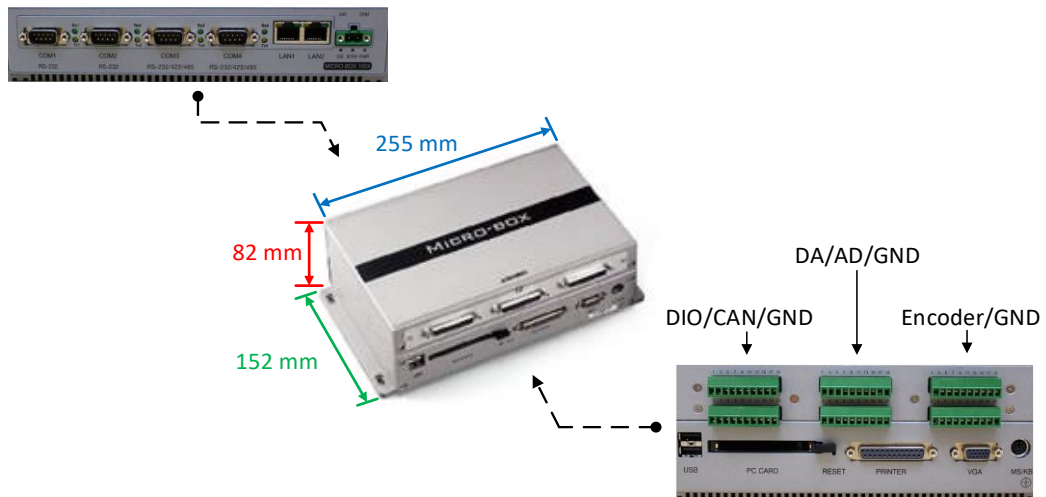


Figure 3.15 Target PC: Terasoft MicroBox 2000.

3.2 Modelling of the BBH1 robot

This section summaries the modelling of the BBH1, which focusses on the hydraulic domain and mechanical domain, and aims to explain the main findings from experiments and to be used to develop controllers. The hydraulic modelling follows well-established theoretical procedures (Merritt et al., 1967), and also incorporates some empirical characteristics found from experiments. The mechanical models are built using SimMechanics[®], a multi-body mechanical simulation tool in the Simulink[®].

3.2.1 Hydraulic models

This section presents the hydraulic model of the BBH1 robot. The equations are written according to the hydraulic circuits shown in Figure 3.5.

3.2.1.1 Actuator model

The hydraulic actuator model includes the piston force balance equation and flow equation. It is assumed that the supply pressure and return pressure are constant plus there is no internal or external leakage. Thus the actuator model is given by:

$$P_c A_p - P_s A_a - F_f = F_h \quad (3-1)$$

$$Q_a = A_p \dot{y} \quad (3-2)$$

where P_c is the full piston side pressure, P_s is the supply pressure (assumed constant), A_p is the full piston area, A_a is the annulus area, F_h is the hydraulic actuation force and F_f is the friction force. Q_a is the piston side flow rate and \dot{y} is the piston velocity.

Additionally, the friction force is modelled by:

$$F_s = f_v \dot{y} \quad (3-3)$$

$$F_f = \begin{cases} F_c & \text{for } F_s \geq F_c \\ F_s & \text{for } |F_s| < F_c \\ -F_c & \text{for } F_s \leq -F_c \end{cases} \quad (3-4)$$

where F_c is the Coulomb friction force, and F_s is velocity-dependent friction at low velocity, introduced to avoid a discontinuity, which can cause numerical issues during the simulation; f_v is a friction coefficient which is relatively large.

3.2.1.2 Valve model

Only one orifice equation is needed to model the proportional valve, as the flow is only metered into one side of the actuator. The spool displacement is considered as a dimensionless variable which ranging from -1 to +1 with the middle position corresponding to 0. The valve model is given by:

$$Q_v = K_v X \sqrt{P_s - P_a} \quad (3-5)$$

where Q_v is the valve flow rate, K_v is the valve flow coefficient, X is the nominalised spool displacement and P_a is the accumulator output pressure. Additionally, a second-order transfer function could be used to represent the valve dynamics, which is given by:

$$X = \frac{\omega_v^2}{s^2 + 2\zeta_v \omega_v s + \omega_v^2} \tilde{u}_c \quad (3-6)$$

where \tilde{u}_c is the spool driving signal, ω_v is the spool natural frequency and ζ_v is the spool damping ratio, which are empirical values determined from the manufacturer data sheet or experimental results.

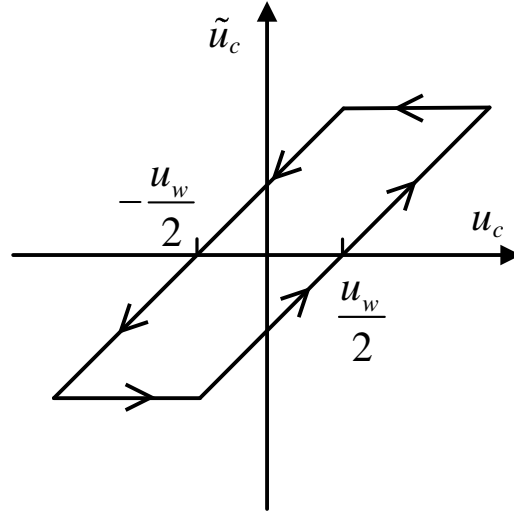


Figure 3.16 Valve hysteresis.

Hysteresis is often a significant non-linearity in valve spool positioning. This is modelled as ‘backlash’ as shown in Figure 3.16, in which u_w is the dead-band width of the backlash. Additionally, the control signal (a voltage signal), u_c , is generated by the motor controller and converted into the driving current of the valve, modelling as a simple proportional gain, $K_{mc}=0.1\text{A/V}$.

3.2.1.3 Accumulator model

The spring accumulator is modelled using equations 3-7, 3-8 and 3-9. And the adiabatic process is assumed due to the quick charge and discharge in robot running.

$$\dot{V} = Q_a - Q_v \quad (3-7)$$

$$V^n P_a = V_m^n P_m \quad (3-8)$$

$$V_0 P_0 = V_m P_m \quad (3-9)$$

where V is the gas volume, V_0 is the initial gas volume, V_m is the gas volume at mean working pressure, P_0 is the gas pre-charge pressure, P_m is the mean working pressure and n is the adiabatic index.

3.2.1.4 Hose pressure loss model

The pressure loss between the valve and the cylinder is modelled. It assumes the flow rate passing through the hose is proportional to the square root of the pressure drop. Thus the hose model is given by:

$$Q_a = K_h \sqrt{P_a - P_c} \quad (3-10)$$

where K_h is the hose pressure loss factor.

3.2.1.5 Hydraulic model implementation in Simulink®

Figure 3.17 shows the implementation of the hydraulic model in Simulink®. The ‘Control Voltage’ port represents the control signal, as well as the ‘Piston Position’ and ‘Piston Velocity’, are sensed from the mechanical models. The ‘Hydraulic Force’ port outputs the actuation force to drive the prismatic joints of the hydraulic actuator. The parameter values for the hydraulic model are listed in Table 3.11.

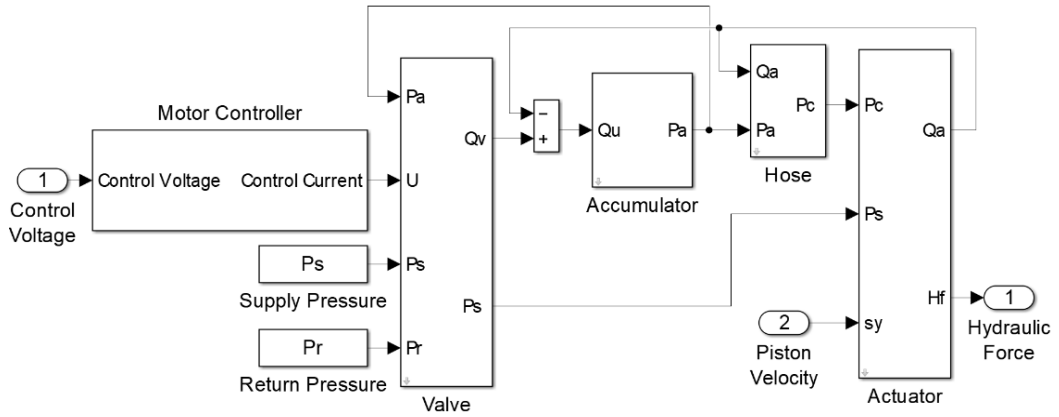


Figure 3.17 Hydraulic models of the BBH1 robot in Simulink®.

Table 3.11 Parameter values of the hydraulic models.

Parameters	Symbol	Value	Unit
Supply pressure	P_s	160×10^5	Pa
Piston area	A_p	1.13×10^{-4}	m^2
Annulus area	A_a	0.63×10^{-4}	m^2

Valve flow coefficient	K_v	4.89×10^{-8}	$\text{m}^4/\text{s}/\text{N}^{1/2}$
Valve spool natural frequency	ω_v	942.48	rad/s
Valve spool damping ratio	ζ_v	0.7	
Backlash dead-band width	u_w	0.2	A
Accumulator pre-charge pressure	P_0	40×10^5	Pa
Accumulator initial gas volume	V_0	7.5×10^{-5}	m^3

3.2.2 Mechanical models

The mechanical model of one robot leg in SimMechanics is shown in Figure 3.18. It includes the inertia parameters and describes the prismatic motion between the piston and the cylinder, which can be expanded into a full mechanical model of the BBH2 in the following chapter including rigid bodies, revolute joints and modelling of a hip actuator.

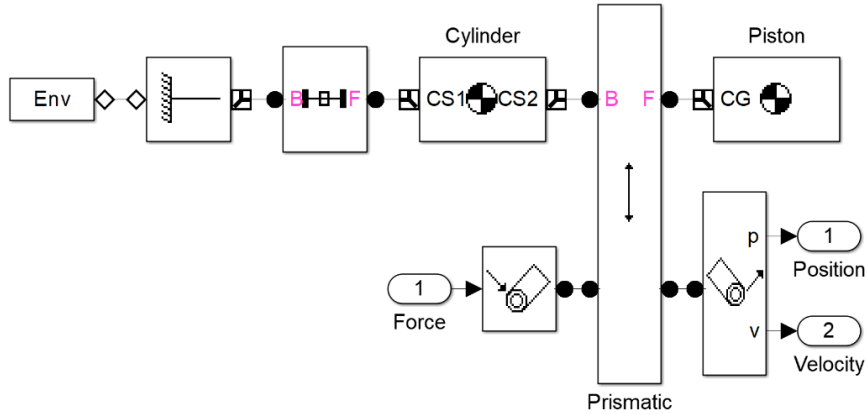


Figure 3.18 One robot leg model of the BBH1.

3.3 Bench test results and analysis

3.3.1 Bench test results

In order to examine the efficacy of the mechanical design of the robot, a series of bench tests have been taken. A proportional-integral (PI) controller is used to

achieve the closed-loop position control of the robot leg, which is common for servo-hydraulic systems. The controller is given by:

$$u_c = K_p e + K_i \int e dt \quad (3-11)$$

where K_p is the proportional gain, K_i is the integral gain and e is the position error.

For BBH1, due to the telescopic type of leg, controlling the leg length is the same as controlling the hydraulic actuator's piston position. The hip actuator is controlled to place the foot underneath the upper body's CoM. The PI controller gains are tuned while the hydraulic actuators are moving. It is necessary to saturate the output of the PI controller in software to avoid the control signal exceeding the limitation of the hardware output voltage, during which time an anti-windup mechanism is activated to drive the integral part towards zero. The controller gains used are: $K_p=200$ (1/m) and $K_i=200$ (1/s/m).

Figure 3.19, Figure 3.20, Figure 3.21 and Figure 3.22 show the experiment results for closed loop position tracking and corresponding piston side pressure change. Note that the actuator piston is stationary at some certain points of the movement, whilst Figure 3.20 and Figure 3.22 indicate that the piston side pressure is increased until the combined force on the piston is large enough to move the piston to the next position. The reason for this performance is mostly due to the friction, which comes from the sealing around the piston, especially at high working pressure. An estimate of the Coulomb friction, F_c , can be found by calculating the pressure increase while the piston is stalled, and is 105 N.

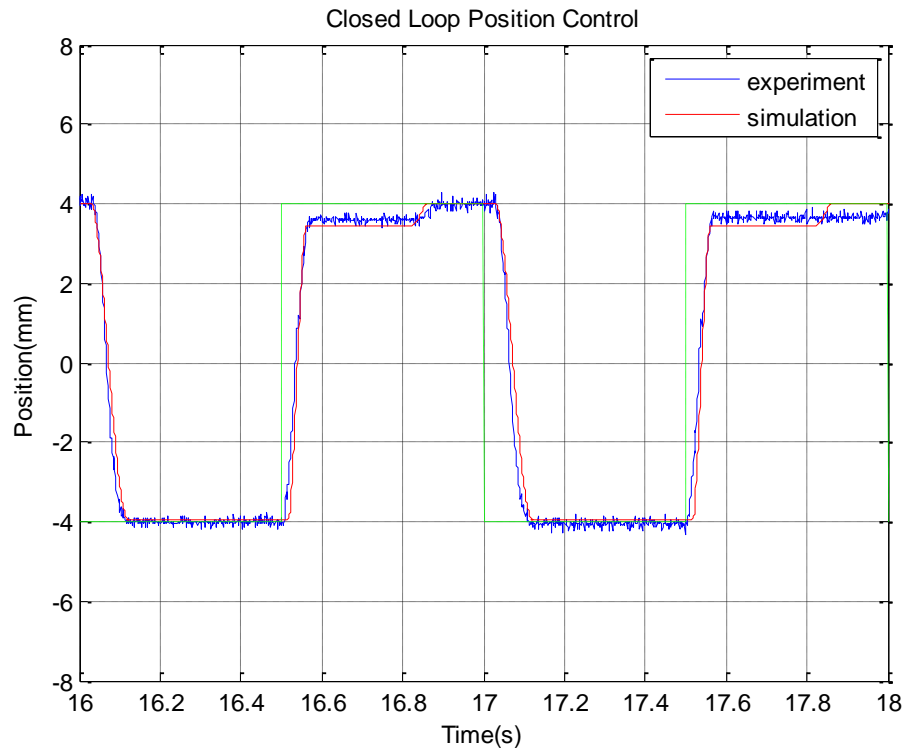


Figure 3.19 Closed loop position control of the leg actuator, using square wave demand.

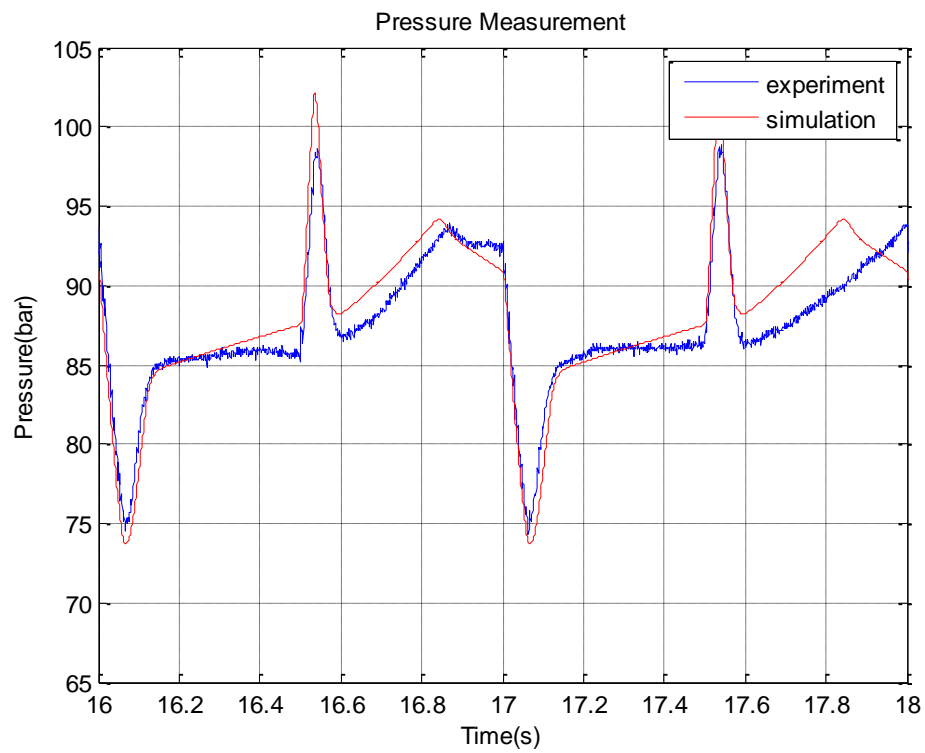


Figure 3.20 Cylinder pressure of the leg actuator, using square wave demand.

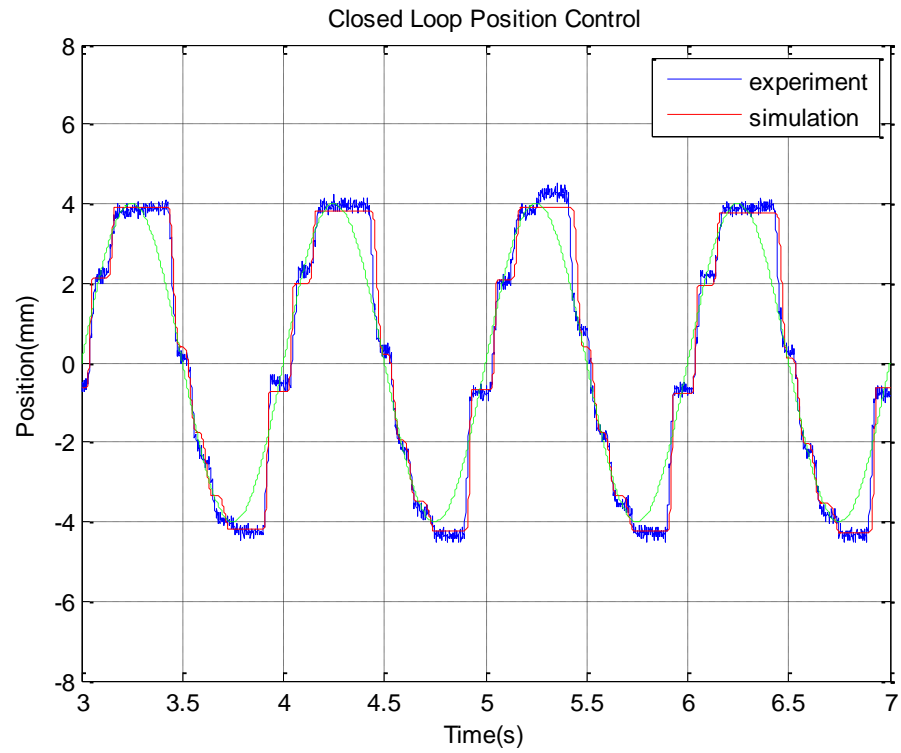


Figure 3.21 Closed loop position control of the leg actuator, using sinusoid wave demand.

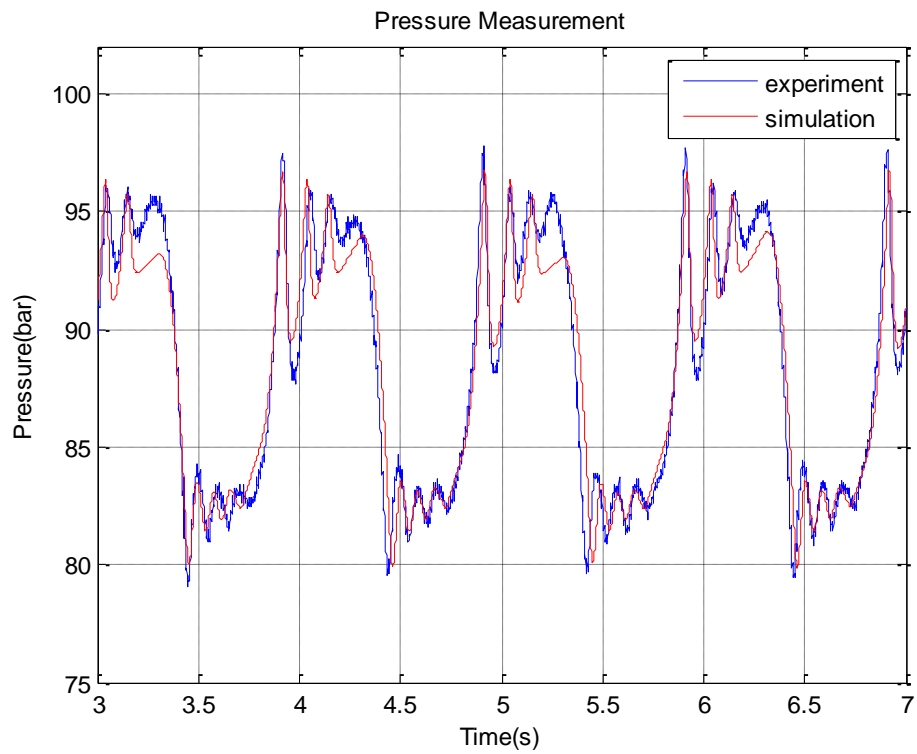


Figure 3.22 Cylinder pressure of the leg actuator, using sinusoid wave demand.

3.3.2 Evaluation of the friction effect

In order to evaluate the friction effect on the compliant actuator, the hydraulic elastance and *error-time integral* are presented in this section. The representations of these factors are given by linearizing the mathematical models in section 3.2. Resulting in the linear valve model is:

$$q_v = C_x x - C_p p_a \quad (3-12)$$

where C_x is the valve flow coefficient corresponding to spool displacement and C_p is the valve flow coefficient corresponding to pressure. Konami (2017) presented a detailed linearization of other components, which is a well-established mathematical procedure.

In hydraulic systems, the change in pressure which results from a certain change in trapped oil volume is termed *Hydraulic Elastance*, which can be understood as another form of hydraulic stiffness. A larger hydraulic elastance gives a faster pressure change for a certain flow. Thus in the closed loop system, generating a large pressure increase only requires a small position tracking error. Moreover, the larger the hydraulic elastance is, the smaller the system compliance would be. The hydraulic elastance for the compliant actuator is:

$$E_c = \frac{nP_m}{V_m} \quad (3-13)$$

where E_c is the hydraulic elastance of the *compliant system*, P_m is mean working pressure and V_m is the corresponding gas volume.

As Figure 3.19 shows, when the piston is stalled, the position error leads to a certain opening area of the valve orifice which allows the flow to be delivered into the accumulator to build up the pressure. In this case, assuming the pressure change in the actuator is small to overcome the friction, then C_p in equation 3-12 is neglectable. Thus, the system block diagram is shown in Figure 3.23 and equation 3-14 describes the required position tracking error in terms of friction when the piston is stationary.

$$e_p = \frac{sF_f}{E_h K_p C_x A_p} \quad (3-14)$$

where e_p is the position tracking error and M is the load mass. Rearranging Equation 3-14 gives an *error-time integral* that is introduced to link the friction effect with system compliance. It is a factor used to represent the length of time that an error must be sustained in order to overcome the Coulomb friction, as Equation 3-15 shows.

$$\int e_p dt = \frac{F_c}{E_h K_p C_x A_p} \quad (3-15)$$

Taking the $F_c=105$ N into account, the theoretical values of hydraulic elastance and *error-time integral* for the compliant actuator are 1.99×10^{14} N/m⁵ and 1.79×10^{-4} mms, respectively. In Figure 3.19, there is a constant e_p of 0.4 mm, theoretically, it takes approximately 0.21 s for the system to build up the pressure, which makes the friction effect is more observable.

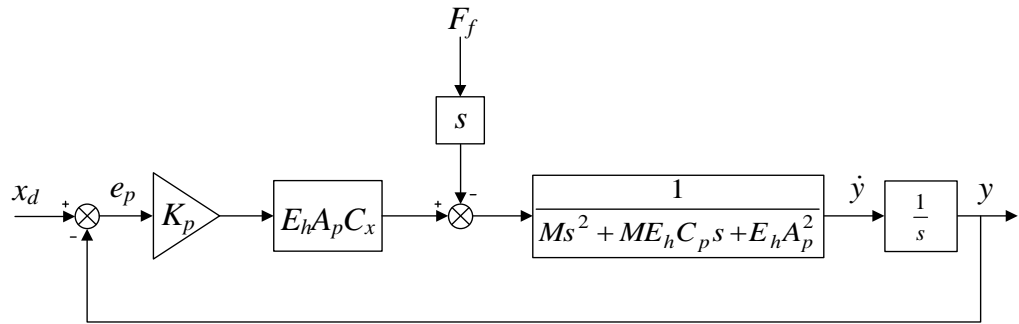


Figure 3.23 Rearranged system block diagram.

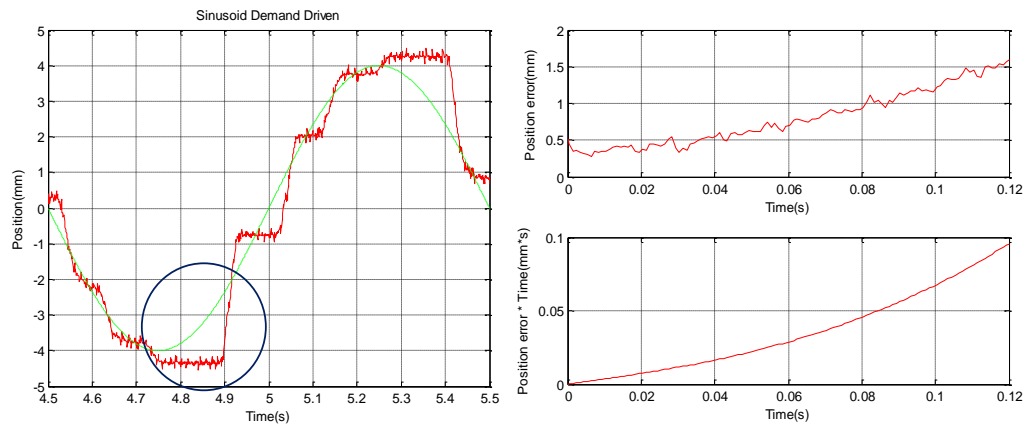


Figure 3.24 Investigating the value of *error-time factor* using sinusoid demand.

With a sinusoidal demand, there is a continually changing position error giving a changing flow rate. As Figure 3.24 shows, if e_p is integrated during the time period when the piston is stalled, the resulting *error-time integral* is 0.09 mms, which is quite similar to the theoretical value.

3.4 Conclusions

A small-sized, hydraulic actuated bipedal hopping robot, BBH1, is described in this chapter. The telescopic type of the leg provides a platform to investigate a novel compliant hydraulic actuator and develop motion controllers. An electro-hydraulic actuation system is used to power the legs. Displacements and pressures – from which forces can be estimated – are measured by the sensory system. A real-time xPC control system enables onboard data acquisition and controller implementation.

The study of this compliant hydraulic actuator for BBH1 has been undertaken in this chapter. A PI controller is used to achieve the position feedback control of the actuator. The non-linear simulation model is successfully developed to explain the main findings of the experimental results, such as the hysteresis in the valve and the friction in the actuator. In particular, an *error-time integral* is used to link the friction effect with system compliance. The quantified analysis of *error-time integral* could help with selecting appropriate components for this application. Moreover, the analysis indicates that in order to reduce the tracking error caused by friction, the options are to:

- Reduce the friction level. In reality, the friction comes from elastomeric seals around the piston head and rod gland, and lower friction is associated with greater leakage.
- Increase hydraulic elastance. The increase of the hydraulic elastance means the increase of system spring stiffness i.e. loss of actuator compliance.

A sensible design approach is to identify the friction level first and then investigate the *error-time integral* to estimate the maximum compliance that is achievable. If

this is not high enough, then another approach to incorporating compliance, i.e. not through hydraulic means, needs to be found.

As a consequence of the friction investigation in this chapter, the BBH2 was developed with a mechanical extension coil spring to provide leg compliance instead of an accumulator, i.e. an articulated type of robot leg is designed. A detailed description of the BBH2 and the corresponding controller development will be given in the next chapters.

4 BBH2 robot

This chapter describes the second prototype of the bipedal hopping robot, namely, the BBH2. This robot has a similar upper body as the BHH1, but an articulated type of leg. This chapter starts with an introduction of the mechanical structure of the BBH2, accompanied by a kinematic transformation calculation of the spring displacement. The description of the hardware implementation, e.g. the actuators and sensors, is the same as described in section 3.1. The next section provides the modelling of the robot, with some essential changes due to the different hydraulic circuit arrangement. In the last section, the bench tests have been undertaken to examine the efficacy of the mechanical design of this robot.

4.1 Mechanical design

A sketch of the BBH2 robot is shown in Figure 4.1. The articulated type of leg is composed of three links:

- The 1st link: a hydraulic actuator, named leg actuator, is placed in parallel with the ‘*thigh*’ to actuate the knee joint.
- The 2nd link: an extension coil spring is mounted in parallel with the ‘*shank*’ to provide the leg compliance.
- The 3rd link: a ‘*foot*’ is used to connect the ankle joint and heel joint.

The length of the ‘*shank*’ is carefully designed so that the ‘*foot*’ is parallel to the ‘*thigh*’ when the spring is unloaded. A 3D printed rubbery foot, which is made of thermoplastic polyurethane (TPU), is attached at the end of the foot to generate sufficient horizontal friction to avoid slipping. A hip actuator is placed under the body to drive the hip joint. At the start of a test, the hip actuator position is controlled by a PI controller to give a 45° hip angle, plus the leg actuator is initially controlled to mid-stroke, resulting in the body’s Centre of Mass (CoM) being aligned with the foot tip, vertically. The main dimensional specifications of the

BBH2 are summarized in Table 4.1. The hydraulic circuit of one of three valve-actuator pairs is shown in Figure 4.2.

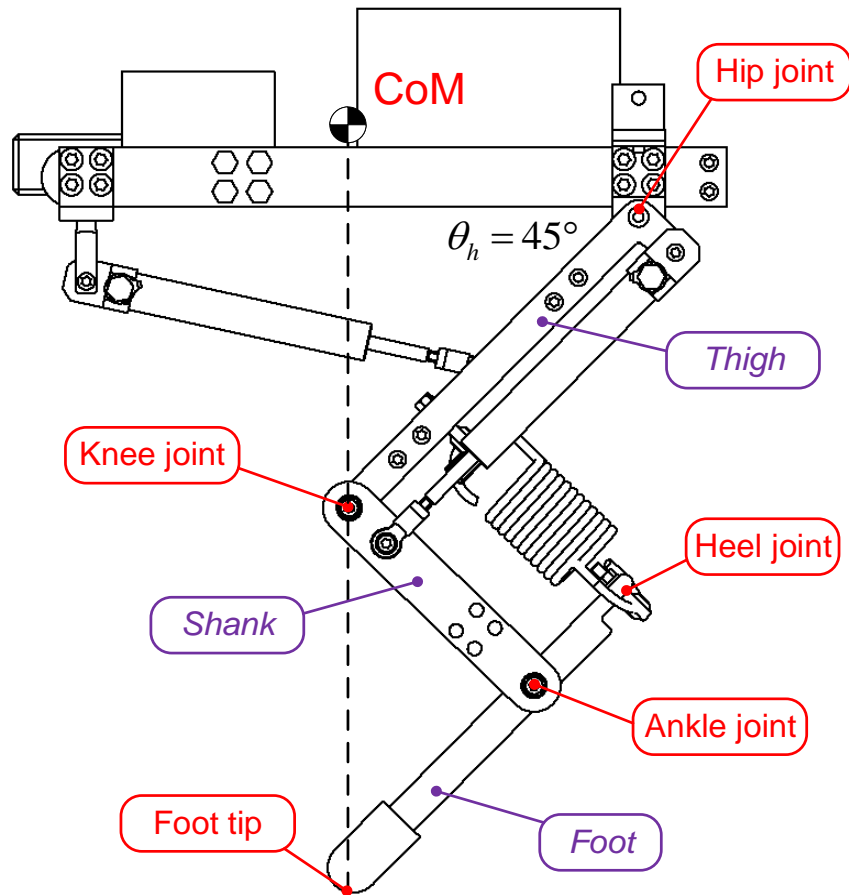


Figure 4.1 Sketch of the BBH2 robot.

Table 4.1 Main dimensional specifications of BBH2.

Height:	552 mm
Length:	400 mm
Width:	315 mm
Weight:	16.8 kg

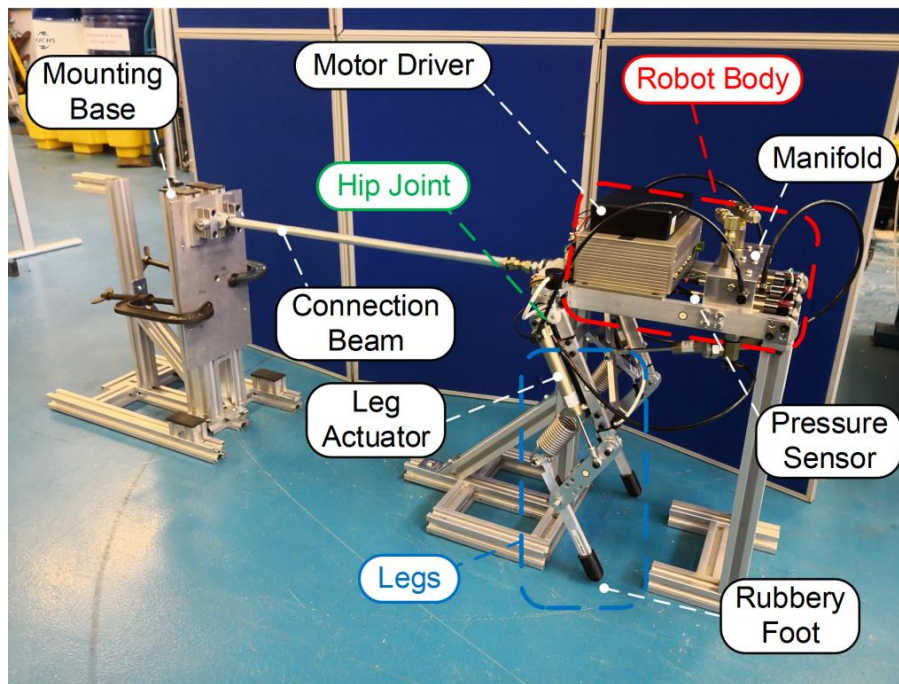


Figure 4.3 The BBH2 robot (showing with a mechanical constraint).

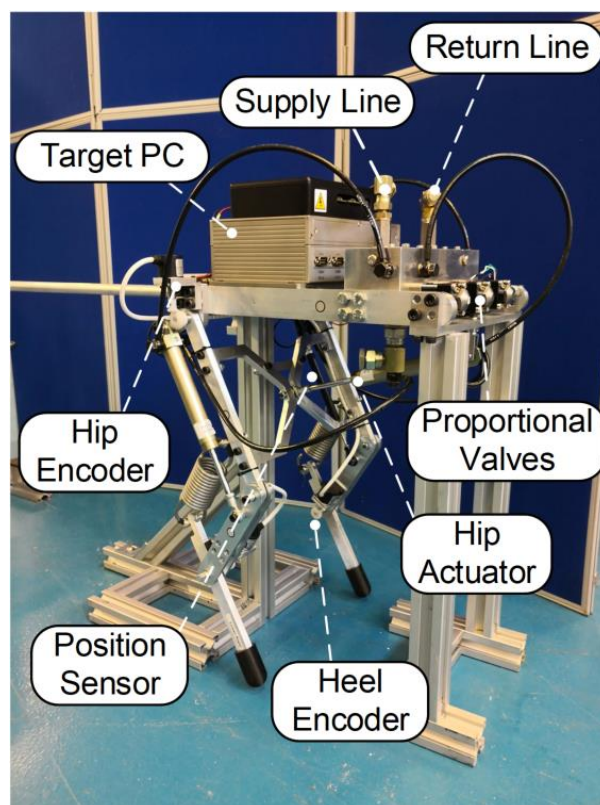


Figure 4.4 The BBH2 robot (showing a close-up view).

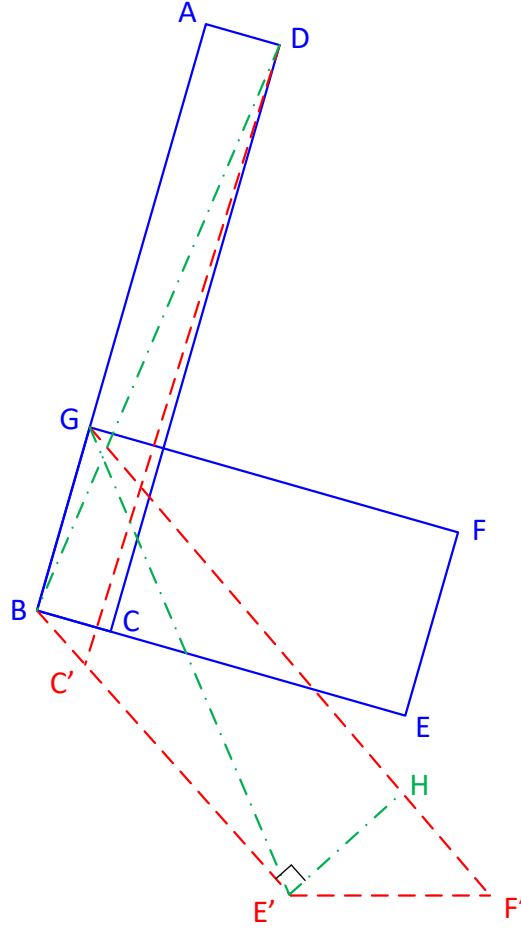


Figure 4.5 Simplified sketch of the robot leg.

For BBH2, the spring displacement can be calculated using a kinematic transformation. Figure 4.5 shows a simplified sketch of the robot leg. The blue lines represent the leg initial structure, the red lines represent the structure after deformation and the green lines are the auxiliary lines. Additionally, l_{DC} is the leg actuator length and l_{GF} is the spring length.

Some of the dimensions of the rigid bodies are known, i.e. $l_{AD} = l_{BC} = l_{BC'} = 30$ mm, $l_{AB} = l_{DC} = l_{DC'} = 240$ mm, $l_{BG} = l_{EF} = l_{EF'} = 75$ mm and $l_{GF} = l_{BE} = l_{BE'} = 150$ mm. Define $\varepsilon = l_{DC} - l_{DC'}$ is the measurement of the position potentiometer, $\alpha = \angle HE'F'$ is the measurement of the incremental encoder. Therefore,

$$\theta = \angle ABE' = \tan^{-1} \left(\frac{l_{AD}}{l_{AB}} \right) + \cos^{-1} \left(\frac{l_{AD}^2 + (l_{AD}^2 + l_{AB}^2) - (l_{AB} + \varepsilon)^2}{2l_{AD}\sqrt{l_{AD}^2 + l_{AB}^2}} \right) \quad (4-1)$$

$$l_{GE'} = \sqrt{l_{BG}^2 + l_{BE}^2 - 2l_{BG}l_{BE} \cos \theta} \quad (4-2)$$

$$\beta = \angle GE'B = \cos^{-1} \left(\frac{l_{BE}^2 + l_{GE'}^2 - l_{BG}^2}{2l_{BE}l_{GE'}} \right) \quad (4-3)$$

$$l_{GF'} = \sqrt{l_{GE'}^2 + l_{BG}^2 - 2l_{GE'}l_{BG} \cos(\angle BE'H - \beta + \alpha)} \quad (4-4)$$

Combining equations 4-1, 4-2, 4-3 and 4-4, gives the spring displacement, $l_s = l_{GF'} - l_{GF}$. This kinematics transformation runs in real-time as an indication of the hopping motion. The implementation of this kinematics transformation is presented in Chapter 7 and Chapter 8, respectively.

4.2 Modelling of the BBH2 robot

This section summaries the modelling of the BBH2 robot, which is similar to the modelling procedure of the BBH1. The notation of the variables used for both robots will not be distinguished, e.g. A_p is the full piston area of the actuator and P_c is the full piston side pressure of the cylinder, etc. However, a more complicated mechanical model will be built using SimMechanics[®], a multi-body mechanical simulation tool in the Simulink[®].

4.2.1 Hydraulic models

As shown in Figure 4.2, since there is no accumulator connected between the cylinder and the valve, the significant changes when modelling the hydraulic system of the BBH2 is that valve outlet flow, Q_v , is directly delivered into the full piston chamber of the cylinder, with a correction for oil compressibility and hose expansion.

The actuator model is given by:

$$P_c A_p - P_s A_a - F_f = F_h \quad (4-5)$$

$$Q_v = A_p \dot{y} + \frac{V_t}{B} \dot{P}_c \quad (4-6)$$

where V_t is the trapped oil volume and B is the effective bulk modulus of the oil which includes hose expansion stiffness.

The valve model is given by:

$$Q_v = K_v X \sqrt{P_s - P_v} \quad (4-7)$$

where P_v is the outlet pressure of the valve.

The hose pressure loss model is given by:

$$Q_v = K_h \sqrt{P_v - P_c} \quad (4-8)$$

4.2.2 Mechanical model

The mechanical properties of the rigid bodies are defined in Autodesk Inventor 2017[®], then uploaded to SimMechanics[®] to create a 3D visualization. The top-level of the mechanical model of BBH2 is shown in Figure 4.6. Only the prismatic primitive is considered when modelling the motion between the actuator piston and cylinder since the piston revolute degree of freedom is constrained by the rod end mounting. Moreover, it is assumed that hip joint friction can be neglected due to the application of low-friction ball bearings.

A ‘spring and damper force’ block is used to represent the spring force between the connections on the *thigh* and *foot*, which is shown in Figure 4.7. Note that the damping force is effectively small according to the manufacturing data.

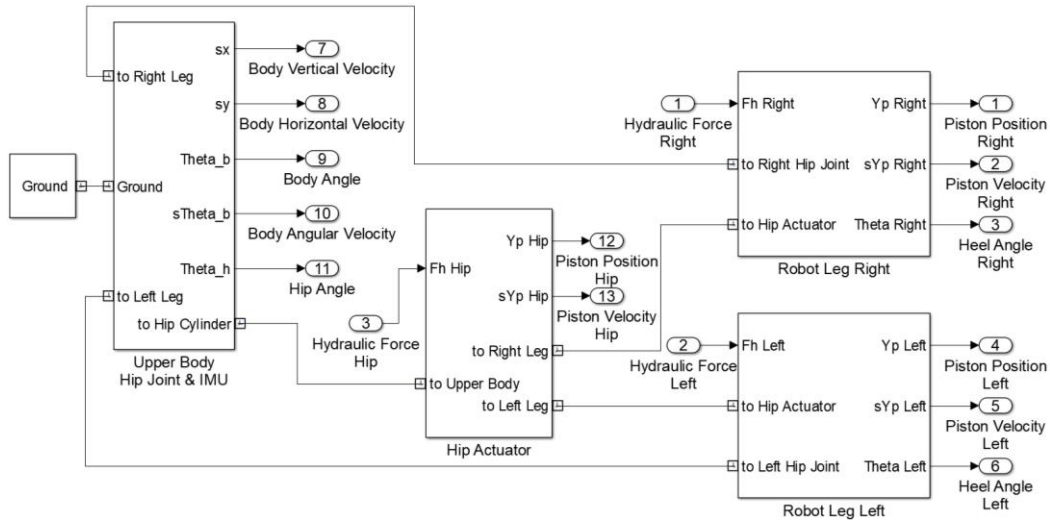


Figure 4.6 Top-level of the mechanical model.

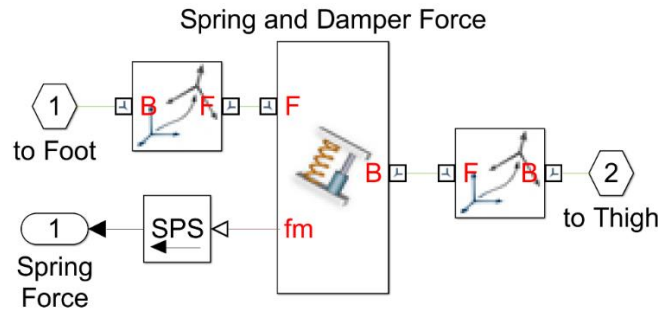


Figure 4.7 Spring and damper model.

Modelling ground contact is an important issue. The reaction force from the ground should support the robot vertically (y-axis) and prevent horizontal foot slip (z-axis) during stance. The other horizontal axis (x-axis) is not relevant as we only consider the planar motion. Define the coordinate of the robot foot as $(0, y_n, z_t)$, and the initial contact point on the ground is $(0, 0, 0)$. The ground reaction force is modelled as a spring and damper both vertically and horizontally. The ground stiffness is relatively large so as not significantly reduce the effective robot leg's stiffness. Thus, the vertical reaction force and the horizontal friction force are given by:

$$F_y = \begin{cases} -k_y y_n - b_y \dot{y}_n & \text{for stance phase} \\ 0 & \text{for flight phase} \end{cases} \quad (4-9)$$

$$F_z = \begin{cases} -k_z z_t - b_z \dot{z}_t & \text{for stance phase} \\ 0 & \text{for flight phase} \end{cases} \quad (4-10)$$

where F_y is the vertical reaction force, k_y is the ground normal spring stiffness and b_y is the ground normal damping coefficient. F_z is the horizontal friction force, k_z is the tangential spring stiffness and b_z is the tangential damping coefficient. Note that F_y is constrained to be a positive value to prevent the robot foot from being stuck when lifting off.

4.2.3 3D visualised model

Integrating the hydraulic models and mechanical model developed above, plus the numerical solution is performed by a stiff/Mod.Rosenbrock solver (Simulink's ODE23s) with variable step size, which is a compromise between the computing speed and the simulation accuracy, the 3D visualised model is shown in Figure 4.8.

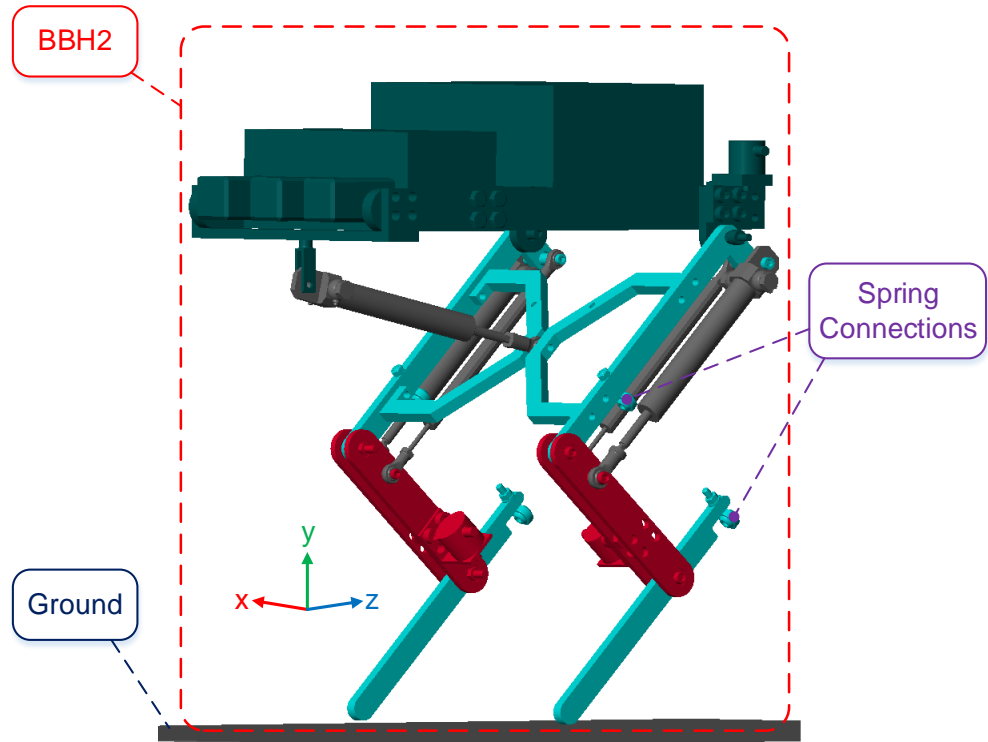


Figure 4.8 3D visualisation of BBH2.

4.3 Bench test results and analysis

The bench tests have been undertaken from two aspects, a simple closed loop position control of the leg actuator and a sinusoid excited hopping to examine the mechanical design.

4.3.1 Leg actuator position tracking performance

For BBH2, the experimental results are shown in Figure 4.9. The piston is tracking the demand position poorly, which is related to the hysteresis in the proportional valve. Dither, a high-frequency sinusoidal signal with low amplitude, is added to the driving signal of the valve to overcome the hysteresis effect. The improved position tracking performance with dither (10% of the maximum amplitude of the valve driving signal at 120 Hz frequency) is shown in Figure 4.10.

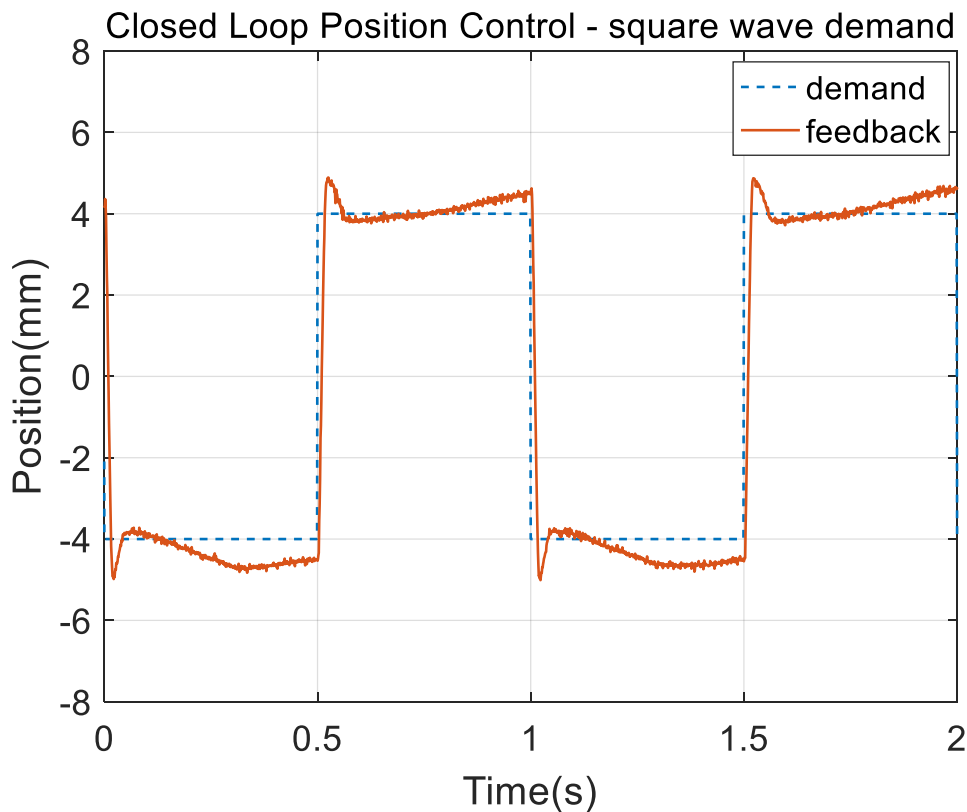


Figure 4.9 Closed loop position control of the leg actuator, using square wave demand (BBH2).

In Figure 4.10, the dither signal can be clearly seen in the collected control signal. Adding the dither is a compromise decision to improve the system performance since the consequent valve spool oscillation generates extra heat which requires efficient cooling and limits the testing time.

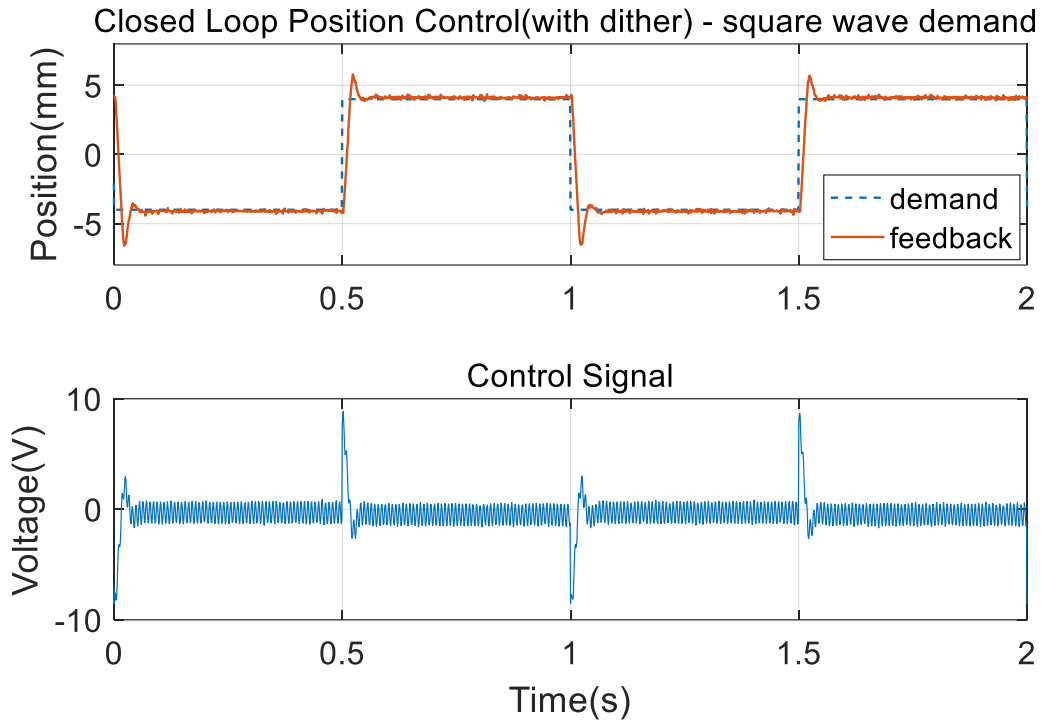


Figure 4.10 Closed loop position control of the leg actuator, using square wave demand, with dither (BBH2).

Additionally, the two leg actuator displacements are synchronised using a ‘Coordinated Controller’, as shown in Figure 4.11. This controls the mean of the leg actuator positions and the corresponding difference, which are called the vertical (or average) position (y_a) and roll position (y_r), respectively. If the demand roll position is zero, the two leg actuator displacements are synchronised. This average leg actuator position will be considered the output variable from now on. Figure 4.12 shows the closed loop position tracking performance using the ‘Coordinated Controller’.

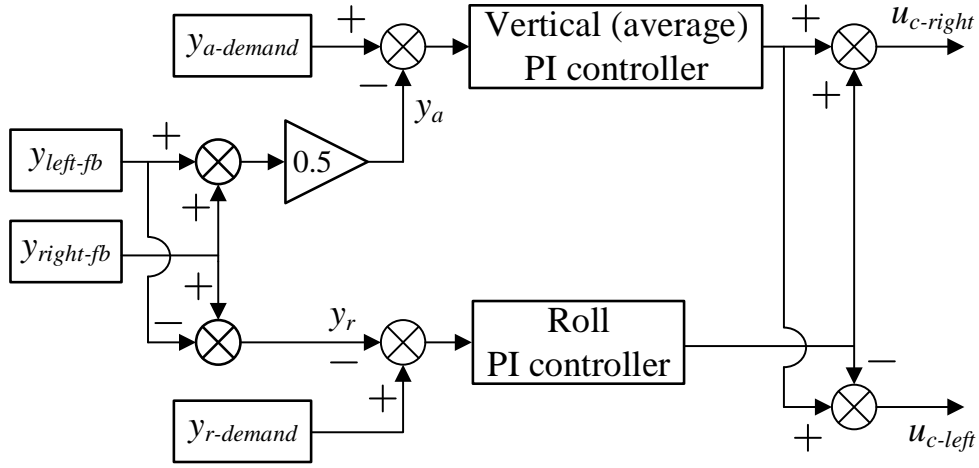


Figure 4.11 Structure of the ‘Coordinated Controller’.

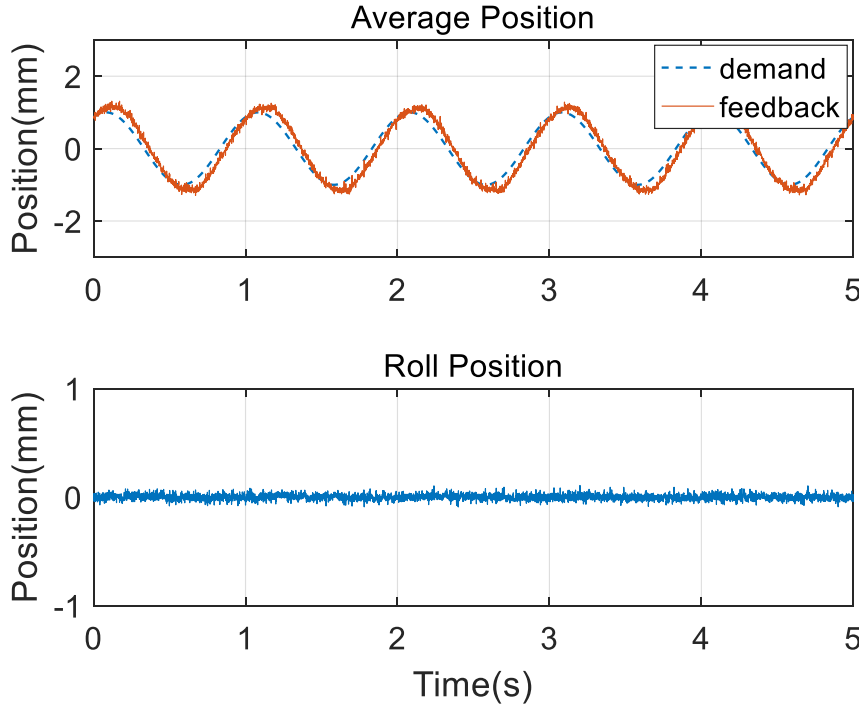


Figure 4.12 Closed loop position control of the leg actuators, using ‘Coordinated Controller’ (BBH2).

4.3.2 Sinusoid excited hopping

The simplified model of BBH is an actuated spring-loaded inverted pendulum (SLIP) model which is able to achieve resonant bouncing/hopping with a sinusoidal or other cyclic signal excitation (Raibert, 1986). Therefore, sinusoidal vertical position demand signals (2 mm amplitude at varying frequencies) are used

to excite the leg actuators to investigate whether hopping is achieved. BBH2 experimental results are shown from Figure 4.13 to Figure 4.15.

Figure 4.13 shows that the leg actuators are tracking the demand well and the spring displacement, l_s is larger than zero, i.e. there is no foot lift-off. Figure 4.14 shows that the robot is hopping momentarily. It can be seen that the system is reaching the ‘beat frequency’ when the 2 Hz excitation signal interferes with the robot resonant frequency, 3 Hz. The consistent spring displacement in Figure 4.15 shows that BBH2 is hopping at a 3 Hz frequency. Moreover, the large roll position error is mainly caused by different friction conditions at each foot touch down.

This series of bench test demonstrates the efficacy of the mechanical design of BBH2, so future controller tests can take place using this platform.

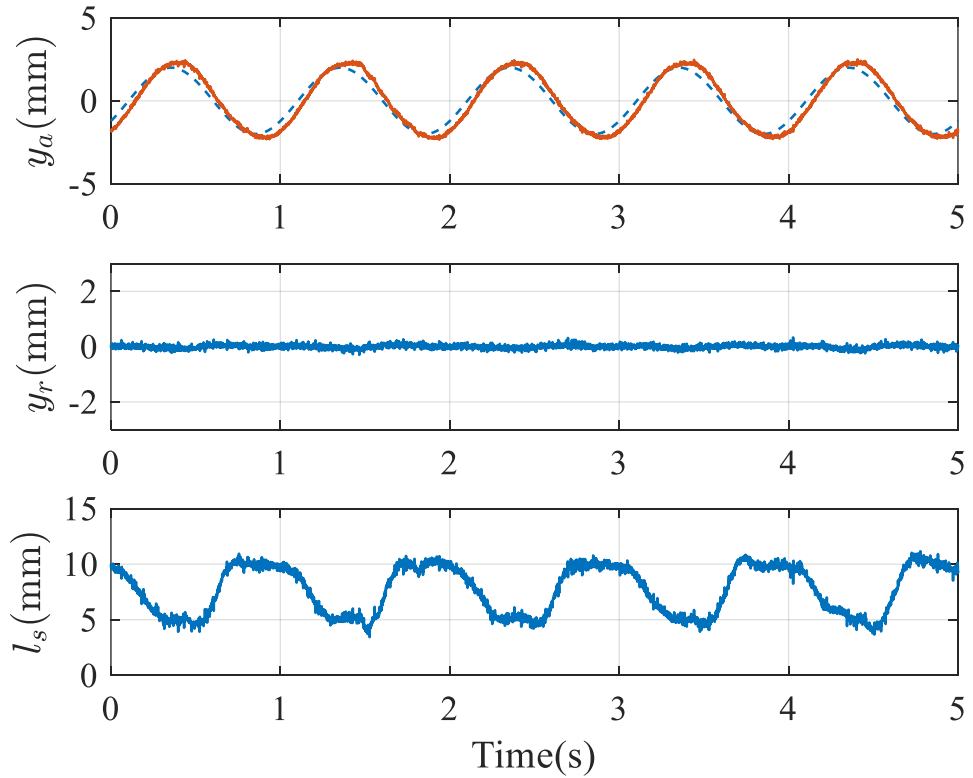


Figure 4.13 1 Hz sinusoid signal excitation.

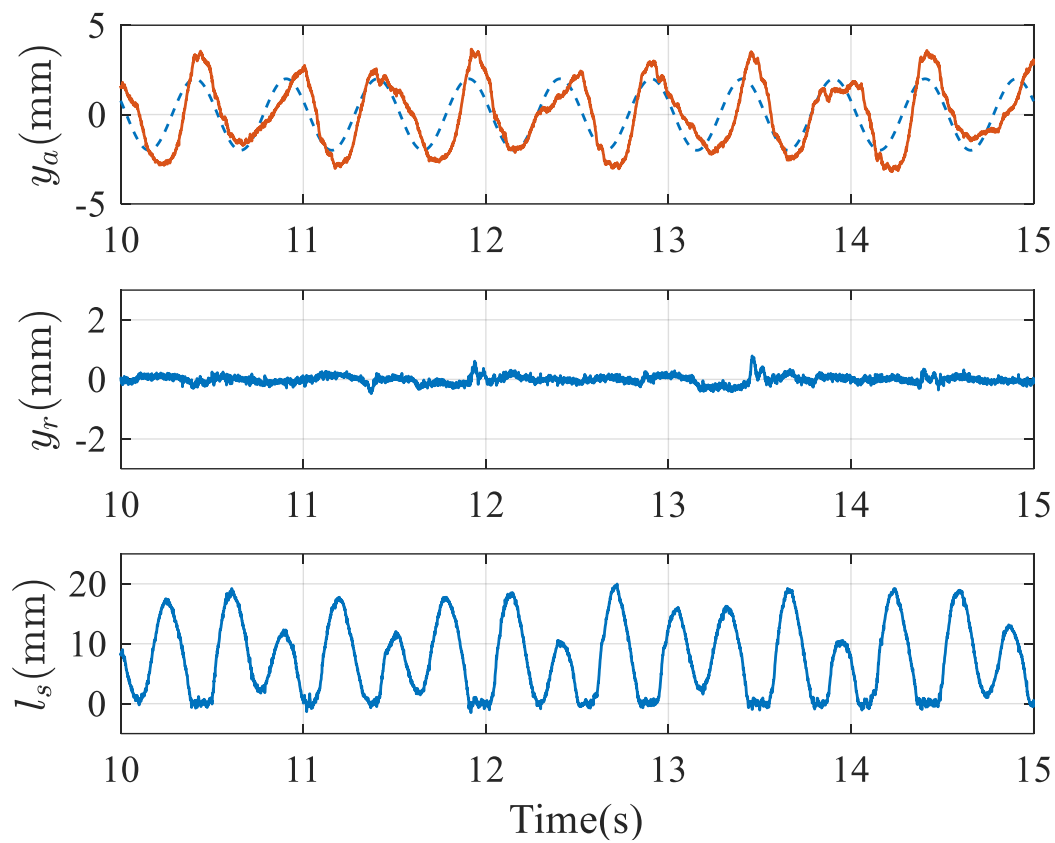


Figure 4.14 2 Hz sinusoid signal excitation.

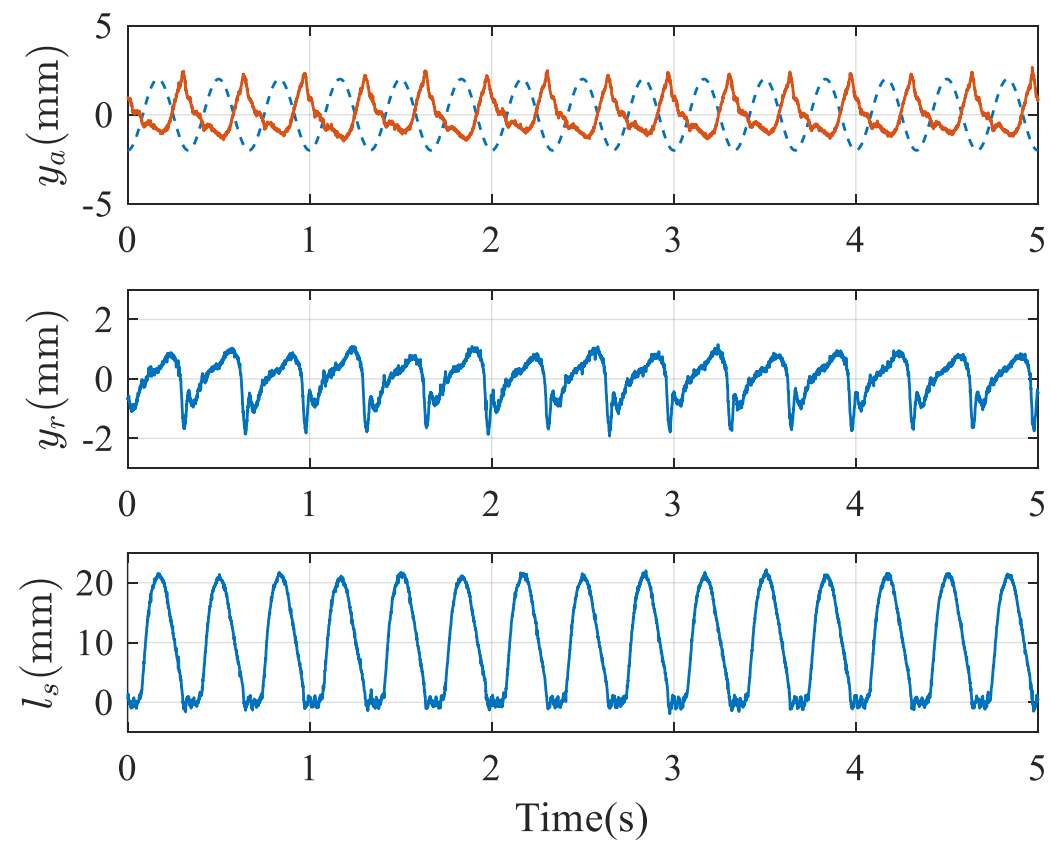


Figure 4.15 3 Hz sinusoid signal excitation.

4.4 Conclusions

The BBH2 robot is described in this chapter. It is designed and built using a similar upper body as the BBH1, but an articulated type of leg, which takes advantage of the mechanical compliance provided by coil spring. The modelling of BBH2 is undertaken, which has the same procedures as described in the last chapter. These detailed non-linear simulation models aim to provide a better explanation of the findings from the experiments. The use of Inventor 2017[®] with SimMechanics[®] provides a time-effective method to have an accurate mechanical model. It is found that the simulation solver needs to be carefully selected, especially when the modelling complexity increases. During the bench test of BBH2, dither is used to overcome the hysteresis effect of the proportional valve. A ‘Coordinated Controller’ is implemented to successfully synchronise the movement of two leg actuators. The BBH2 hardware refinement is promising since hopping is successfully achieved using sinusoidal actuator position demand signals at the robot’s resonant frequency.

5 Motion control

This chapter presents the research of motion control for bipedal hopping robot, e.g. balancing control while the robot is in a standing position, vertical hopping height control and balancing control while the robot is hopping. The main contents are summarised from three research papers, which the details are included in appendix.

5.1 Balancing control while standing

5.1.1 Introduction

For bipedal robots, static balancing, i.e. at the standing position, is easy to achieve if there is a sufficient foot contact area. A small foot supporting area can increase the capability of traversing through rough or uneven terrain. However, it is challenging to maintain balance when this contact area is small. A generic model of the standing position for BBH1 and BBH2 is a modified double inverted pendulum model, of which the foot is pivoted on the ground and only one actuation at the hip joint is considered. Rather than control the upper body towards a so-called balanced position, it is possible to keep the combined centre of mass (CoM) align with the foot, vertically. This concept results in complex system characteristics and a suitable control method is needed, e.g. pole-placement control method.

5.1.2 Modelling

The inverted pendulum model has been successfully used to help design one-leg hopping robots (Kajita, 1989). A modified double inverted pendulum model is appropriate to analyse the motion of the BBH. As shown in Fig. 3, the model consists of two rigid bodies, an upper body and a lower body (representing the leg-pair), connected with revolute joint 1 (hip joint). The bottom of the lower body, i.e. the foot is connected to the ground using revolute joint 2 in the model. Using small angle approximations, we are trying to maintain the combined centre of mass

(CoM) of the overall model vertically above revolute joint 2 by applying an active torque at revolute joint 1.

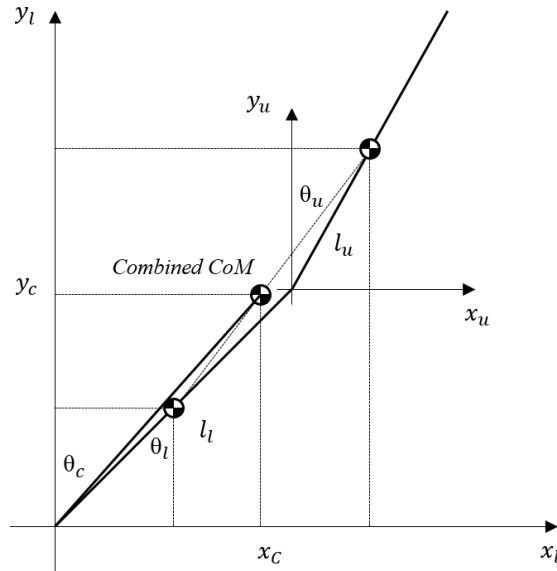


Figure 5.1 The modified double inverted pendulum model.

According to a detailed force analysis using free body diagram, the plant model is given by:

$$\frac{\theta_c}{T_{act}} = \frac{3k_2k_{l1}s^2 + 3k_lk_{u3} + 3k_2k_{l2}}{4k_{u1}k_{l1}s^4 + (k_{l1}k_{u2} + 4k_{u1}k_{l2})s^2 + k_{u2}k_{l2}} \quad (5-1)$$

where $k_{u1} = 4M_u l_u^2$, $k_{u2} = 3M_u g l_u$, $k_{u3} = M_u l_u$, $k_{l1} = \frac{1}{3}M_l l_l - M_u l_l$ and

$$k_{l2} = M_u g + \frac{1}{2}M_l g .$$

5.1.3 Controller design

According to the plant model, the pole-placement method can be used to develop the controller. The closed-loop block diagram is shown in Figure 5.2. The controller is implemented using two digital filters, $1/F(s)$ and $G(s)$, where $1/F(s)$ is a forward path compensator and $G(s)$ plays the same role as the state feedback gains in a state-feedback controller.

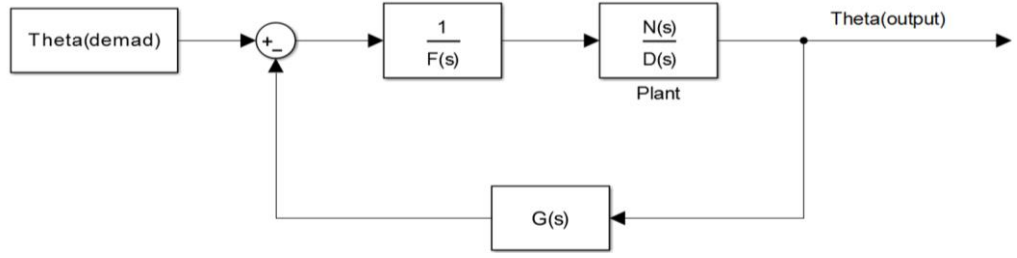


Figure 5.2 Block diagram of pole placement controller.

The closed-loop transfer function of the block diagram is:

$$\frac{\theta_c}{\theta_d} = \frac{N(s)}{D(s)F(s) + N(s)G(s)} \quad (5-2)$$

If,

$$A(s) = D(s)F(s) + N(s)G(s) \quad (5-3)$$

Then,

$$\frac{\theta_c}{\theta_d} = \frac{N(s)}{A(s)} \quad (5-4)$$

The roots of polynomial $A(s)$ indicate the stability and the time domain response of the whole system. By specifying different polynomials of $G(s)$ and $F(s)$, the roots of $A(s)$ can be arranged at any desired positions. According to the plant model:

$$N(s) = n_2s^2 + n_0 \quad (5-5)$$

$$D(s) = d_4s^4 + d_2s^2 + d_0 \quad (5-6)$$

It is necessary to have the same number of equations and unknowns, which determines the degrees of polynomials $G(s)$ and $F(s)$ (Plummer, A. R. 1991).

Define n and m as the degree of $G(s)$ and $F(s)$, respectively. Using,

$$\deg F(s) = n - 1 = 1 \quad (5-7)$$

$$\deg G(s) = m - 1 = 3 \quad (5-8)$$

$$\deg A(s) = n + m - 1 = 5 \quad (5-9)$$

Therefore,

$$F(s) = f_1 s + f_0 \quad (5-10)$$

$$G(s) = g_3 s^3 + g_2 s^2 + g_1 s + g_0 \quad (5-11)$$

$$A(s) = a_5 s^5 + a_4 s^4 + a_3 s^3 + a_2 s^2 + a_1 s + a_0 \quad (5-12)$$

The coefficients in $G(s)$ and $F(s)$ can be calculated by solving Equation 5-13 with polynomials as given in equations 5-5, 5-6, 5-10, 5-11 and 5-12, i.e. solving the following matrix equation:

$$\begin{bmatrix} a_5 \\ a_4 \\ a_3 \\ a_2 \\ a_1 \\ a_0 \end{bmatrix} = \begin{bmatrix} d_4 & 0 & n_2 & 0 & 0 & 0 \\ 0 & d_4 & 0 & n_2 & 0 & 0 \\ d_2 & 0 & n_0 & 0 & n_2 & 0 \\ 0 & d_2 & 0 & n_0 & 0 & n_2 \\ d_0 & 0 & 0 & 0 & n_0 & 0 \\ 0 & d_0 & 0 & 0 & 0 & n_0 \end{bmatrix} \times \begin{bmatrix} f_1 \\ f_0 \\ g_3 \\ g_2 \\ g_1 \\ g_0 \end{bmatrix} \quad (5-13)$$

$A(s)$ will be chosen as the denominator of a fifth-order Butterworth filter. A Butterworth filter has a flat frequency response in the passband. Therefore, determining the vector of $G(s)$ and $F(s)$ coefficients gives a controller achieving these desired closed-loop poles. A simple simulation test can be done by using the physical configuration parameters of the BBH, as Table 5.1 shows. Figure 5.3 shows the step response with these parameters. With a higher cut-off frequency, the system presents a faster step response (as expected) and acceptable overshoot. However, in SimMechanics®, in order to avoid breaking down the structure, the cut-off frequency of the desired polynomial should be selected appropriately to compromise between the step response time and the overshoot.

Table 5.1 Physical parameters.

Parameters	Symbol	Value	Unit
Mass of the upper body	M_u	7.5	kg
Mass of the lower leg	M_l	0.75	kg
Length of the upper body	l_u	44.4	mm
Length of the lower leg	l_l	95	mm
Gravitational acceleration	g	9.81	m/s ²

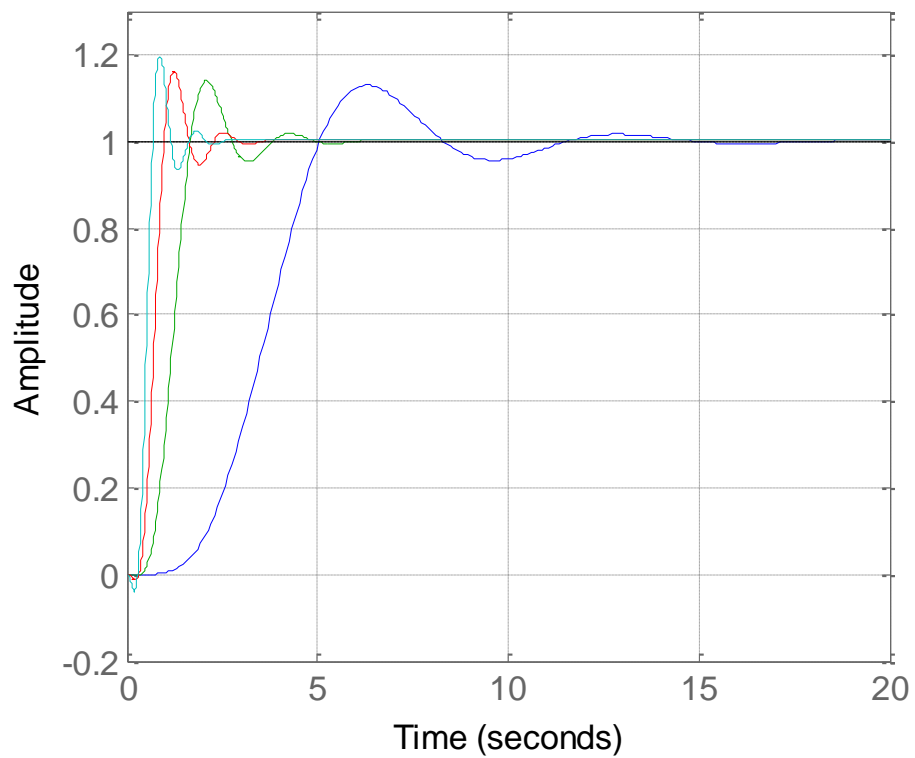


Figure 5.3 Step response with closed-loop poles for cut-off frequencies of 7 rad/s, 5 rad/s, 3 rad/s and 1 rad/s..

5.1.4 Evaluation of the controller

5.1.4.1 Minimize the jerk gain

There are four unknowns in $G(s)$, which are the feedback gains related to the output angle, angular velocity, angular acceleration and the derivative of angular acceleration, also named the jerk. It is necessary to minimize the jerk gain, or even

make it as zero, because of the noise caused by derivative calculations. By setting the jerk gain as zero, $G(s)$ is going to be a second-order polynomial and $F(s)$ can be a constant value. Such as:

$$F(s) = f_0 \quad (5-14)$$

$$G(s) = g_2 s^2 + g_1 s + g_0 \quad (5-15)$$

Additionally, $A(s)$ should be a fourth-order polynomial, which is:

$$A(s) = a_4 s^4 + a_3 s^3 + a_2 s^2 + a_1 s + a_0 \quad (5-16)$$

Then, there will be four unknowns in five equations, which will not give a minimal degree of the solution. In order to solve this set of equations, an extra unknown τ can be introduced by setting the $A(s)$ as:

$$A(s) = (\tau s + 1)(a_{m3} s^3 + a_{m2} s^2 + a_{m1} s + a_{m0}) \quad (5-17)$$

Combining Equations 5-5, 5-6, 5-7, 5-14, 5-15 and 5-17 gives:

$$\begin{bmatrix} 0 \\ a_{m3} \\ a_{m2} \\ a_{m1} \\ a_{m0} \end{bmatrix} = \begin{bmatrix} d_4 & n_2 & 0 & 0 & -a_{m3} \\ 0 & 0 & n_2 & 0 & -a_{m2} \\ d_2 & n_0 & 0 & n_2 & -a_{m1} \\ 0 & 0 & n_0 & 0 & -a_{m0} \\ d_0 & 0 & 0 & n_0 & 0 \end{bmatrix} \times \begin{bmatrix} f_0 \\ g_2 \\ g_1 \\ g_0 \\ \tau \end{bmatrix} \quad (5-18)$$

As in the last section, this can be solved for the $G(s)$ and $F(s)$ coefficients and the extra unknown τ . However, τ needs to be evaluated to ensure that it is always a positive value, which means it is a stable pole position. τ can be calculated from Equation 5-18, which for the plant parameters in Table 5.1, gives:

$$\tau = -\frac{a_{m1}}{a_{m0} + 0.0095a_{m2}} - \frac{a_{m3}}{105.1349a_{m0} + a_{m2}} \quad (5-19)$$

$A(s)$ is specified to represent stable poles, as a result, a_{m0} , a_{m1} , a_{m2} and a_{m3} are positive values. According to Equation 5-19, τ is always negative. In other words, a pole in $A(s)$ is always placed in the right half plane, so the closed-loop system is

not stable. Therefore, the jerk feedback cannot be cancelled or avoided in the controller.

5.1.4.2 Noise tolerance

Rather than simply attempting to avoid using jerk feedback, a more general approach to reducing the effect of noisy feedback signals on control performance is considered in this section. As Figure 5.4 shows, by including $H(s)$ as a command filter, Equation 5-20, 5-21 and 5-22 indicate that the reciprocal of $H(s)$ can be used as a low pass filter within the closed loop controller to attenuate the noise without altering the response of the whole system.

$$y = \frac{N(s)H(s)}{D(s)F(s) + N(s)G(s)} r + \frac{D(s)F(s)}{D(s)F(s) + N(s)G(s)} e \quad (5-20)$$

If,

$$D(s)F(s) + N(s)G(s) = A_m(s)H(s) \quad (5-21)$$

Substituting 5-21 into 5-20:

$$y = \frac{N(s)}{A_m(s)} r + \frac{D(s)F(s)}{A_m(s)H(s)} e \quad (5-22)$$

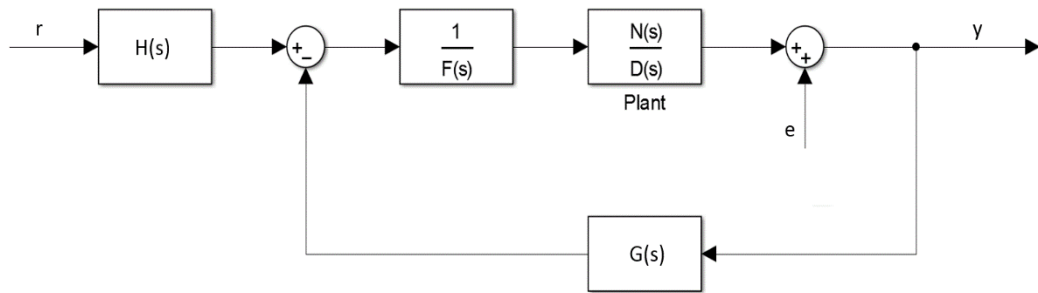


Figure 5.4 Closed-loop block diagram with $H(s)$ filter.

Here, e is measurement noise. According to the previous discussion, $A_m(s)H(s)$ can be given by a polynomial with desired stable poles, and the steady-state gain is calculated to give unity gain in the closed loop. If $H(s)$ is specified as the denominator of a second-order low-pass filter, which includes two roots of the full

characteristic polynomial $A(s)$, it can be used to attenuate the noise without influencing the servo performance of the system. In order to give a unity steady state gain:

$$N(0) = A_m(0) \quad (5-23)$$

However, it is necessary to evaluate how the noise is affected by using different $H(s)$. Figure 5.5 is the noise amplitude against frequency according to different $H(s)$. Here $A_m(s)$ has the poles of a third order Butterworth filter with cut-off frequency. As the cut-off frequency of $H(s)$ reduces, noise above 2Hz is increasingly attenuated, at the expense of low-frequency noise amplification. However, another aspect also needs to be investigated which is the sensitivity of the control signal to noise, as Figure 5.6 shows.

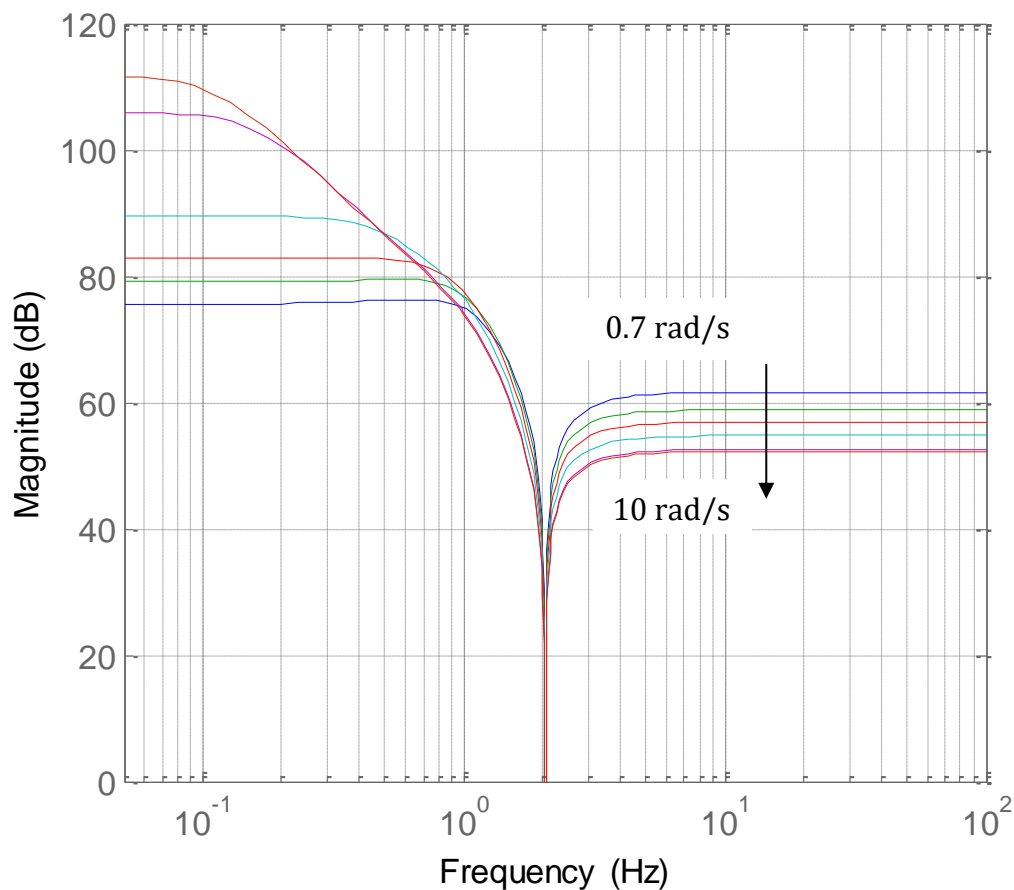


Figure 5.5 Frequency response of output angle (y) over noise (e) for different cut-off frequency of $H(s)$, as 0.7 rad/s, 1 rad/s, 3 rad/s, 5 rad/s, 7 rad/s and 10 rad/s.

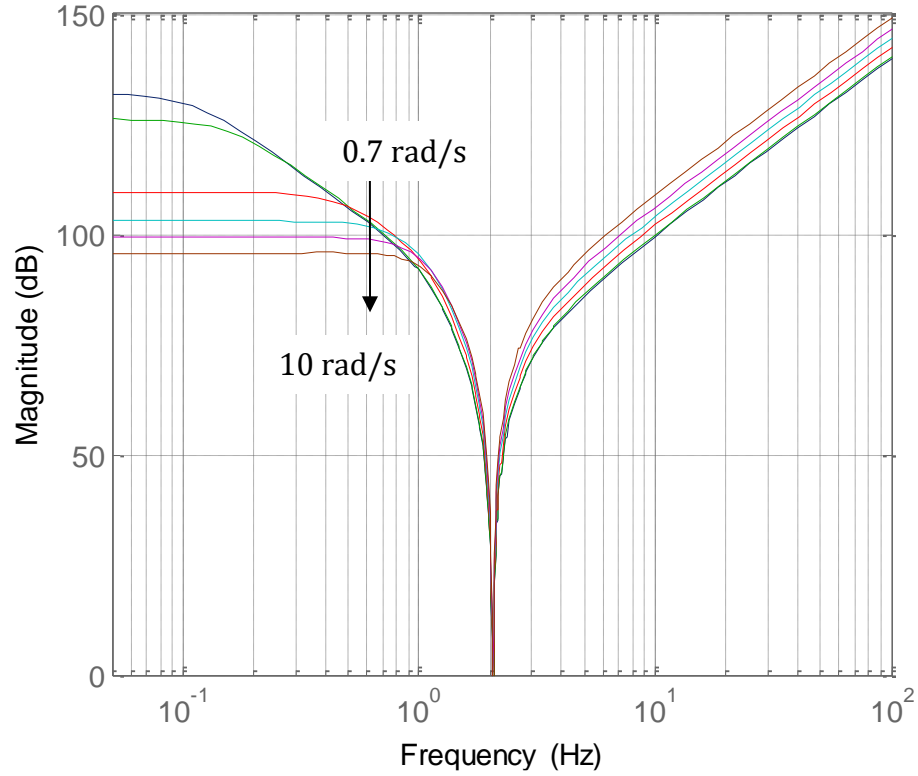


Figure 5.6 Frequency response of control signal (u) over noise (e) for different cut-off frequency of $H(s)$, as 0.7 rad/s, 1 rad/s, 3 rad/s, 5 rad/s, 7 rad/s and 10 rad/s.

At high frequencies, the noise amplification is increasing dramatically, but it is lower with $H(s)$ which has a lower cut-off frequency. This might be caused by the unstable $D(s)$. These results are influenced by pole selection, which is discussed further in (Chen, 1995).

5.1.5 Summary

This section presents the development of a balancing controller for the BBH in a standing position. The controller is developed using a pole-placement control method and investigated via simulation. The calculation results indicate that up to a third-order motion derivative is required, i.e. jerk. The potential high-frequency noise issues when sensing the state variables in practice can be handled using a command filter without influencing the servo performance of the controller. Another promising way to obtain the ‘jerk’ without requiring differentiation of measured signals is to build a state estimator or observer. The performance of this estimator or observer needs to be studied carefully in future research.

5.2 Vertical hopping height control

5.2.1 Introduction

For legged hopping robots, vertical hopping control can be investigated before the dynamic balancing issues are considered by constraining movement to be in the vertical direction. According to the reviewed literature in Chapter 2, most hopping height controllers require detection of ground contact to enable different control actions to handle the rapid change of system characteristics between the flight and stance phases. This transition can be provided either mechanically or electrically. Moreover, several state variables usually need to be measured, e.g. the actual body position, and the corresponding velocity or acceleration. This section presents a novel hopping height controller that significantly reduces the number of measured variables without the need to explicitly detect the ground contact. The conditions for self-excited hopping are theoretically derived and the method is successfully demonstrated experimentally on the BBH2 robot.

5.2.2 Control concept

5.2.2.1 Simple models

The controller development starts from analysing the motion of a spring-loaded inverted pendulum (SLIP) model, as shown in Figure 5.7.

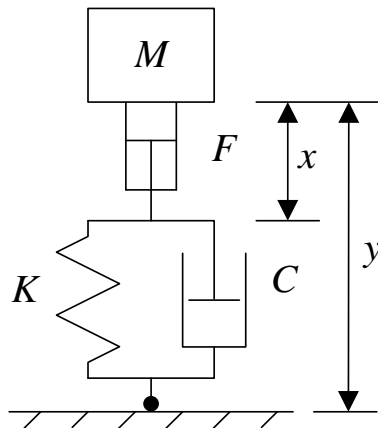


Figure 5.7 Modified SLIP model.

The equation of motion of the mass is given by:

$$M\ddot{y} = -C(\dot{y} - \dot{x}) - K(y - x) \quad (5-24)$$

where x is the actuator displacement from mid-stroke, y is the body displacement, K is the spring stiffness, C is damping coefficient and M is the body mass. Displacement y is chosen to be zero with the actuator at mid-stroke in steady state conditions.

A simple linear model of the valve and actuator is useful to understand the proposed control technique, in which a gain is used to represent the valve characteristic relating driving signal to flow rate, and the actuator position is a scaled integral of the valve flow output, which is given by:

$$x = \frac{C_x}{A_p s} u_c \quad (5-25)$$

where C_x is the valve flow coefficient, A_p is the piston area of the hydraulic actuator and u_c is the valve driving signal.

Thus, a linear model from the valve driving signal to the resultant force is given by:

$$F = \frac{C_x M s (C s + K)}{A_p (M s^2 + C s + K)} u_c \quad (5-26)$$

where F is the resultant force.

Note that C_x is derived from a linearized valve model that varies due to the actuator's working conditions. It is assumed that the pressure drop across the valve is constant, result in a constant C_x .

5.2.2.2 Controller design

A self-excited hopping controller as shown in Figure 5.8, is proposed to control the body height, y . It is composed of an outer positive force feedback loop with a saturation limit dictating the hopping height, plus a closed-loop actuator position

control loop, for which the demand is generated by the force loop. Additionally, a command velocity feedforward loop is used to improve the system response.

A first-order high pass filter is used to remove the mean value due to the weight component in the force measurement. The resultant force feedback signal can be considered as a command velocity:

$$u_d = \frac{s}{s + \omega_u} a_s \quad (5-27)$$

where u_v is the command velocity, a_s is the output of the saturation limit relating to the resultant force, and ω_u is the cut-off frequency of the high pass filter. The corresponding command position signal is given by:

$$x_d = \frac{1}{s + \omega_u} a_s \quad (5-28)$$

where x_d is the command position signal. One interpretation of this arrangement is as an impedance controller, where the impedance model relating force to motion is a damper with negative damping coefficient, thus reducing stability margins.

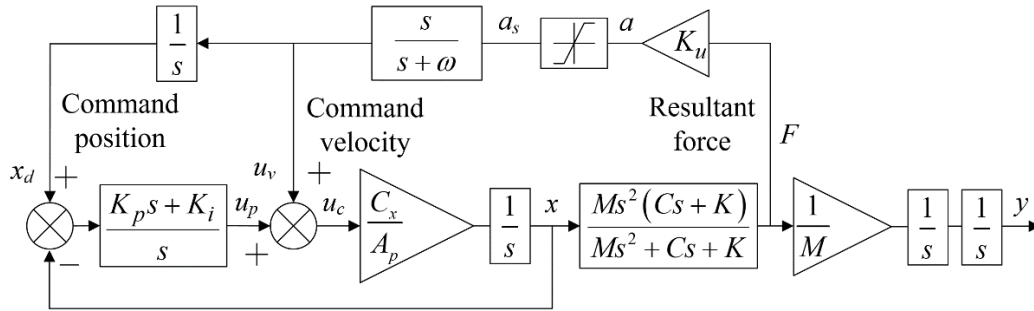


Figure 5.8 Controller structure.

A PI controller is used to achieve closed-loop position control of the actuator, as is widely used in servohydraulic:

$$u_p = K_p e + K_i \int e dt \quad (5-29)$$

where u_p is the control signal from the position loop, K_p is the proportional gain, K_i is the integral gain and e is the position error. Therefore, the valve control signal is given by:

$$u_c = u_p + u_v \quad (5-30)$$

5.2.2.3 Describing function analysis

The describing function technique can be used to analyse the controller performance as there is only one non-linear element, i.e. the saturation characteristic in the force feedback loop. Assuming a gradient of 1 in the linear region, define a sinusoid input as:

$$a(t) = A \sin \omega_a t \quad (5-31)$$

where A is the amplitude and ω_a is the frequency. Thus, the saturation output is:

$$a_s(t) = \begin{cases} -S & a(t) \leq -S \\ a(t) & -S < a(t) < S \\ S & a(t) \geq S \end{cases} \quad (5-32)$$

where S is the saturation limit.

The describing function of the saturation non-linearity is shown to be:

$$N(A) = \begin{cases} 1 & A < S \\ \frac{2}{\pi} \left[\arcsin \frac{S}{A} + \frac{S}{A} \sqrt{1 - \left(\frac{S}{A} \right)^2} \right] & A \geq S \end{cases} \quad (5-33)$$

Note that when $A \geq S$, $N(A)$ represents a variable gain which is determined by the saturation limit and is independent of the frequency of the input.

Table 5.2 Parameter values.

Variable	Symbol	Value	Unit
Mass	M	15	kg
Spring stiffness	K	4750	N/m
Damping coefficient	C	8	Ns/m
Piston area	A_p	1.13×10^{-4}	m ²

Valve coefficient	C_x	3.56×10^{-8}	L/min
Supply pressure	P_s	160×10^5	Pa
Return pressure	P_r	0	Pa
Force feedback gain	K_u	5×10^{-3}	m/N
The cut-off frequency of high pass filter	ω_u	1.885	rad/s
Proportional gain	K_p	320	1/m
Integral gain	K_i	120	1/(sm)

$$\frac{N(s)}{D(s)} = \frac{-0.503s^6 - 461s^5 - 9.658 \times 10^4 s^4 - 2.163 \times 10^5 s^3 - 6.761 \times 10^4 s^2}{15s^6 + 4092s^5 + (2.368s^4 + 133.2s^3 + 531.9s^2 + 633.7s + 169.9) \times 10^2} \quad (5-34)$$

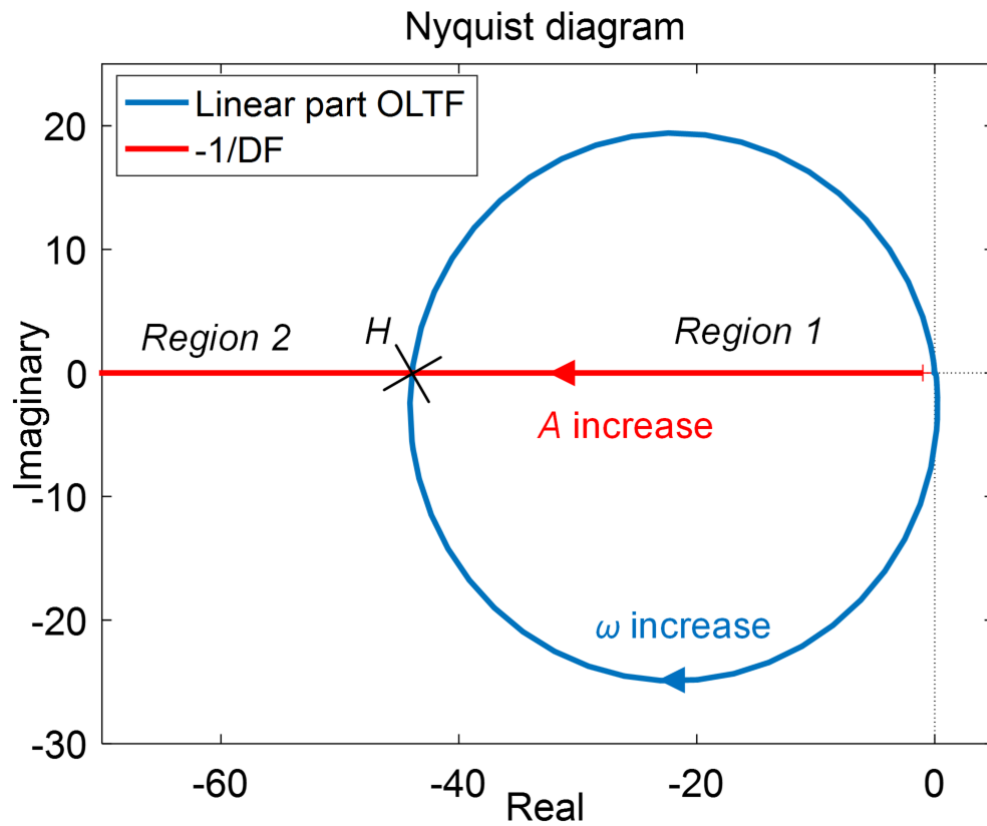


Figure 5.9 Nyquist diagram of the OLTF and -1/DF.

The aim of this controller is to build a self-excited oscillation system, thus, the stability of the non-linear system should be examined. Table 5.2 presents the parameter values of the linear parts. Note that the control signal u_c is defined as dimensionless. The open-loop transfer function (OLTF) is given as Equation 5-34.

To study the stability of the system, the Nyquist diagram of the linear OLTF is plotted together with the negative reciprocal of the describing function (DF) of the saturation limit, as is shown in Figure 5.9.

There is an intersection point, H , of the OLTF and $-1/DF$ curves, which indicates that a limit cycle occurs, in other words, the system exhibits an inherent self-sustaining oscillation. This can be explained from the fact that H separates the $-1/DF$ plot into 2 regions. According to the Nyquist stability criteria:

If $-1/N(A)$ falls in region 1, the closed-loop system is unstable;

If $-1/N(A)$ falls in region 2, the closed-loop system is stable.

Therefore, any disturbance tending to increase the amplitude will move from H to region 2, i.e. stability. Thus, the amplitude will reduce back to H . Vice versa for any disturbance trying to reduce the amplitude. Therefore, H is a stable self-excitation oscillation point.

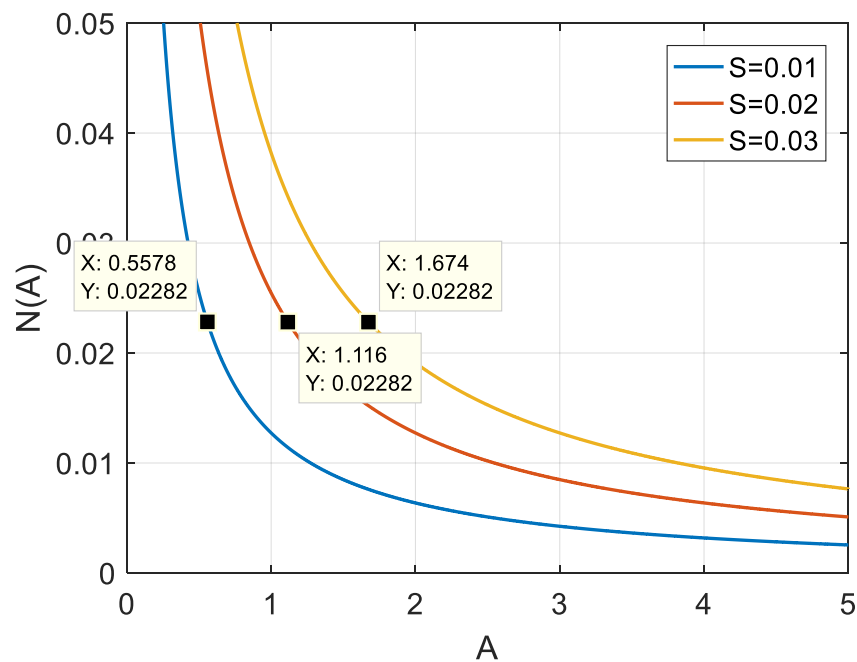


Figure 5.10 Using DF to predict amplitude A.

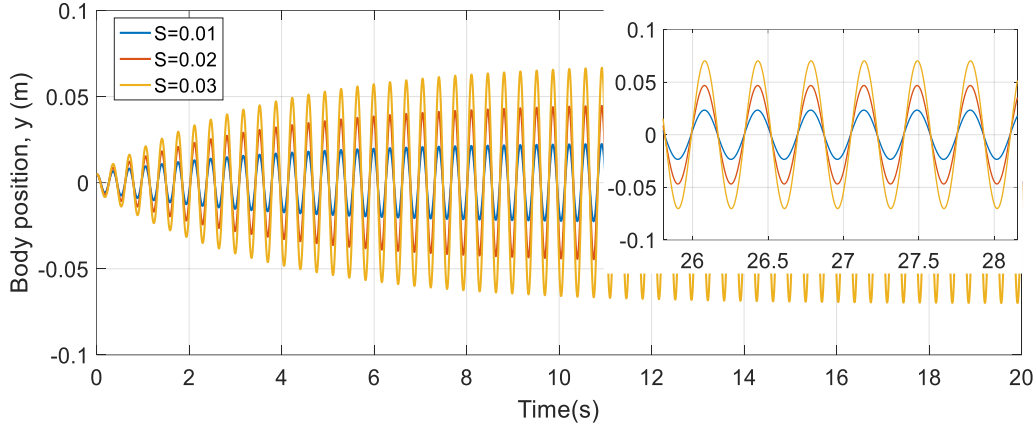


Figure 5.11 Simulation results of using saturation limit to dictate body position.

Figure 5.10 shows the relationship between A and $N(A)$ for different saturation limits, S . The value of $N(A)$ at H is 0.02282, which is used to explain the amplitude of y in terms of S . Figure 5.11 shows via simulation that when the system is exhibiting steady oscillation, A is proportional to S , and so the amplitude of body position y is also proportional to S . The oscillation frequency, ω_s , is found from Equation 5-34 to be 17.844 rad/s. This is very close to the natural frequency, ω_n , given by $\sqrt{K/M}$ to be 17.795 rad/s.

5.2.2.4 Model with foot free to lift off the ground

A more realistic model allows the foot to lift off the ground. Therefore, the transition between the stance phase and flight phases can occur. Note that during the flight phase, the body vertical motion has a parabolic trajectory due to gravity, and the spring is only functional in the stance phase, as shown in Figure 5.12.

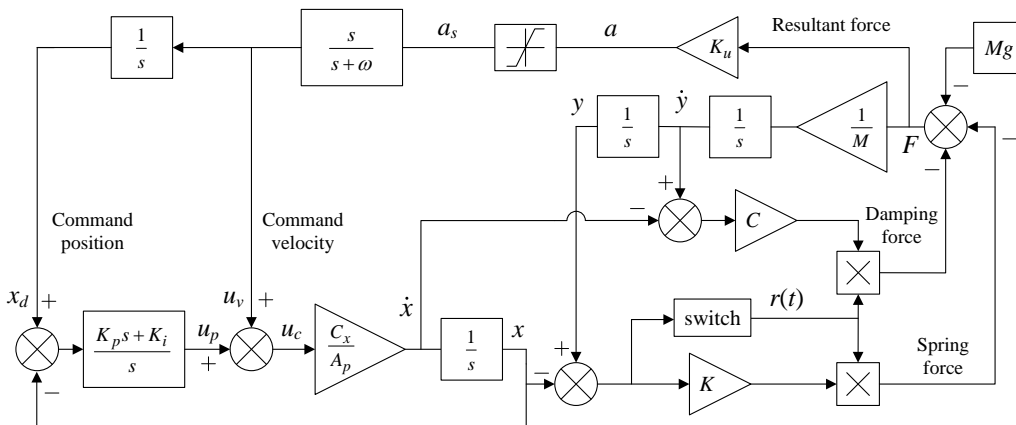


Figure 5.12 Simulation model considering foot lift off the ground.

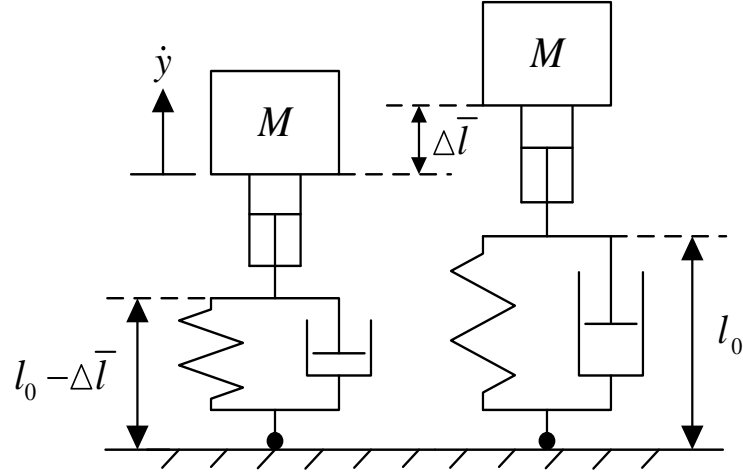


Figure 5.13 The threshold of spring displacement.

A ‘switch’ is used to represent the transition between the flight phase and the stance phase. It is assumed that the natural length of the spring, l_0 , is zero. Therefore, the ‘switch’ outputs 1 if the foot is on the ground and 0 for lift-off, respectively:

$$r(t) = \begin{cases} 1 & y - x \leq 0 \\ 0 & y - x > 0 \end{cases} \quad (5-35)$$

where $r(t)$ is the output of the switch. There is a threshold for S that determines if the foot lifts off the ground during the oscillation. In the steady state, the spring displacement, $\Delta \bar{l}$, is given by:

$$\Delta \bar{l} = \left| \frac{Mg}{K} \right| = 0.031 \text{ m} \quad (5-36)$$

Assuming the damping is small and can be neglected, to have the foot lift off the ground, the spring should return to natural length as shown in Figure 5.13. Defining Y as the amplitude of $y(t)$, from Figure 5.8 or Figure 5.12, assuming no foot lift-off, the amplitudes Y and A are related by:

$$A = \left| MK_u \omega_s^2 \right| Y \quad (5-37)$$

where A_t is the amplitude threshold for foot lift off. Therefore, combining equations 5-32 and 5-37, the corresponding saturation limit is:

$$S_t = 0.0133 \quad (5-38)$$

where S_t is the saturation threshold above which hopping (i.e. foot lift off) will occur. This is demonstrated via simulation. Figure 5.14 shows that when $S=0.01$, the foot stays on the ground. When S is greater than 0.0133, e.g. for the cases of $S=0.02$ or 0.03, results in a larger hopping height. Thus, the flight phase duration increases and the hopping height is still determined by the saturation limit. Figure 5.15 shows that when $S=0.0133$, the foot leaves the ground momentarily in the ‘free foot’ case, which is caused by the approximation when operating the describing function technique.

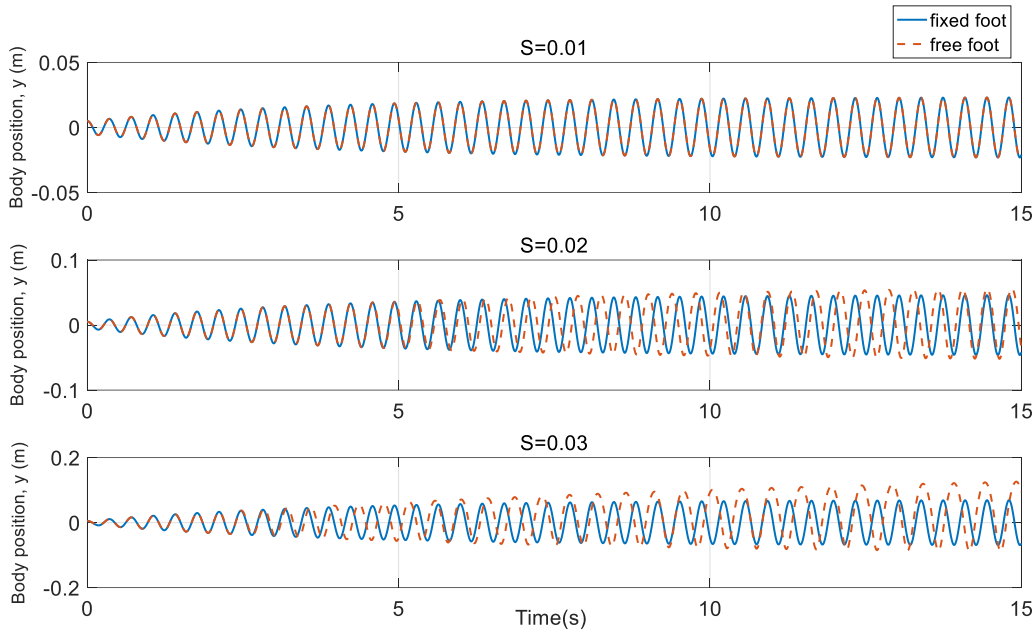


Figure 5.14 Simulation results of $S=0.01$, $S=0.02$ and $S=0.03$.

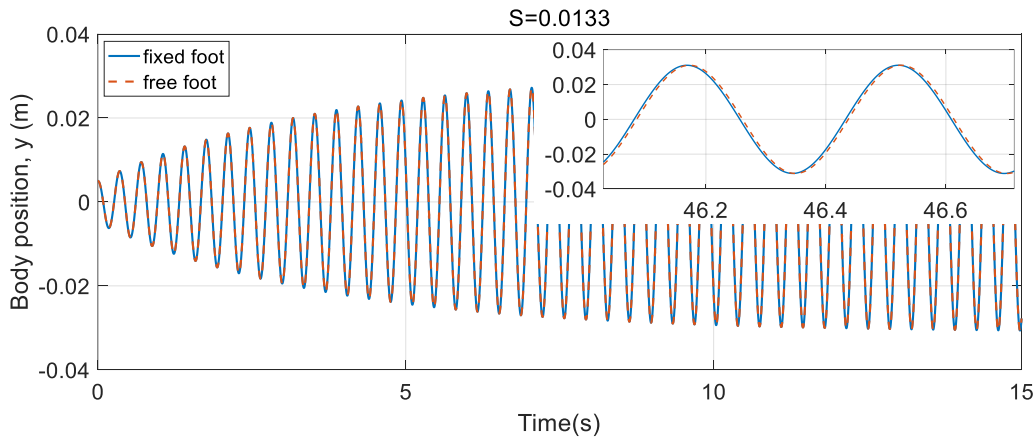


Figure 5.15 Simulation results of $S=0.0133$. The close-up figure shows a small difference between ‘fixed foot’ and ‘free foot’ cases, which indicate the foot leaves the ground momentarily.

5.2.3 Results and discussion

The experimental and simulation results are shown in Figure 5.16. As the saturation limit reduces, the spring displacement also reduces. Even though there is no direct measurement of the hopping height, the decrease of spring displacement indicates a decrease in hopping height since less impact energy is stored in the spring. Therefore, the saturation limit does dictate the hopping height. The hopping frequency has a small variation due to the change of saturation limit. When $S=0.02$, the hopping frequency is 2.15 Hz, when $S=0.01$, the hopping frequency is 2.25 Hz. This is consistent with the results of using the simple model in Section 2. The supplementary video provides a visual demonstration. Note that doubling the saturation limit is not doubling the spring displacement, plus there is a sustained oscillation when $S=0$. Figure 5.17 shows that when the robot exhibits sustained oscillation, at each ‘touch-down’, the ground impact force acting on the robot foot results in the actuator piston retracting slightly due to the compressibility of the oil. Then the piston is moved back towards the zero position by the closed-loop position controller. This effect tends to excite the robot into a resonant oscillation. As these oscillations build in amplitude, the foot may leave the ground momentarily. This characteristic is not seen with the simple model, i.e. the simple model gives no sustained oscillation when $S=0$, as it does not include the oil compressibility effect.

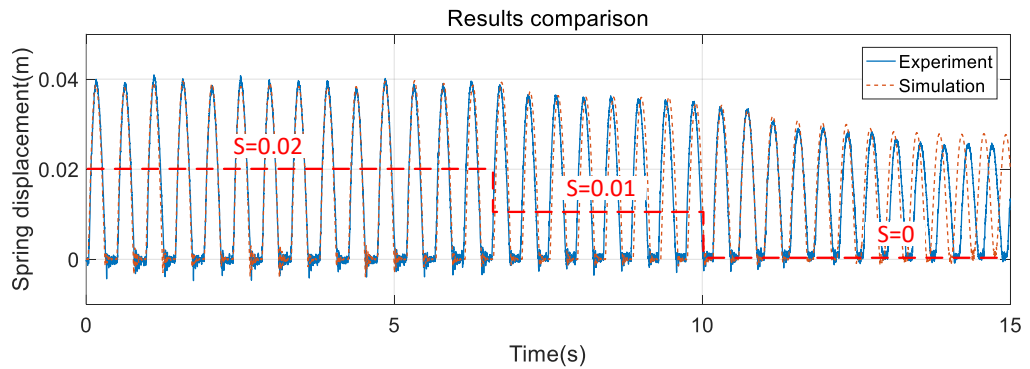


Figure 5.16 Results comparison.

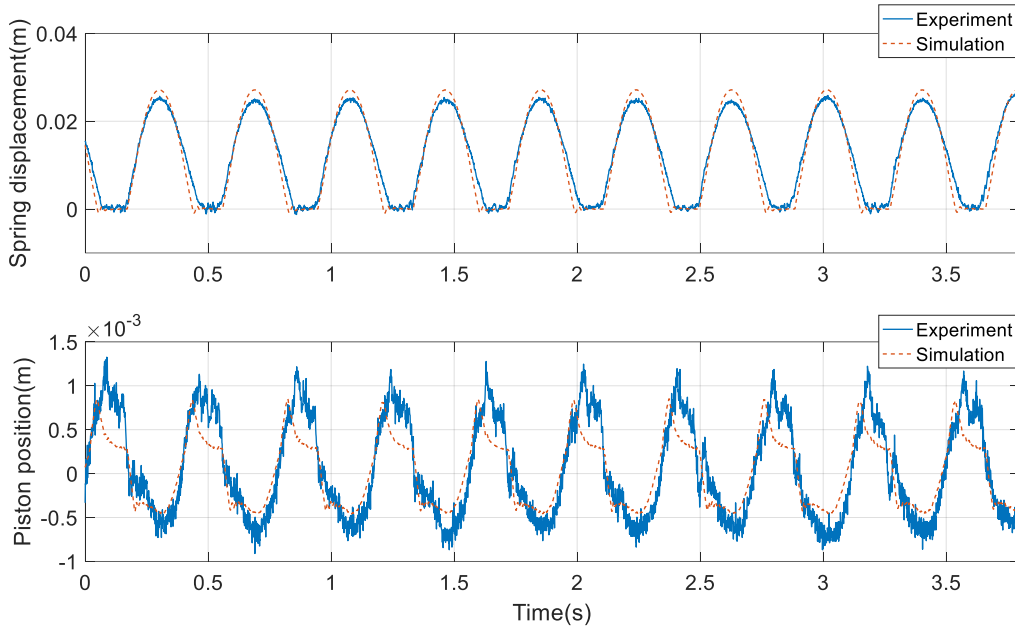


Figure 5.17 Results comparison.

5.2.4 Summary

A self-excited hopping height controller is successfully developed in this section. It is composed of a positive pressure feedback loop and a saturation limit which dictates the hopping height. The position of the robot leg actuator is controlled using a PI controller and the command position signal is generated from the force feedback loop, plus a command velocity feedforward loop is used to improve the system response. A simple system model, in which all aspects but the saturation limit are linearized is used to analyse the controller performance via the describing function technique. Additionally, this controller is studied using a more realistic model, in which the robot foot can lift off the ground. Consequently, the conditions of self-excited hopping are theoretically derived and successfully experimental tested on the BBH2 robot. A detailed simulation model is developed to explain the main findings from the experiments, in which a sustained robot body oscillation is found even when the pressure feedback signal is zero. This is related to the compressibility of the oil, a characteristic which is not included in the simple models. For legged robots, control strategies are closely linked to the mechanical design and components selection. The main contribution of this controller is to significantly reduce the complexity of running robots, from mechanical design and/or sensor measurement perspectives.

5.3 Balancing control while hopping

5.3.1 Introduction

For bipedal hopping robots, dynamic balancing control is challenging, especially when the foot contact area is small. The distinction between the flight phase and stance phase, i.e. detection of the ground contact, is required to accomplish different control actions, which can be provided either mechanically or electrically. This section presents the investigation of balancing control while the BBH2 robot is hopping. The controller developed follows the well-established structure of the ‘Three-part’ control algorithm and is investigated using a detailed simulation model.

5.3.2 Controller implementation

To simplify the controller implementation, the distance between the body CoG and the foot is introduced as a ‘*virtual leg*’. The leg displacement is calculated using a kinematics transformation. Figure 5.18 is a simplified diagram of one hopping cycle.

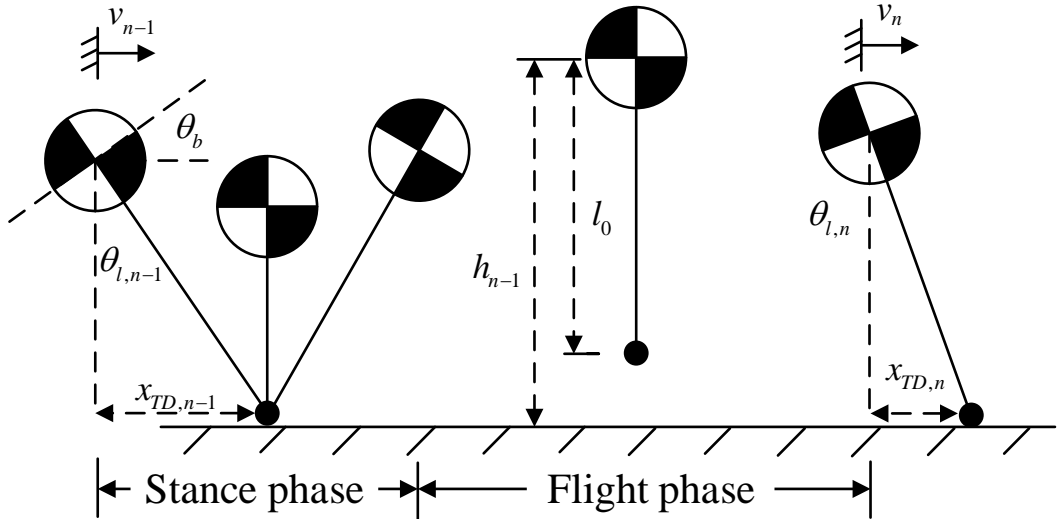


Figure 5.18 Simplified diagram of one hopping cycle.

5.3.2.1 Control of the hopping height

Bhatti et al. developed a simple hopping height control technique for a planar robot travelling over discontinuous surfaces. The leg actuator demand velocity during the stance phase is derived using the achieved height of the previous hop, denoted $h_{n-1,a}$, and the desired height for the next hop, $h_{n,d}$, and is given by:

$$q_{n,d} = K_{h1}\sqrt{h_{n,d}} + K_{h2}\left(\sqrt{h_{n,d}} - \sqrt{h_{n-1,a}}\right) \quad (5-39)$$

where $q_{n,d}$ is the desired extension velocity of the leg, K_{h1} and K_{h2} are the controller gains. Integrating this desired velocity gives the demand position, which is common for a servo-hydraulics system. Additionally, the virtual leg is controlled to return to mid-length during the flight phase to be ready for the next touchdown, plus the demand hopping height remains constant in this simulation, i.e. $h_{n,d}=0.43$ m. The closed-loop leg length control is achieved using a PI controller:

$$u_c = K_p e + K_i \int e dt \quad (5-40)$$

where K_p is the proportional gain, K_i is the integral gain and e is the leg position error.

5.3.2.2 Control of the longitudinal velocity

During the flight phase, the robot has a parabolic trajectory, thus moving the hip actuator results in different rotation angle for the body and legs due to the moment of inertia. The leg angle, θ_l , is controlled to place the foot on the ground at a horizontal position, x_{TD} , relative to the body CoG, to achieve the required longitudinal velocity. An appropriate leg angle for the next touch-down can be calculated from the previous hop. Thus, the foot placement at the previous touch-down, $x_{TD,n-1,a}$, is given by:

$$x_{TD,n-1,a} = \frac{1}{2} v_{n-1,a} T_{s,n-1,a} \quad (5-41)$$

where $v_{n-1,a}$ is the achieved body longitudinal velocity at previous touch-down and $T_{s,n-1,a}$ is the corresponding stance duration. Thus the leg angle is given by:

$$\theta_{l,n-1,a} = \sin^{-1} \frac{x_{n-1,TD,a}}{l_0} \quad (5-42)$$

where $\theta_{l,n-1,a}$ is the achieved leg angle of the previous hop, and l_0 is the nominal length of the virtual leg, which is 0.4 m. According to small perturbation approximation, define:

$$\Delta\theta_l = K_l(v_{n,d} - v_{n-1,a}) \quad (5-43)$$

where $v_{n,d}$ is the desired body longitudinal velocity for the next touchdown, $\Delta\theta_l$ is the corresponding leg angle change and K_l is the feedback gain. Thus, the desired leg angle for the next touch-down, $\theta_{l,n,d}$, is given by:

$$\theta_{l,n,d} = \theta_{l,n-1} + \Delta\theta_l \quad (5-44)$$

If hip torque is the control variable, leg angle can be controlled in a closed loop.

$$\tau_l = K_{l1}(\theta_{l,n} - \theta_{l,n,d}) + K_{l2}(\dot{\theta}_{l,n}) \quad (5-45)$$

where τ_l is the control torque for the hip during flight phase, K_{l1} and K_{l2} are feedback gains, and $\theta_{l,n}$ is the actual leg angle.

5.3.2.3 Control of the body attitude

Controlling the leg angle during flight phase changes the body pitch angle, which can be corrected during the stance phase. It is assumed there is sufficient friction at the ground to avoid the robot foot slipping. The body angle, θ_b , is controlled towards a horizontal position, i.e. $\theta_{b,d}=0^\circ$, using a simple servo given by:

$$\tau_b = K_{b1}(\theta_b - \theta_{b,d}) + K_{b2}(\dot{\theta}_b) \quad (5-46)$$

where τ_b is the control torque for the hip during stance phase, K_{b1} and K_{b2} are feedback gains, and $\theta_{b,d}$ is the desired body angle. Table 3 shows the values of the controller gains and feedback gains used in this simulation.

Table 5.3 Controller and feedback gains.

Parameters	Value	Unit
K_{h1}	0.02	$\text{m}^{1/2}/\text{s}$
K_{h2}	1	$\text{m}^{1/2}/\text{s}$
K_{l1}	100	Nm/rad
K_{l2}	0.02	Nms/rad
K_{b1}	1×10^5	Nm/rad
K_{b2}	9×10^3	Nms/rad
K_p	320	1/m
K_i	100	1/(sm)

5.3.3 Simulation results

Figure 5.19 shows the simulation results. The simulation starts with a free drop of the robot from a small initial body height. The achieved hopping frequency is approximately 3 Hz, and the hopping height controller is able to correct the robot motion within several hops when the longitudinal velocity is changing. The leg angle is adjusted by the controller to achieve different velocity demands. At $t=6$, a sudden movement of the hip actuator is found due to a large step change of the velocity demand, so more hops are needed to allow the robot to gradually achieve the demand velocity. Between $t=5$ and 10, the forward travelling speed is 0.24 m/s; between $t=15$ and 20, the backward speed is 0.08 m/s; between $t=20$ and 25, the backward speed is 0.15 m/s. The body angle is successfully controlled to

maintain balance, not only when hopping on a spot, i.e. $\dot{x}(t)=0$, but also to be balanced with different moving speed.

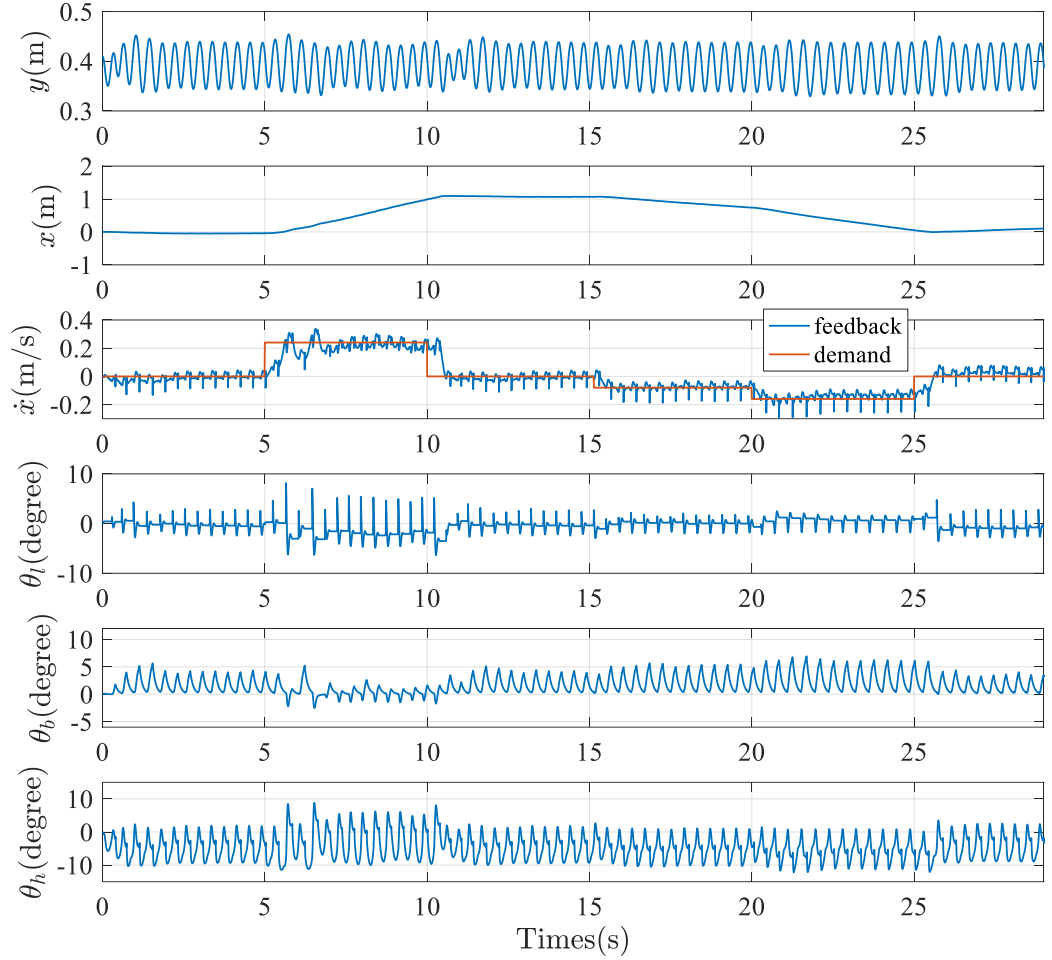


Figure 5.19 Simulation results.

5.3.4 Summary

The section describes the successful implementation of a dynamic balancing controller for the BBH2 robot. The robot motion control is separated into three parts: the hopping height, the longitudinal velocity and body attitude. An adaptive demand actuator velocity is derived using the achieved height of the previous hop and the desired height for the next cycle; integrating this velocity gives an actuator position demand, which can input to a PI controller. Different longitudinal velocities are achieved by controlling the leg angle to place the foot at the required position at each touchdown. The body attitude is corrected during the stance phase to maintain balance. Simulation results indicate that this controller can in principle

successfully balance the BBH2 robot, not only hopping on a spot but also travelling with different velocities. Sensor selection and signal processing are challenging when implementing this controller in practice, as sufficiently quick response and high measurement accuracy are required to obtain the robot motion.

6 Conclusions and further work

This chapter summaries the findings reported in this thesis along with some recommended further research which should be done.

6.1 Conclusions

This thesis presents several studies relate to legged locomotion, especially focussing on the design of a compliant hydraulic actuator for robot leg actuation and the development of control strategies for bipedal hopping.

Two small-sized, hydraulically actuated bipedal hopping robots (BBH1 and BBH2) are successfully developed. The different types of the leg (telescopic and articulated) provide an experimental basis to study a novel compliant hydraulic actuator and to validate motion controllers. An electro-hydraulic actuation system is used to power the legs. Essential variables, for feedback control purposes, are measured by the sensory system. A real-time xPC control system enables onboard data acquisition and controller implementation. The detailed nonlinear simulation models of these two robots are developed, which mainly focuses on the hydraulic and mechanical domains. These models provide a better explanation of the findings from the experiments. Moreover, a series of bench tests are taken to examine the efficacy of the mechanical design of the robots.

The study of a compliant hydraulic actuator for running robots has been undertaken in Section 3.3. This actuator is used as a telescopic type of robot leg, which is experimentally tested on the BBH1. A PI controller is used to achieve the position feedback control of the actuator. The non-linear simulation model is used to explain the main findings of the experimental results, such as the hysteresis in the valve and the friction in the actuator. In particular, an *error-time integral*, which is derived using a set of linear models, is introduced to link the friction effect with the system compliance. The quantified analysis of *error-time integral* could help with selecting appropriate components for this application. Moreover, the

analysis indicates that in order to reduce the position tracking error caused by friction, the options are to:

- Reduce the friction level. In reality, the friction comes from elastomeric seals around the piston head and rod gland, and lower friction is associated with greater leakage.
- Increase hydraulic elastance. The increase of the hydraulic elastance means the increase of system spring stiffness, i.e. loss of actuator compliance.

Therefore, a sensible design approach is to identify the friction level first and then investigate the *error-time integral* to estimate the maximum compliance that is achievable.

The investigation of the standing balance control of this robot was undertaken in Section 5.1. The pole placement method is used to develop the controller, based on a double inverted pendulum robot model. According to the calculation, the minimal degree of solution indicates the minimal number of motion feedback states (or position derivatives); in this case, up to the third derivative (jerk) is required. Although the balancing servo-performance appears promising, frequency response analysis shows that measurement noise could be problematic, particularly as it affects the control signal. High-frequency noise can be reduced to some extent by including lower frequency desired closed loop poles which are cancelled by a command filter.

In Section 5.2, a novel hopping controller is developed and experimentally tested on the BBH2 robot. The controller is composed of a positive force feedback loop with a saturation limit dictating the amplitude; a conventional position feedback loop is implemented plus a command velocity feedforward loop to improve the system response. The condition for guaranteed self-excited hopping is theoretically derived using the describing function technique and demonstrated via simple simulation models. A threshold for the saturation limit is derived which indicates the condition for robot foot lift off the ground. Without direct measuring the hopping height, the spring displacement is consistently following the trend expected from the saturation limit change. The variation of hopping frequency caused by different hopping heights is as expected. It is found that practical details

affect the stabilisation of the system. Thus, the detailed nonlinear simulation model is used to explain these findings. Particularly, the sustained robot oscillation, when the pressure feedback signal is zero, is identified to be caused by the compressibility of the oil.

In Section 5.3, the dynamic balancing control while a bipedal robot is hopping is investigated using the BBH2 robot via simulation. The controller is built following a well-established structure of the ‘Three-part’ control algorithm. The hopping height is controlled using an adaptive controller; changing the leg angle during the flight phase to place the foot in the desired position achieves longitudinal velocity control; the body attitude is controlled during the stance phase to maintain balance. Simulation results demonstrate that the controller can successfully balance the robot while hopping with different longitudinal velocities both forwards and backwards. In practice, the direct measurement of the robot hopping height and longitudinal velocity is challenging due to the requirements of sufficiently quick response and high measurement accuracy of the sensors. If necessary, state estimators or observers can be built, i.e. derive the hopping height or longitudinal velocity from the estimated state variables.

The research in legged locomotion is likely to continue over a long period. Impressive progress has been made in designing and demonstrating agile legged robots, although in many cases they are only capable of simple motions in structured environments. However, ultimately there is real potential for legged robots to be involved in our daily lives, e.g. for rescue operations, transportation across rough terrain, and assistance within the built environment.

6.2 Further work

It is never easy to make a robot that can actually hop. Although the work is done in this thesis presents some success in several studies of legged locomotion, some recommendations for future work are:

- Lower friction hydraulic cylinders can be used to accomplish the hardware refinement for the BBH1 using the same application of the compliant

hydraulic actuator. However, the friction effect still needs to be rigorously investigated using *error-time integral* since it commonly exists.

- For the balancing control of the robot in a standing position, a state estimator or observer can be built to estimate state variable values without requiring differentiation of measured signals. Plus, the damping at the actuated joint should be taken into account.
- Although the novel self-excited hopping controller has been successfully implemented on the BBH2, a small oscillation of the piston is found when the robot lifts off the ground. This is mainly due to the small mass of the robot leg. Thus, further controller improvement is looking for an adaptive algorithm to attenuate this unnecessary oscillation.
- It is possible to use another nonlinear element, e.g. relay, to replace the saturation limit in the novel hopping height control. In fact, the selection of this nonlinearity can be investigated by applying the describing function technique, similarly as described in Chapter 7.
- Several hardware refinements are needed to optimise the mechanical design of the robot used for experimental verification, e.g. the mass of some parts can be reduced. Pressurised hydraulic accumulators for untethered operation are promising to provide high-density energy storage for this small-sized hopping robot. Servo valves could replace the current proportional valves due to a significantly less hysteresis level, although null leakage would have to be considered. Hydraulic hoses with a larger inner diameter and fittings should be used to minimise the pressure loss.

Bibliography

Active Sensors Ltd. (2015). *CLS 1302 series position sensor* [Online]. Available: <http://www.activesensors.com/datasheet/linear-potentiometer/cls1300.pdf>

Ahmadi, M. and Buehler, M., 1999. The ARL monopod II running robot: Control and energetics. In *Proceedings 1999 IEEE International Conference on Robotics and Automation (Cat. No. 99CH36288C)* (Vol. 3, pp. 1689-1694). IEEE.

Al-Shuka, H.F., Corves, B., Zhu, W.H. and Vanderborght, B., 2016. Multi-level control of zero-moment point-based humanoid biped robots: a review. *Robotica*, 34(11), pp.2440-2466.

Bekey, G.A., 2005. *Autonomous robots: from biological inspiration to implementation and control*. MIT press.

Bhatti, J., Plummer, A.R., Iravani, P. and Ding, B., 2015, August. A survey of dynamic robot legged locomotion. In *2015 International Conference on Fluid Power and Mechatronics (FPM)* (pp. 770-775). IEEE

Bhatti, J., Plummer, A.R., Sahinkaya, M.N., Iravani, P., Guglielmino, E. and Caldwell, D.G., 2012, July. Fast and adaptive hopping height control of single-legged robot. In *ASME 2012 11th Biennial Conference On Engineering Systems Design And Analysis*.

Boston Dynamics. <http://www.bostondynamics.com/>

Bottaro, A., Casadio, M., Morasso, P.G. and Sanguineti, V., 2005. Body sway during quiet standing: is it the residual chattering of an intermittent stabilization process?. *Human movement science*, 24(4), pp.588-615.

Bretl, T. and Lall, S., 2008. Testing static equilibrium for legged robots. *IEEE Transactions on Robotics*, 24(4), pp.794-807.

Chen, C.T., 1998. *Linear system theory and design*. Oxford University Press, Inc.

Chen, Y.G. and Hsu, M.H., 2007. Searching ancient inventions from modern techniques-a research of walking horses with 8-link type leg mechanisms. In *Proceedings of twelfth world congress in mechanism and machine science*.

Chou, C.P. and Hannaford, B., 1996. Measurement and modelling of McKibben pneumatic artificial muscles. *IEEE Transactions on robotics and automation*, 12(1), pp.90-102.

Cotton, S., Olaru, I.M.C., Bellman, M., van der Ven, T., Godowski, J. and Pratt, J., 2012, May. Fastrunner: A fast, efficient and robust bipedal robot. concept and planar simulation. In *2012 IEEE International Conference on Robotics and Automation* (pp. 2358-2364). IEEE.

Daerden, F. and Lefeber, D., 2002. Pneumatic artificial muscles: actuators for robotics and automation. *European journal of mechanical and environmental engineering*, 47(1), pp.11-21.

De Santos, P.G., Gálvez, J.A., Estremera, J. and Garcia, E., 2003. SIL04: a true walking robot for the comparative study of walking machine techniques. *IEEE Robotics & Automation Magazine*, 10(4), pp.23-32.

Ding, B., Plummer, A. and Iravani, P., 2016. Investigating balancing control of a standing bipedal robot with point foot contact. *IFAC-PapersOnLine*, 49(21), pp.403-408.

Ding, B., Plummer, A. and Iravani, P., 2018, July. A Study of a Compliant Hydraulic Actuator for Running Robots. In *2018 Global Fluid Power Society PhD Symposium (GFPS)* (pp. 1-6). IEEE.

Erbatur, K., Okazaki, A., Obiya, K., Takahashi, T. and Kawamura, A., 2002. A study on the zero moment point measurement for biped walking robots. In *7th International Workshop on Advanced Motion Control. Proceedings (Cat. No. 02TH8623)* (pp. 431-436). IEEE.

Geyer, H., Seyfarth, A. and Blickhan, R., 2003. Positive force feedback in bouncing gaits?. *Proceedings of the Royal Society of London. Series B: Biological Sciences*, 270(1529), pp.2173-2183.

Hardarson, F., 1998. Locomotion for difficult terrain. KTH.

Hengstler. (2014). *RI32 series incremental encoder* [Online]. Available: https://www.hengstler.de/gfx/file/shop/encoder/RI32/Datasheet_RI32_en.pdf

Hirose, M. and Ogawa, K., 2006. Honda humanoid robots development. *Philosophical Transactions of the Royal Society A: Mathematical, Physical and Engineering Sciences*, 365(1850), pp.11-19.

Hodgins, J.K. and Raibert, M.N., 1991. Adjusting step length for rough terrain locomotion. *IEEE Transactions on Robotics and Automation*, 7(3), pp.289-298.

Hoerbiger. (2008). *LB6 series hydraulic actuator* [Online]. Available: <https://www.hoerbiger.com/upload/file/zyylinder.pdf>

HYDAC Technology Ltd. (2015). *SBO series diaphragm accumulator* [Online]. Available: <https://www.hydac.com/de-en/products/hydraulic-accumulators.html>

Hyon, S.H. and Mita, T., 2002. Development of a biologically inspired hopping robot-" Kenken". In *Proceedings 2002 IEEE International Conference on Robotics and Automation (Cat. No. 02CH37292)* (Vol. 4, pp. 3984-3991). IEEE.

Hyon, S.H., Emura, T. and Mita, T., 2003. Dynamics-based control of a one-legged hopping robot. *Proceedings of the Institution of Mechanical Engineers, Part I: Journal of Systems and Control Engineering*, 217(2), pp.83-98.

Jelali, M. and Kroll, A., 2012. *Hydraulic servo-systems: modelling, identification and control*. Springer Science & Business Media.

Kajita, S., Agency of Industrial Science, Japan International Trade and Industry Ministry of, 1989. *Method and apparatus for dynamic walking control of robot*. U.S. Patent 4,834,200.

Konami, S. and Nishiumi, T., 2016. *Hydraulic Control Systems: Theory and Practice*. World Scientific Publishing Company.

Liu, G.H., Lin, H.Y., Lin, H.Y., Chen, S.T. and Lin, P.C., 2014. A bio-inspired hopping kangaroo robot with an active tail. *Journal of Bionic Engineering*, 11(4), pp.541-555.

Maxon Motor. (2014). *ESCON Module 24/2 motor controller* [Online]. Available: https://www.maxonmotor.nl/medias/sys_master/8815105572894/466023-ESCON-Module-24-2-Hardware-Reference-En.pdf

McGeer, T., 1990. Passive dynamic walking. *I. J. Robotic Res.*, 9(2), pp.62-82.

McGhee, R.B., 1976. Robot locomotion. In *Neural control of locomotion* (pp. 237-264). Springer, Boston, MA.

Merritt, H., Merritt, H.E. and Merritt, H.E., 1967. *Hydraulic control systems*. John Wiley & Sons.

Michael, K., 2012. Meet Boston dynamics' LS3-the latest robotic war machine.

MIT Leg Laboratory.<http://www.ai.mit.edu/projects/leglab/robots/robots.html>

Moog Inc. (2009). *E242 series proportional valve* [Online]. Available: <https://www.moog.com/literature/ICD/E242CartridgeDDV-ds.pdf>

Palmer, L.R., Orin, D.E., Marhefka, D.W., Schmiedeler, J.P. and Waldron, K.J., 2003, September. Intelligent control of an experimental articulated leg for a galloping machine. In *2003 IEEE International Conference on Robotics and Automation (Cat. No. 03CH37422)* (Vol. 3, pp. 3821-3827). IEEE.

Plummer, A.R., 1991. *Digital control techniques for electro-hydraulic servosystems* (Doctoral dissertation, University of Bath).

Plummer, A.R., 2008. A detailed dynamic model of a six-axis shaking table. *Journal of earthquake engineering*, 12(4), pp.631-662.


Poulakakis, I., Papadopoulos, E. and Buehler, M., 2006. On the stability of the passive dynamics of quadrupedal running with a bounding gait. *The International Journal of Robotics Research*, 25(7), pp.669-687.

- Pratt, G.A., 2000. Legged robots at MIT: What's new since Raibert?. *IEEE Robotics & Automation Magazine*, 7(3), pp.15-19.
- Pratt, J., Chew, C.M., Torres, A., Dilworth, P. and Pratt, G., 2001. Virtual model control: An intuitive approach for bipedal locomotion. *The International Journal of Robotics Research*, 20(2), pp.129-143.
- Raibert, M., 2010, December. Dynamic legged robots for rough terrain. In *2010 10th IEEE-RAS International Conference on Humanoid Robots* (pp. 1-1). IEEE.
- Raibert, M., 2012. Alphadog, the rough-terrain robot. In *Adaptive Mobile Robotics* (pp. 07-07).
- Raibert, M., Blankespoor, K., Nelson, G. and Playter, R., 2008. Bigdog, the rough-terrain quadruped robot. *IFAC Proceedings Volumes*, 41(2), pp.10822-10825.
- Raibert, M., Blankespoor, K., Nelson, G. and Playter, R., 2008. Bigdog, the rough-terrain quadruped robot. *IFAC Proceedings Volumes*, 41(2), pp.10822-10825.
- Raibert, M., Chepponis, M. and Brown, H.B.J.R., 1986. Running on four legs as though they were one. *IEEE Journal on Robotics and Automation*, 2(2), pp.70-82.
- Raibert, M.H. and Sutherland, I.E., 1983. Machines that walk. *Scientific American*, 248(1), pp.44-53.
- Raibert, M.H., 1984. Hopping in legged systems—modelling and simulation for the two-dimensional one-legged case. *IEEE Transactions on Systems, Man, and Cybernetics*, (3), pp.451-463.
- Raibert, M.H., 1986. *Legged robots that balance*. MIT press.
- Sakagami, Y., Watanabe, R., Aoyama, C., Matsunaga, S., Higaki, N. and Fujimura, K., 2002. The intelligent ASIMO: System overview and integration. In *IEEE/RSJ international conference on intelligent robots and systems* (Vol. 3, pp. 2478-2483). IEEE.
- Sayyad, A., Seth, B. and Seshu, P., 2007. Single-legged hopping robotics research—A review. *Robotica*, 25(5), pp.587-613.

- Schwarzenbach, J. and Gill, K.F., 1978. *System modelling and control*. J. Wiley.
- Semini, C., Tsagarakis, N.G., Guglielmino, E. and Caldwell, D.G., 2010, October. Design and experimental evaluation of the hydraulically actuated prototype leg of the HyQ robot. In *2010 IEEE/RSJ International Conference on Intelligent Robots and Systems* (pp. 3640-3645). IEEE.
- Silva, M.F. and Tenreiro Machado, J.A., 2007. A historical perspective of legged robots. *Journal of Vibration and Control*, 13(9-10), pp.1447-1486.
- Terasoft Ltd. (2014). *Micro-Box 2000 industrial PC* [Online]. Available: https://www.terasoft.com.tw/product/doc/microbox_en.pdf
- Todd, D.J., 2013. *Walking machines: an introduction to legged robots*. Springer Science & Business Media.
- Variohm. (2014). *EPT 1200 series pressure transducer* [Online]. Available: https://www.variohm.com/images/datasheets/EPT1200%20_%201500.pdf
- Waldron, K.E.N.N.E.T.H.J. and McGhee, R.O.B.E.R.T.B., 1986. The adaptive suspension vehicle. *IEEE Control Systems Magazine*, 6(6), pp.7-12.
- Yao, B., Bu, F., Reedy, J. and Chiu, G.C., 2000. Adaptive robust motion control of single-rod hydraulic actuators: theory and experiments. *IEEE/ASME Transactions on Mechatronics*, 5(1), pp.79-91.
- Yost Labs. (2016). *3-SpaceTM USB/RS232 inertial measurement unit* [Online]. Available: <https://yostlabs.com/wp/wp-content/uploads/pdf/3-Space-Sensor-Users-Manual-USB-1.pdf>
- Zhou, X. and Bi, S., 2012. A survey of bio-inspired compliant legged robot designs. *Bioinspiration & Biomimetics*, 7(4), p.041001.

Appendix 1

Statement of Authorship

This declaration concerns the article entitled:							
A study of a compliant hydraulic actuator for running robots							
Publication status (tick one)							
draft manuscript	<input type="checkbox"/>	Submitted	<input type="checkbox"/>	In review	<input type="checkbox"/>	Accepted	<input type="checkbox"/>
Published	<input checked="" type="checkbox"/>						
Publication details (reference)	<p>Ding, B., Plummer, A. and Iravani, P., 2018, July. A Study of a Compliant Hydraulic Actuator for Running Robots. In <i>2018 Global Fluid Power Society PhD Symposium (GFPS)</i> (pp. 1-6). IEEE.</p> <p>Conference title: '2018 IEEE Global Fluid Power Society PhD Symposium (GFPS2018)'</p>						
Candidate's contribution to the paper (detailed, and also given as a percentage).	<p>Formulation of ideas: The initial idea was formulated by A.Plummer; the key idea of introducing a novel factor is formulated by the candidate (80%).</p> <p>Design of methodology: Experimental/simulation methodology is mostly by the candidate (70%). Results analysis methodology is mostly by the candidate (80%).</p> <p>Experimental work: Solely the candidate (100%).</p> <p>Presentation of data in conference format: Solely the candidate (100%).</p>						
Statement from Candidate	This paper reports on original research I conducted during the period of my Higher Degree by Research candidature.						
Signed					Date	06/03/2019	

© 2018 IEEE. Personal use of this material is permitted. Permission from IEEE must be obtained for all other uses, in any current or future media, including reprinting/republishing this material for advertising or promotional purposes, creating new collective works, for resale or redistribution to servers or lists, or reuse of any copyrighted component of this work in other works.

PAPER 1: A study of a compliant hydraulic actuator for running robots

Beichen Ding*, Andrew Plummer*, Pejman Iravani*

*Centre for PTMC, Department of Mechanical Engineering, University of Bath, Bath, UK

Abstract

In the legged locomotion research area, it is known that efficient running or hopping in either animal or legged robots require leg actuator compliance. Springy legs interacting with body mass gives a natural hopping/running frequency. Servo-hydraulics is highly suitable for robot leg actuation due to its high power density and fast response. In this paper, we investigate using a hydraulic accumulator connected to a hydraulic cylinder to provide both actuation and the required leg compliance. This approach is experimentally applied to a bipedal hopping robot, and closed loop leg position control is implemented. A non-linear simulation model is used to explain the main findings from the experimental results. The effect of friction in this type of compliant hydraulic actuator is found to be very significant. An *error-time factor* is introduced to enable an understanding of the friction effect and aids component selection for this application.

1. Introduction

One of the aims of legged robot research is to develop legged moving machines, which can traverse rough terrain, for example, as required in disaster rescue. Some successfully developed legged robot platforms and their control strategies have been reviewed in [1]. In order to design advanced robots, one approach is to mimic animals. Legged animals moving on rough terrain require leg actuator compliance for agile locomotion. This compliance is mainly provided by the musculoskeletal distributed in the legs which have potential advantages that are listed in [2]. From biomechanical studies, the design of legged robots requires careful integration of the actuation approach and leg compliance solutions. Compressed gas and coil springs are possible solutions, which have been studied in [3].

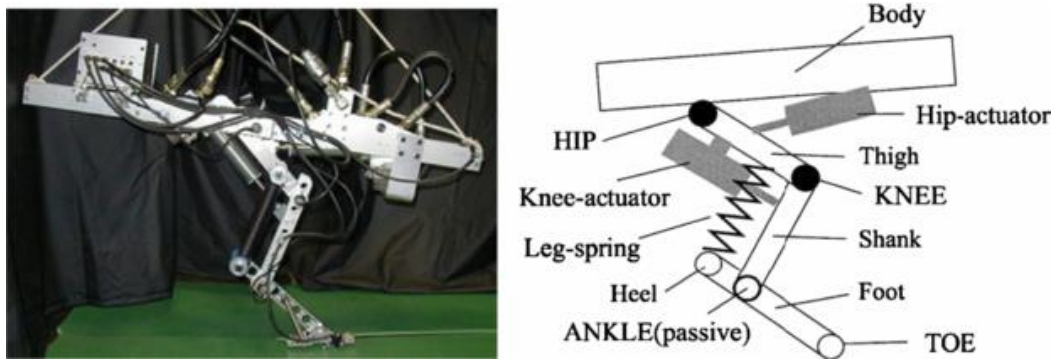


Figure 1. Kenken: one-legged hopping robot [8].

In [4], a planar two-legged running machine is developed using a hydraulic actuator acting in series with a pneumatic spring. The significant compressibility of gas is able to provide high energy storage capacity. More applications of pneumatic actuators for robot design can be found in [5] and [6]. However, the dynamic response and non-linearities of the pneumatic system bring control challenges [7]. Servo-hydraulics could be a solution due to the quick dynamic response and high power density.

Using a coil spring is another effective approach to provide the robot leg's compliance. In [8], the one-legged hopping robot, Kenken, use an extension spring in parallel with the shank beam, which is shown in Fig. 1. Due to the parallelogram mechanism, the coil spring can be passively extended to absorb the impact when the knee joint is controlled to be fixed by the actuator. Other applications of coil springs can be found in [9] and [10].

In this paper, we investigate a compliant hydraulic actuated robot leg using a hydraulic accumulator connected to the piston side of a hydraulic cylinder. Due to the compressibility of the pre-charged gas in the accumulator, the actuator compliance is much higher than a conventional valve controlled actuator system. In order to achieve a quick response, a fast proportional valve is used to control the fluid flow into the full-piston side of the actuator, as shown in Fig. 2. A non-linear simulation model is developed to explain the main findings of the experimental results and the analysis of these results illustrates the significant friction effect on this type of compliant actuator. The quantified representation of this effect is given by introducing an *error-time factor*, which also aids component selection for this application.

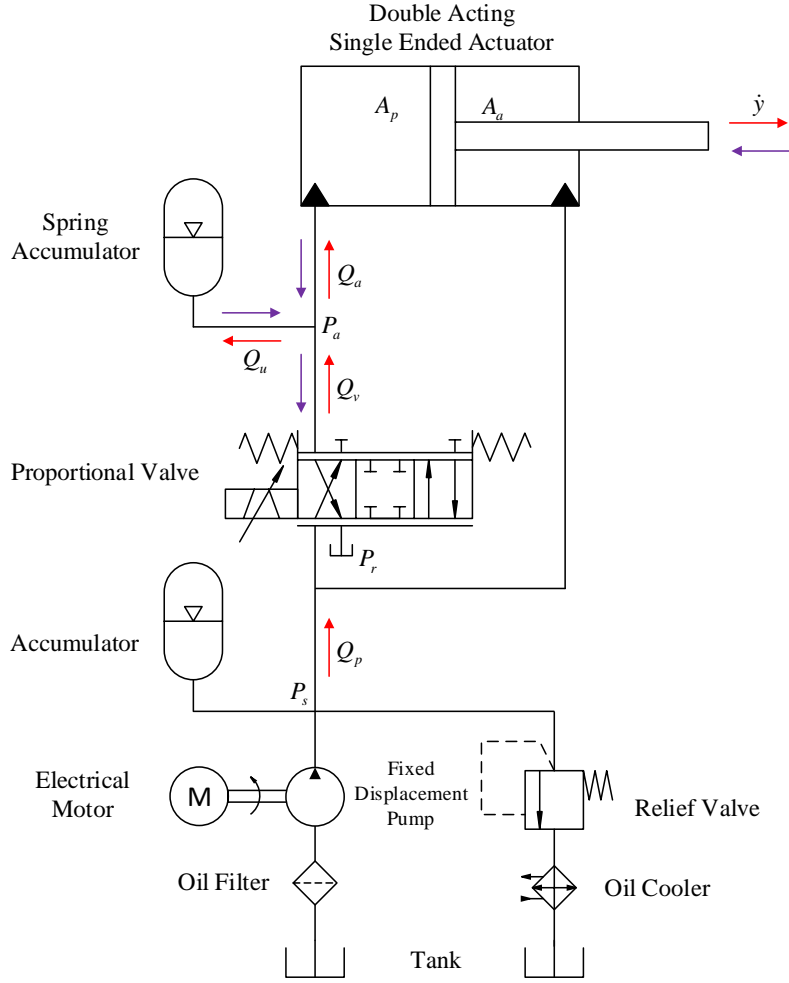


Figure 2. Hydraulic circuit for one compliant leg actuator.

2. Experimental setup

The compliant actuator is experimentally tested on a bipedal hopping robot, which is 414 mm in length, 275 mm in width and 394 mm in height. As shown in Fig. 3, a position sensor is placed in parallel with the leg actuator to measure the piston position. The proportional valves and accumulators are mounted on a manifold. The current test rig is driven by a hydraulic power pack placing in the adjacent area, which could be eventually replaced by a pressurized supply accumulator for untethered operation. Table 1 provides the details of the key components.

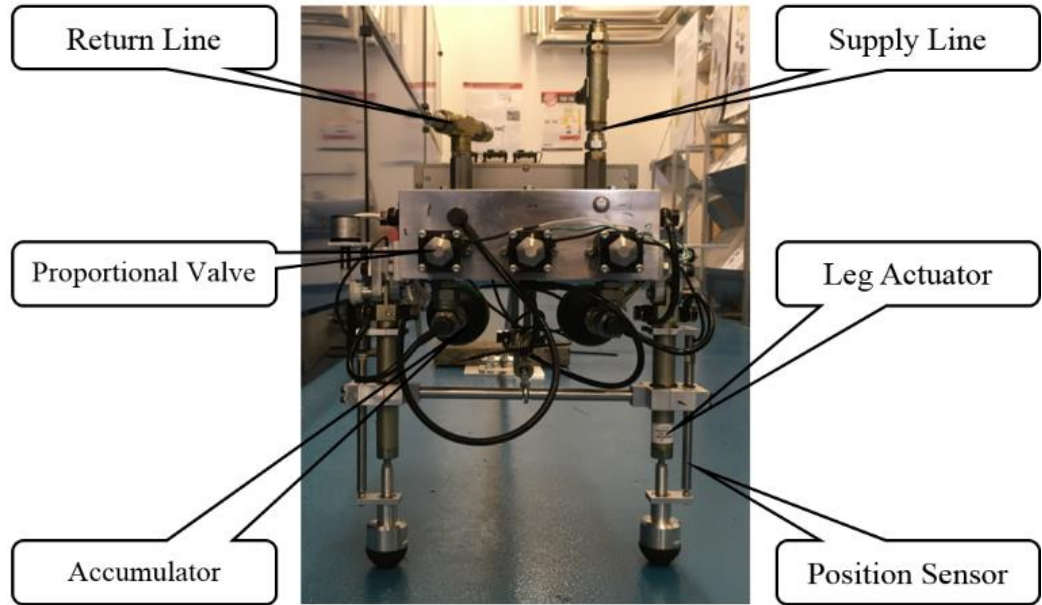


Figure 3. Bipedal hopping robot.

Table 1. Key components

Components	Model	Quantity
Valves	Moog E242	2
Cylinders	Hoerbigger LB6 series	2
Position sensors	Active Sensor PLS0956	2
Accumulators	HYDAC SBO250-0.075E1	2
Controller PC	Terasoft Microbox 2000	1

3. Modelling

3.1 Hydraulic models

This section presents the modelling of the dynamic characteristics of the hydraulic actuator, the proportional valve, the hydraulic accumulator and the hose. The equations are written according to the hydraulic circuit shown in Fig.2.

3.1.1 Actuator model

The actuator model includes the piston force balance equation (1) and the flow equation (4). It is assumed that the supply pressure and return pressure are constant plus there is no inner or outer leakage.

$$P_c A_p - P_s A_a - F_f = F_h \quad (1)$$

where P_c is the full piston side pressure, P_s is the supply pressure, A_p is the full piston area, A_a is the annulus area, F_h is the hydraulic force and F_f is the friction force. Additionally, (2) and (3) are used to represent F_f .

$$F_s = f_v \dot{y} \quad (2)$$

$$F_f = \begin{cases} F_c & \text{for } F_s \geq F_c \\ F_s & \text{for } |F_s| < F_c \\ -F_c & \text{for } F_s \leq -F_c \end{cases} \quad (3)$$

where F_s is the static friction, f_v is a static friction coefficient and F_c is the Coulomb friction. The cylinder flow equation is given by:

$$Q_a = A_p \dot{y} \quad (4)$$

where Q_a is the piston side flow rate and \dot{y} is the piston velocity.

3.1.2 Valve model

The spool displacement is considered as a dimensionless variable which ranging from -1 to +1 with the middle position corresponding to 0. The spool orifice equation is:

$$Q_v = K_v X \sqrt{P_s - P_a} \quad (5)$$

where Q_v is the valve flow rate, K_v is the valve flow coefficient and X is the nominalised spool displacement.

Additionally, a second-order transfer function (6) could be used to represent the valve dynamics [11].

$$X = \frac{\omega_v^2}{s^2 + 2\zeta_v\omega_v + \omega_v^2} \tilde{u}_c \quad (6)$$

where \tilde{u}_c is the spool driving signal, ω_v is the spool natural frequency, ζ_v is the spool damping ratio.

Backlash is introduced as a simplified model of the valve hysteresis as shown in Fig. 4, in which u_c is the control signal, and u_w is the deadband width of the backlash.

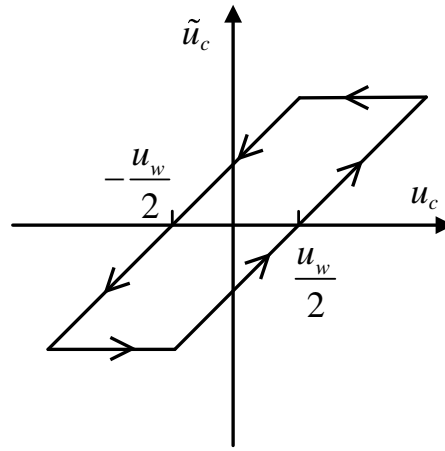


Figure 4. Valve hysteresis.

3.1.3 Accumulator model

The accumulator model gives the pressure corresponding to the gas volume change. An adiabatic process is assumed due to the quick charge and discharge in robot running.

$$\dot{V} = Q_a - Q_v \quad (7)$$

$$V^n P_a = V_m^n P_m \quad (8)$$

$$V_0 P_0 = V_m P_m \quad (9)$$

where V is the gas volume, V_0 is the initial gas volume, V_m is the gas volume at mean working pressure, P_0 is the gas pre-charge pressure, P_a is the accumulator output pressure, P_m is the mean working pressure and n is the adiabatic index.

3.1.4 Hose model

The hose model is used to investigate the potential pressure loss between the accumulator and the cylinder. It assumes the flow rate passing through the hose is proportional to the square root of the pressure drop.

$$Q_a = K_h \sqrt{P_a - P_c} \quad (10)$$

where K_h is the hose pressure loss factor.

3.2 Mechanical model

From (1) to (10), the hydraulic actuator force can be determined based on actuator velocity and valve control signal. In order to complete the simulation model, a mechanical model of the robot leg is needed, which is built using SimMechanics[®], a multi-body mechanical simulation tool in the Simulink[®], as shown in Fig. 5.

This model presents the inertia parameters of the robot leg actuator and describes the prismatic motion between the piston and the cylinder. Additionally, it will be expanded into a full mechanical model of the robot in the future including rigid bodies, revolute joints and the modelling of a hip actuator.

3.3 Closed loop controller

A PI controller is used to achieve the position feedback control of the system, which has been well studied [12] and described in (11).

$$u_c = K_p e + K_i \int e dt \quad (11)$$

where K_p is the proportional gain, K_i is the integral gain and e is position error.

The model equations developed in Section 3.1 are used to create a Simulink[®] simulation model, plus the mechanical model and the PI controller are implemented. Table 2 presents the parameter values in the models.

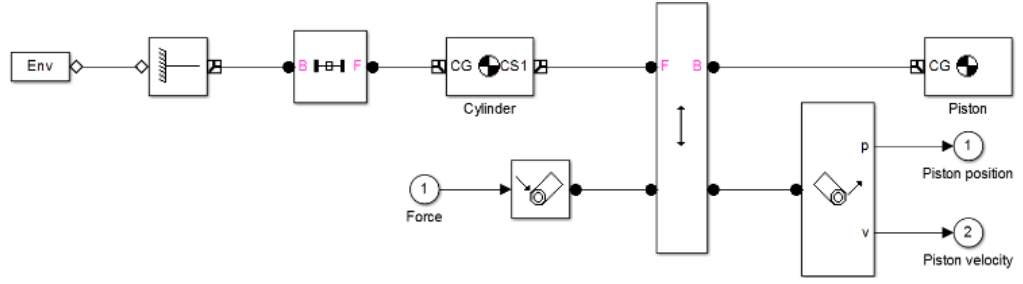


Figure 5. Robot leg model.

Table 2. Values of the physical parameters

Parameters	Symbol	Value	Unit
Supply Pressure	P_s	160×10^5	Pa
Piston Area	A_p	1.13×10^{-4}	m^2
Annulus Area	A_a	0.63×10^{-4}	m^2
Valve Flow Coefficient	K_v	4.89×10^{-8}	$\text{m}^4/\text{s}/\text{N}^{1/2}$
Valve Spool Natural Frequency	ω_v	942.48	rad/s
Valve Spool Damping Ratio	ζ_v	0.7	
Backlash Deadband Width	u_w	0.2	A
Accumulator Pre-charge Pressure	P_0	40×10^5	Pa
Accumulator Initial Gas Volume	V_0	7.5×10^{-5}	m^3
Controller Proportioanl Gain	K_p	2	1/m
Controller Integral Gain	K_i	2	1/(sm)

4. Experimental and simulation results

In order to get a better understanding of this type of compliant hydraulic actuator, the experimental and simulation results are provided according to hydraulic circuits either using or without using the accumulators, which are named the *compliant system* and *stiff system*, respectively. For the *stiff system*, Fig. 6 shows that the piston position is tracking the demand square wave signal poorly, which is related to the hysteresis of the proportional valve. Dither, a high-frequency sinusoidal signal with low amplitude, is added to the driving signal of the valve to overcome the hysteresis effect. The improved position tracking performance of using dither (10% of the maximum amplitude of the valve driving signal at 120 Hz frequency) is shown in Fig. 7.

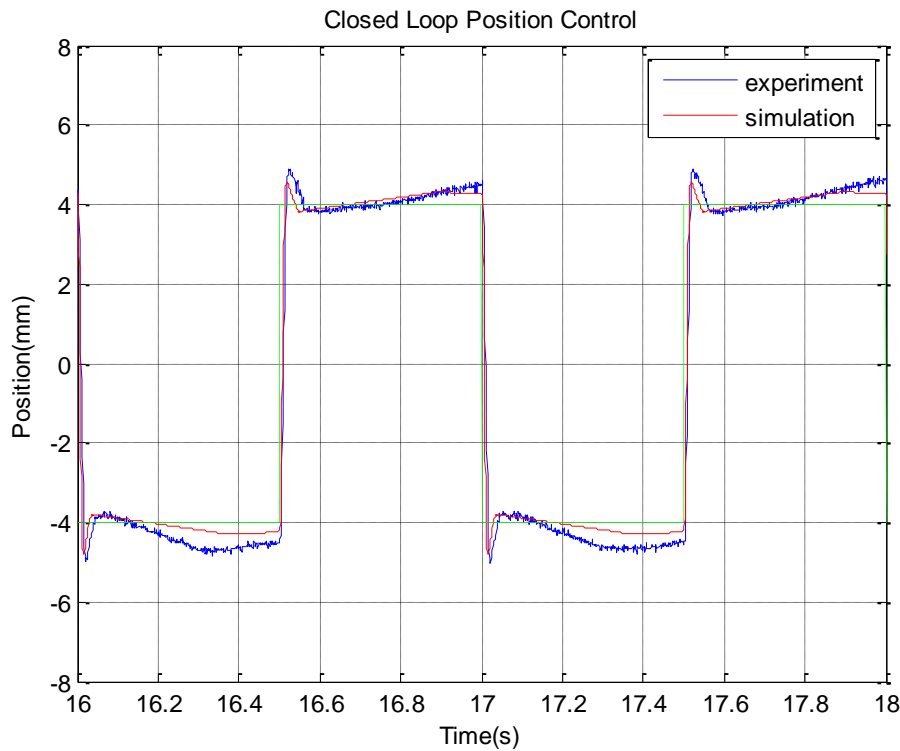


Figure 6. Position tracking of the *stiff system*.

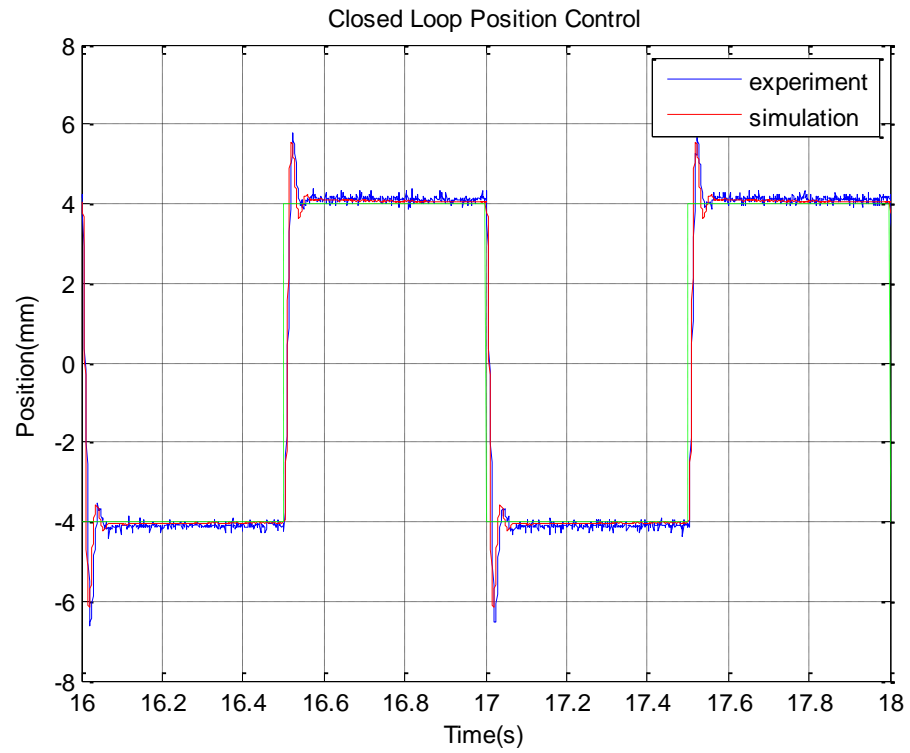


Figure 7. Position tracking of the *stiff* system by adding dither.

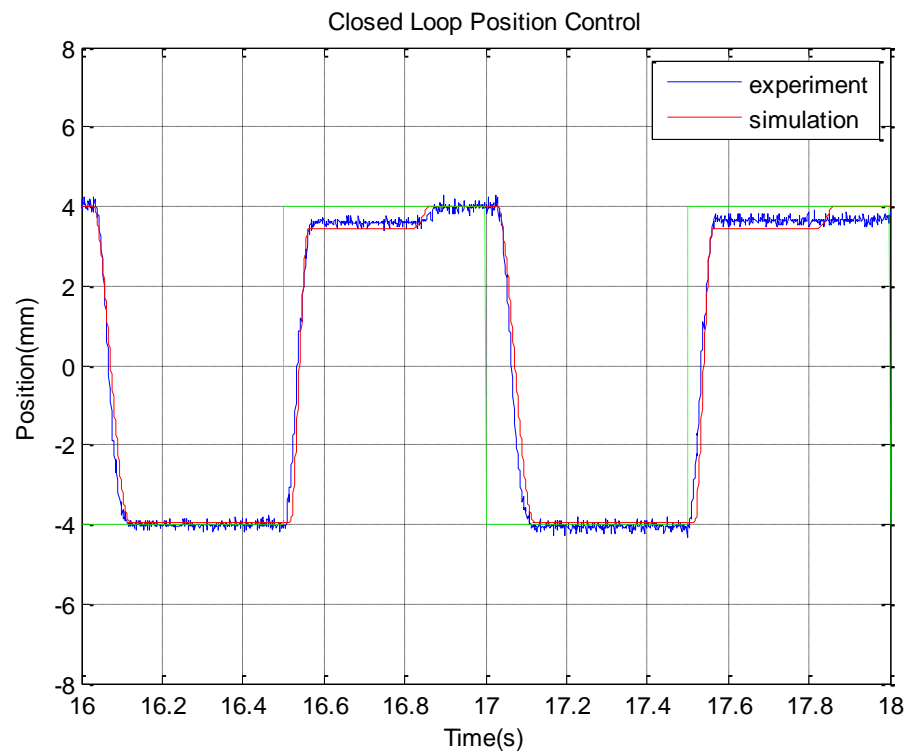


Figure 8. Position tracking of the *compliant* system with square wave demand.

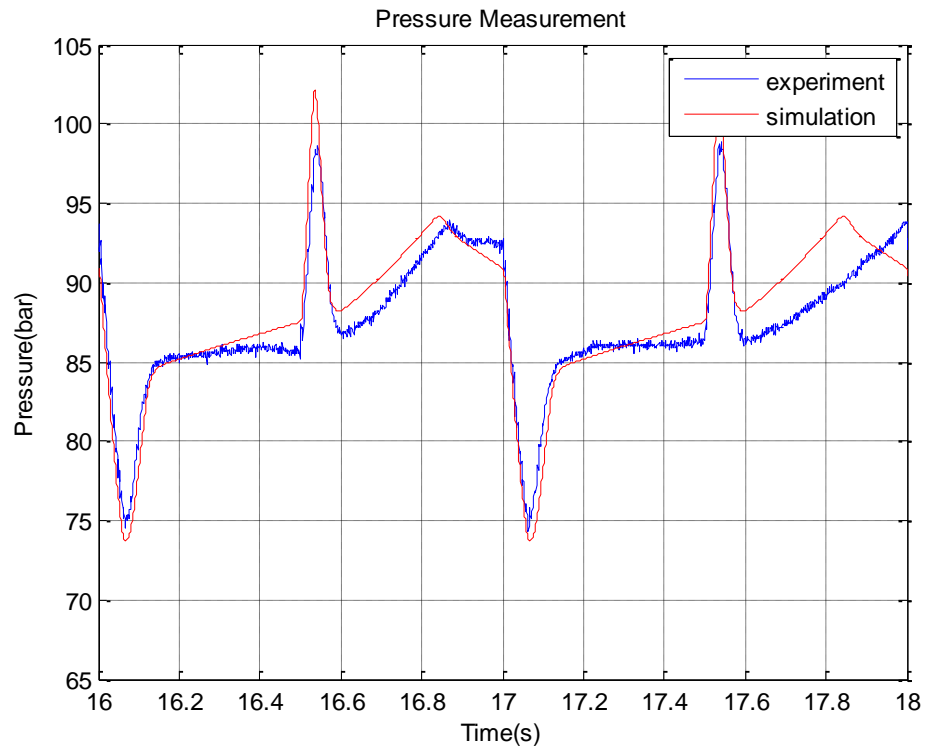


Figure 9. Cylinder pressure for the *compliant system* with square wave demand.

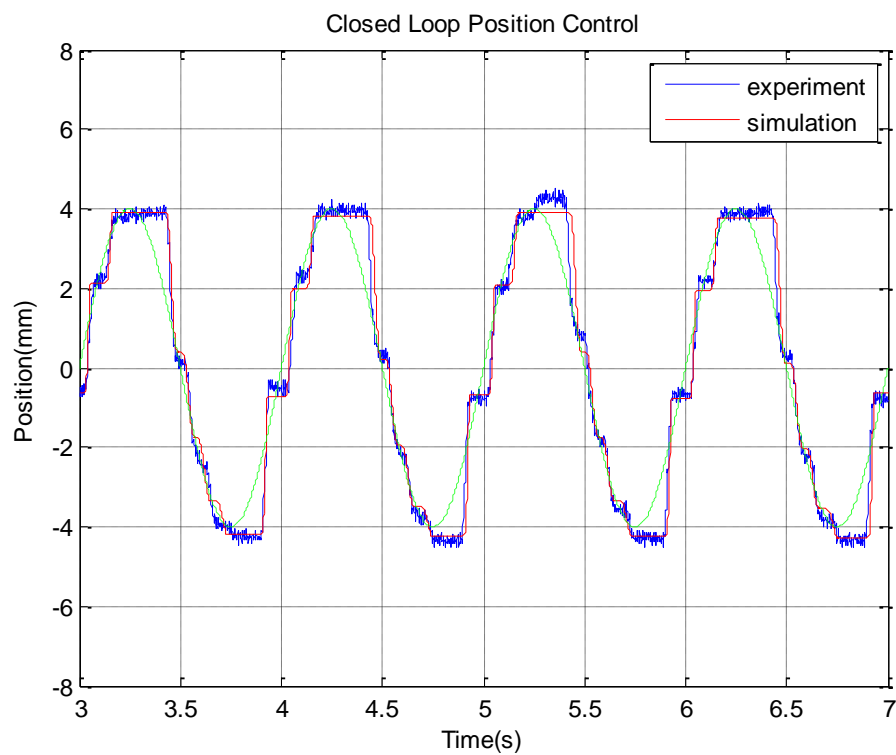


Figure 10. Position tracking of the *compliant system* with sinusoidal demand.

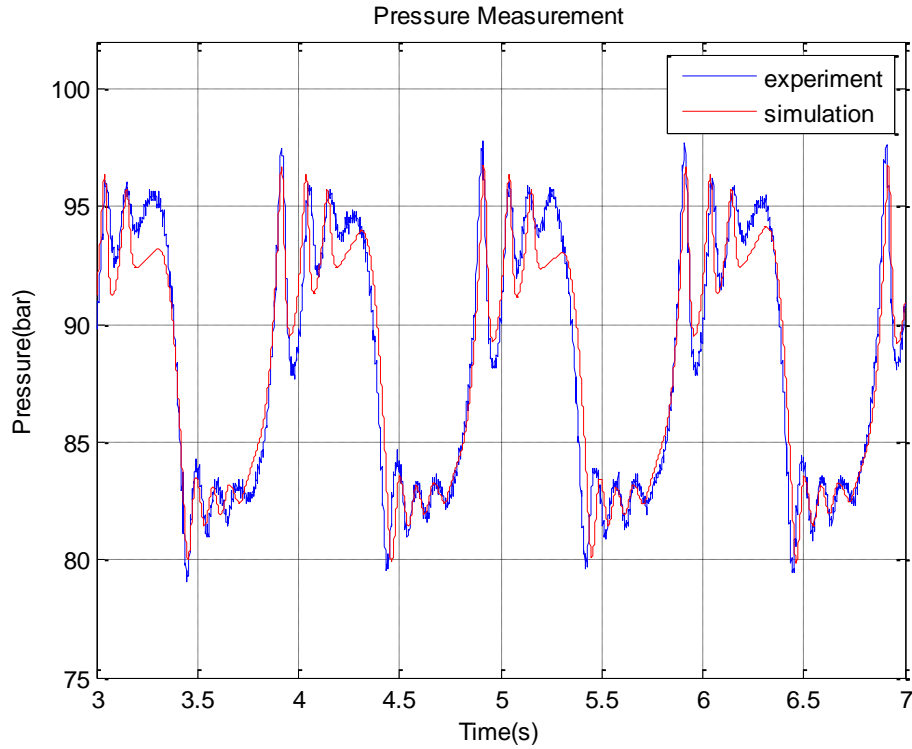


Figure 11. Cylinder pressure of *compliant system* with sinusoidal demand.

For the *compliant system*, the closed loop position tracking is investigated using square wave and sinusoidal demand signals respectively, plus the piston side pressure is measured accordingly.

Fig. 8 and Fig. 10 show that the actuator piston is stationary at some certain points during the movement, whilst Fig. 9 and Fig. 11 indicate that the piston side pressure is increased until the combined force on the piston is large enough to move the piston to the next position. The reason for this performance is mostly due to the friction effect. An estimate of the Coulomb friction, F_c , can be found by calculating the pressure increase while the piston is stalled, and is 105 N.

5. Evaluation of the friction effect

In order to evaluate the friction effect on the compliant actuator, the hydraulic elastance and *error-time factor* are presented in this section. The representations of these factors are given by linearizing the mathematical models in section 3. Resulting in the linear valve model is:

$$q_v = C_x x - C_p p_a \quad (12)$$

where C_x is the valve flow coefficient corresponding to spool displacement and C_p is the valve flow coefficient corresponding to pressure. A detailed linearization of other components is in [12].

5.1 Hydraulic elastance

The fundamental difference between the *compliant system* and *stiff system* is the change in pressure which results from a certain change in trapped oil volume. This property is termed *Hydraulic Elastance*. A larger hydraulic elastance gives a faster pressure change for a certain flow. Thus in the closed loop system, generating a large pressure increase only requires a small position tracking error. Moreover, the larger the hydraulic elastance is, the smaller the system compliance would be. The hydraulic elastance for each system is given in (13) and (14).

$$E_s = \frac{B}{V_t} \quad (13)$$

where E_s is the hydraulic elastance of *stiff system*, B is the oil bulk modulus and V_t is the trapped oil volume in the actuator.

$$E_c = \frac{nP_m}{V_m} \quad (14)$$

where E_c is the hydraulic elastance of the *compliant system*, P_m is mean working pressure and V_m is the corresponding gas volume.

5.2 Error-time factor

As Fig. 8 shows, when the piston is stalled, the position error leads to a certain opening area of the valve orifice which allows the flow to be delivered into the accumulator to build up the pressure. In this case, assuming the pressure change in the actuator is small to overcome the friction, then C_p in (12) is neglectable. Thus, the system block diagram is shown in Fig. 12 and (15) describes the required position tracking error in terms of friction when the piston is stationary.

$$e_p = \frac{sF_f}{E_h K_p C_x A_p} \quad (15)$$

where e_p is the position tracking error and M is the load mass. Rearranging (15) gives an *error-time factor* that is introduced to link the friction effect with system compliance. It is a factor used to represent the length of time that an error must be sustained in order to overcome the Coulomb friction, as (16) shows.

$$\int e_p dt = \frac{F_c}{E_h K_p C_x A_p} \quad (16)$$

Taking the $F_c=105$ N into account, Table 3 presents the theoretical values of hydraulic elastance and *error-time factor* for each system. In Fig. 8, there is a constant e_p of 0.4 mm, theoretically, it takes approximately 0.21 s for the *compliant system* to build up the pressure and only 4.47×10^{-4} s for the *stiff system*. This significant difference makes the friction effect is more observable for the *compliant system*.

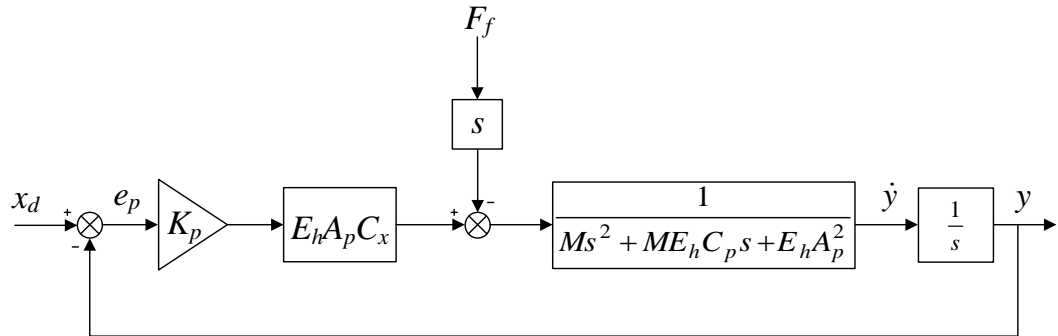


Figure 12. Rearranged system block diagram.

Table 3. Theoretical values

Parameters	Compliant System	Stiff System	Unit
Hydraulic Elastance	4.24×10^{11}	1.99×10^{14}	N/m ⁵
Error-time Factor	8.4×10^{-2}	1.79×10^{-4}	mms

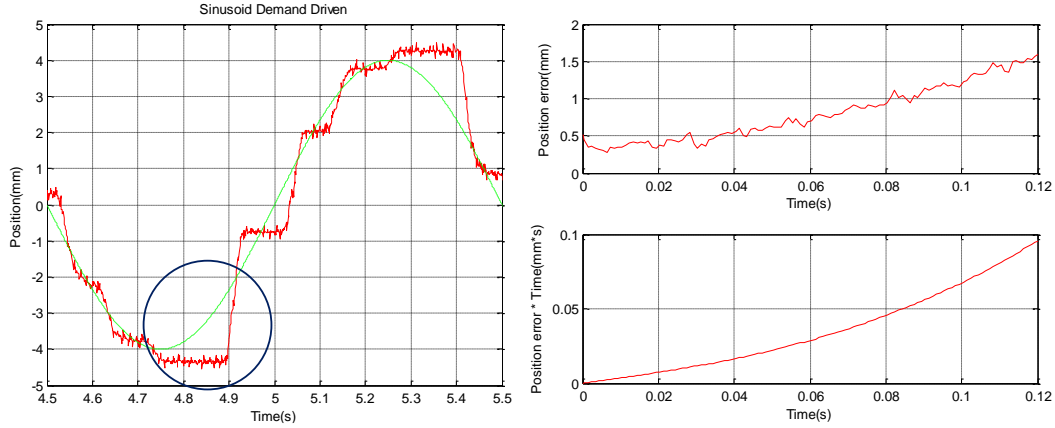


Figure 13. Investigating the value of *error-time factor* using sinusoid demand.

With a sinusoidal demand, there is a continually changing position error giving a changing flow rate. As Fig.13 shows, if e_p is integrated during the time period when the piston is stalled, the resulting *error-time factor* is 0.09 mms, which is quite similar to the theoretical value.

6. Conclusion

The study of a compliant hydraulic actuator for running robots has been undertaken in this paper. This actuator is experimentally tested on a bipedal hopping robot. A PI controller is used to achieve the position feedback control of the actuator. The non-linear simulation model is successfully developed to explain the main findings of the experimental results, such as the hysteresis in the valve and the friction in the actuator. In particular, an *error-time factor* is used to link the friction effect with system compliance. The quantified analysis of *error-time factor* could help with selecting appropriate components for this application.

Moreover, the analysis indicates that in order to reduce the tracking error caused by friction, the options are to:

- Reduce the friction level. In reality, the friction comes from elastomeric seals around the piston head and rod gland, and lower friction is associated with greater leakage.

- Increase hydraulic elastance. The increase of the hydraulic elastance means the increase of system spring stiffness i.e. loss of actuator compliance.

A sensible design approach is to identify the friction level first and then investigate the *error-time factor* to estimate the maximum compliance that is achievable. If this is not high enough, then another approach to incorporating compliance, i.e. not through hydraulic means, needs to be found.

References


- [1] Bhatti, Jawaad, A. R. Plummer, Pejman Irvani, and Beichen Ding. "A survey of dynamic robot legged locomotion." In Fluid Power and Mechatronics (FPM), 2015 International Conference on, pp. 770-775. IEEE, 2015.
- [2] Zhou, Xiaodong, and Shusheng Bi. "A survey of bio-inspired compliant legged robot designs." *Bioinspiration & biomimetics* 7, no. 4 (2012): 041001.
- [3] Liu, Guan-Hong, Hou-Yi Lin, Huai-Yu Lin, Shao-Tuan Chen, and Pei-Chun Lin. "A bio-inspired hopping kangaroo robot with an active tail." *Journal of Bionic Engineering* 11, no. 4 (2014): 541-555.
- [4] Hodgins, Jessica K., and M. N. Raibert. "Adjusting step length for rough terrain locomotion." *IEEE Transactions on Robotics and Automation* 7, no. 3 (1991): 289-298.
- [5] F. Daerden, and D. Lefeber, "Pneumatic artificial muscles: actuators for robotics and automation." *European journal of mechanical and environmental engineering* 47, no. 1 (2002): 11-21.
- [6] Raibert, Marc H. *Legged robots that balance*. MIT Press, 1986.
- [7] Chou, Ching-Ping, and Blake Hannaford. "Measurement and modelling of McKibben pneumatic artificial muscles." *IEEE Transactions on Robotics and Automation* 12, no. 1 (1996): 90-102.
- [8] Hyon, S. H., T. Emura, and T. Mita. "Dynamics-based control of a one-legged hopping robot." *Proceedings of the Institution of Mechanical Engineers, Part I: Journal of Systems and Control Engineering* 217, no. 2 (2003): 83-98.
- [9] Poulakakis, Ioannis, Evangelos Papadopoulos, and Martin Buehler. "On the stability of the passive dynamics of quadrupedal running with a

bounding gait." *The International Journal of Robotics Research* 25, no. 7 (2006): 669-687.

- [10] Palmer, Luther R., David E. Orin, Duane W. Marhefka, James P. Schmiedeler, and Kenneth J. Waldron. "Intelligent control of an experimental articulated leg for a galloping machine." In *Robotics and Automation, 2003. Proceedings. ICRA'03. IEEE International Conference on*, vol. 3, pp. 3821-3827. IEEE, 2003.
- [11] Plummer, Andrew R. "A detailed dynamic model of a six-axis shaking table." *Journal of earthquake engineering* 12, no. 4 (2008): 631-662.
- [12] Konami, Shizurou, and Takao Nishiumi. *Hydraulic Control Systems: Theory and Practice*. 2017.

Appendix 2

Statement of Authorship

This declaration concerns the article entitled:							
Investigating balancing control of a standing bipedal robot with point foot contact							
Publication status (tick one)							
draft manuscript	<input type="checkbox"/>	Submitted	<input type="checkbox"/>	In review	<input type="checkbox"/>	Accepted	<input type="checkbox"/>
Published	<input checked="" type="checkbox"/>						
Publication details (reference)	<p>Ding, B., Plummer, A. and Iravani, P., 2016. Investigating balancing control of a standing bipedal robot with point foot contact. <i>IFAC-PapersOnLine</i>, 49(21), pp.403-408.</p> <p>Conference title: 'the 7th IFAC Symposium on Mechatronic Systems & 15th Mechatronics Forum International Conference (Mechatronics 2016)'</p>						
Candidate's contribution to the paper (detailed, and also given as a percentage).	<p>Formulation of ideas: Jointly with supervisors (50%).</p> <p>Design of methodology: Modelling was developed solely by the candidate (100%). Results/analysis/methodology mainly by the candidate (70%).</p> <p>Simulation work: Solely the candidate (100%)</p> <p>Presentation of data in conference format: Solely the candidate (100%)</p>						
Statement from Candidate	This paper reports on original research I conducted during the period of my Higher Degree by Research candidature.						
Signed						Date	06/03/2019

PAPER 2: Investigating balancing control of a standing bipedal robot with point foot contact

Beichen Ding*, Andrew Plummer*, Pejman Iravani*

*Centre for PTMC, Department of Mechanical Engineering, University of Bath, Bath, UK

Abstract

Comparing with wheeled or tracked moving machines, legged robots have potential advantages, especially when considering moving on discontinuous or rough terrain. For many bipedal robots, balance in the standing position is easy to maintain by having sufficient contact area with the ground. For some bipedal robots, the Zero Moment Point (ZMP) control method has been successfully implemented in which the centre of mass is aligned above the support area. However, the balancing issue while standing becomes challenging when the contact area is very small. This paper presents a controller which is developed to balance a bipedal robot with coupled legs which have point foot contact. It is necessary to investigate the non-linear characteristics of the system. A pole-placement control method is used, and noise issues with sensing higher motion derivatives are investigated. The simulation-based evaluation indicates limitations that need to be addressed before experimental implementation.

7. Introduction

Considering moving on rough terrains, such as soft and uneven surfaces, legged robots have potential advantages comparing with wheeled or tracked vehicles (Hardarson, 1970). The isolated foot support area avoids the requirement for continuous ground. In the last few decades, bipedal robots have attracted researchers' attention. Several successful two-leg walking robots have been presented to show the motion mechanism principles, such as Asimo (Sakagami, 2002), ATLAS and PETMAN (Raibert, 2010). Considering the standing position, most of these platforms solve the balancing problem by having sufficient foot contact area with the ground. The Zero Moment Point control method has been successfully implemented to maintain balance by controlling the centre of mass above the support area while the robot is standing or slowly walking (Erbatur, 2002). An intermittent control strategy might be a solution to solve the body sway

issue with a smaller foot contact (Bottaro, 2005). However, the problem is still very challenging when the support area is limited to point contact.

The Bath Bipedal Hopper (BBH) is a small size hydraulic actuated bipedal hopping robot, which is developed to design and test advanced controllers. The foot support area of the BBH is very small and can be approximated by a point. One mode of operation is balancing while standing rather than hopping, and control for this mode is considered in this paper. A double inverted pendulum model is used to represent the BBH. A pole placement controller is developed and tested in simulation. Evaluation indicates the feasibility of this method and makes suggestions for further research.

8. Hardware of the Bath Bipedal Hopper

As Fig. 1 shows, the basic design concept of the BBH comes from kangaroos, which are the largest animal using a bipedal hopping mechanism on the planet. The BBH has an upper body and two lower legs. The upper body consists of the main controller, which is an industrial PC (PC104 format), a manifold integrated with proportional valves and supporting framework. A hydraulic cylinder actuates the fore-aft hip rotation of both legs, i.e. this motion of the legs is coupled together. The two lower legs are hydraulic actuators with position sensors in parallel. There is an inertial measurement unit (IMU) attached to the upper body to measure the body rotation angle. An encoder is used to measure the angle at the hip point. Each foot consists of an aluminium alloy hemisphere covered in hard rubber. The BBH was designed to achieve locomotion using kangaroo-like hopping. Fig. 2 shows a simplified 3D model of BBH. Table 1 shows a list of some key components.

Table 1. Key components.

Components	Model	Quantity
Valves	Moog E242	3
Cylinder	Hoerbigger LB6 series	3
Position sensor	Active sensor PLS0956	2
Encoder	Hengstler RI32	1
IMU	ADIS16300	1
Controller PC	Terasoft Microbox 2000	1

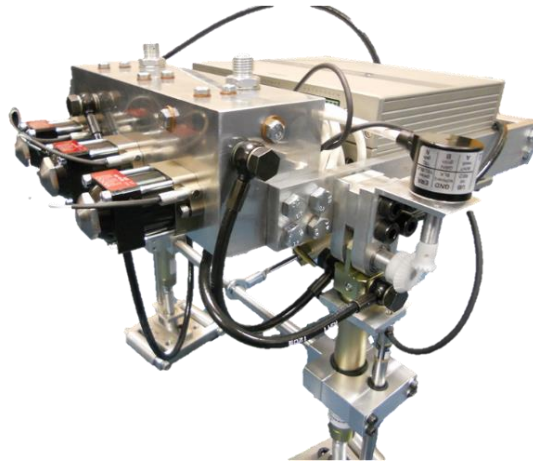


Figure 1. Hardware of the Bath Bipedal Hopper.

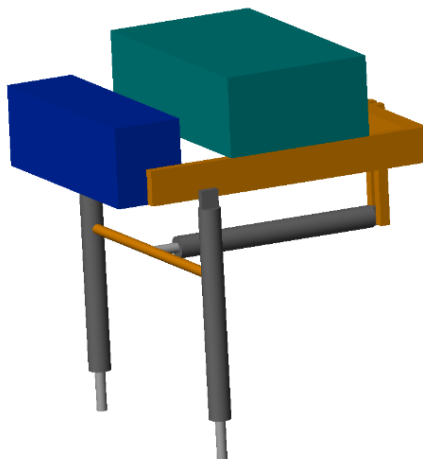


Figure 2. Simplified 3D model of the BBH.

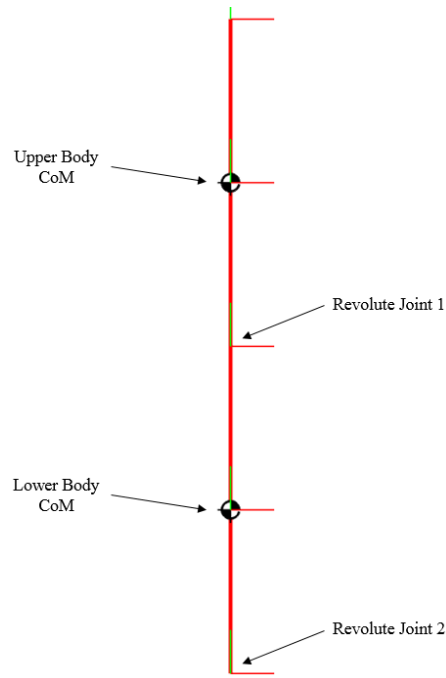


Figure 3. The modified double inverted pendulum model.

9. Modelling

9.1 Double inverted pendulum model

The inverted pendulum model has been successfully used to help design one-leg hopping robots (Kajita, 1989). A modified double inverted pendulum model is appropriate to analyse the motion of the BBH. As shown in Fig. 3, the model consists of two rigid bodies, an upper body and a lower body (representing the leg-pair), connected with revolute joint 1 (hip joint). The bottom of the lower body, i.e. the foot is connected to the ground using revolute joint 2 in the model. Using small angle approximations, we are trying to maintain the combined centre of mass (CoM) of the overall model vertically above revolute joint 2 by applying an active torque at revolute joint 1.

9.2 Dynamic analysis

The force analysis of the upper body is shown in Fig. 4.

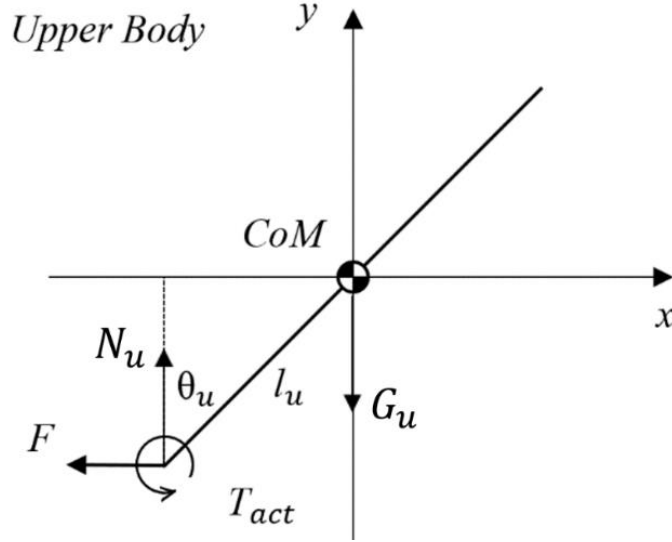


Figure 4. Upper body force analysis.

Consider the force on the upper body and taking moments about the revolute joint 1 gives (1), (2) and (3):

$$-F = M_u (l_u \ddot{\theta}_u + l_l \ddot{\theta}_l) \quad (1)$$

$$T_{act} - M_u g l_u \theta_u = J_u \ddot{\theta}_u \quad (2)$$

$$J_u = \frac{4}{3} M_u l_u^2 \quad (3)$$

where M_u is the mass of the upper body, l_u is the length from the upper body's CoM to revolute joint 1, l_l is the length of the lower body, J_u is the moment of inertia of the upper body. Combine (1), (2) and (3) gives:

$$\frac{\theta_u}{T_{act}} = \frac{3}{4M_u l_u^2 s^2 + 3M_u g l_u} \quad (4)$$

Fig. 5 presents the force analysis of the lower body; taking a moment about revolute joint 2 gives (5) and (6).

$$-Fl_l - M_u g l_l \theta_l - \frac{1}{2} M_l g l_l \theta_l = J_l \ddot{\theta}_l \quad (5)$$

$$J_l = \frac{1}{3} M_l l_l^2 \quad (6)$$

M_l is the mass and J_l is the moment of inertia of the lower body. Combining (1), (5) and (6) gives:

$$\frac{\theta_u}{\theta_l} = \frac{\left(\frac{1}{3} M_l l_l - M_u l_l \right) s^2 + M_u g + \frac{1}{2} M_l g}{M_u l_u s^2} \quad (7)$$

Considering the overall model, the combined CoM position is shown in Fig. 6.

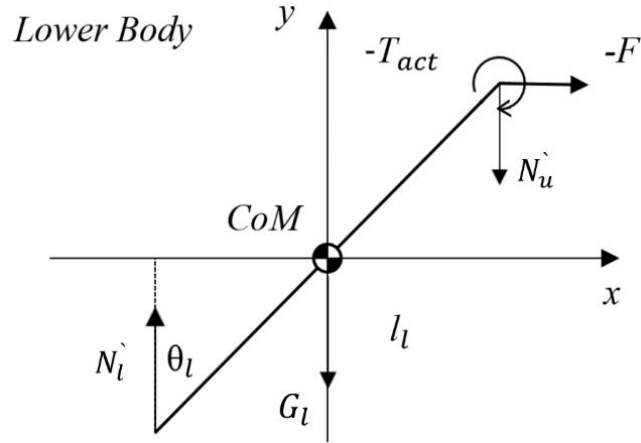


Figure 5. Lower body force analysis.

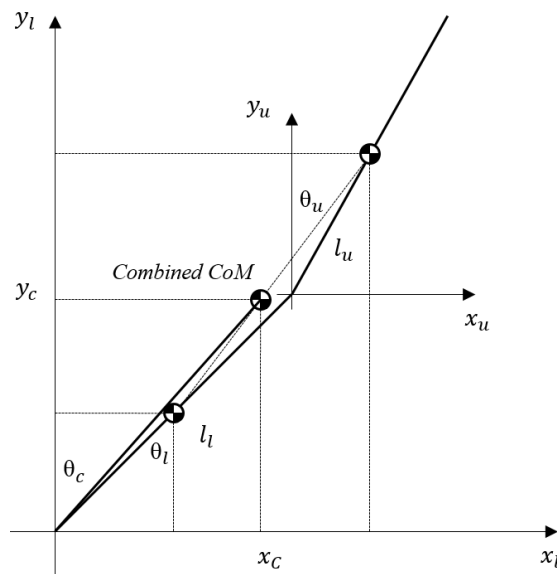


Figure 6. The position of combined CoM.

According to the geometry relations, the position of the combined CoM can be expressed as (8) and (9):

$$x_c = \left(\frac{1}{2} l_l \theta_l + l_u \theta_u \right) \frac{M_l}{M_l + M_u} + \frac{1}{2} l_l \theta_l \quad (8)$$

$$y_c = \left(\frac{1}{2} l_l + l_u \right) \frac{M_l}{M_l + M_u} + \frac{1}{2} l_l \quad (9)$$

Considering small angle approximation:

$$\tan \theta_c = \frac{x_c}{y_c} = \frac{l_l \theta_l (2M_l + M_u) + 2l_u \theta_u M_l}{l_l (2M_l + M_u) + 2l_u M_l} \approx \theta_c \quad (10)$$

If,

$$p = \frac{2l_u M_u}{l_l (2M_u + M_l)} \quad (11)$$

Then,

$$\theta_c = k_1 \theta_l + k_2 \theta_u \quad (12)$$

where

$$k_1 = \frac{1}{p+1} \quad (13)$$

$$k_2 = \frac{p}{p+1} \quad (14)$$

Combining (4), (7) and (12) gives the plant model:

$$\frac{\theta_c}{T_{act}} = \frac{3k_2 k_{l1} s^2 + 3k_l k_{u3} + 3k_2 k_{l2}}{4k_{u1} k_{l1} s^4 + (k_{l1} k_{u2} + 4k_{u1} k_{l2}) s^2 + k_{u2} k_{l2}} \quad (15)$$

Where,

$$k_{u1} = 4M_u l_u^2;$$

$$k_{u2} = 3M_u g l_u ;$$

$$k_{u3} = M_u l_u ;$$

$$k_{l1} = \frac{1}{3} M_l l_l - M_u l_l ;$$

$$k_{l2} = M_u g + \frac{1}{2} M_l g .$$

10. Controller design

According to the plant model, the pole-placement method can be used to develop the controller. The closed-loop block diagram is shown in Fig. 7. The controller is implemented using two digital filters, $1/F(s)$ and $G(s)$, where $1/F(s)$ is a forward path compensator and $G(s)$ plays the same role as the state feedback gains in a state-feedback controller.

The closed-loop transfer function of the block diagram is:

$$\frac{\theta_c}{\theta_d} = \frac{N(s)}{D(s)F(s) + N(s)G(s)} \quad (16)$$

If,

$$A(s) = D(s)F(s) + N(s)G(s) \quad (17)$$

Then,

$$\frac{\theta_c}{\theta_d} = \frac{N(s)}{A(s)} \quad (18)$$

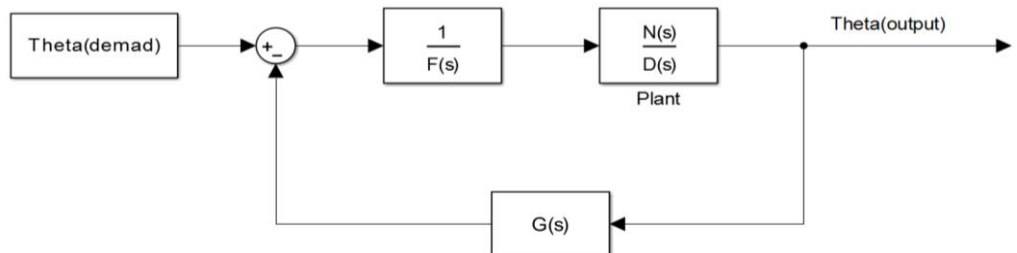


Figure 7. Block diagram of pole placement controller.

The roots of polynomial $A(s)$ indicate the stability and the time domain response of the whole system. By specifying different polynomials of $G(s)$ and $F(s)$, the roots of $A(s)$ can be arranged at any desired positions. According to the plant model:

$$N(s) = n_2 s^2 + n_0 \quad (19)$$

$$D(s) = d_4 s^4 + d_2 s^2 + d_0 \quad (20)$$

It is necessary to have the same number of equations and unknowns, which determines the degrees of polynomials $G(s)$ and $F(s)$ (Plummer, A. R. 1991).

Define n and m as the degree of $G(s)$ and $F(s)$, respectively. Using,

$$\deg F(s) = n - 1 = 1 \quad (21)$$

$$\deg G(s) = m - 1 = 3 \quad (22)$$

$$\deg A(s) = n + m - 1 = 5 \quad (23)$$

Therefore,

$$F(s) = f_1 s + f_0 \quad (24)$$

$$G(s) = g_3 s^3 + g_2 s^2 + g_1 s + g_0 \quad (25)$$

$$A(s) = a_5 s^5 + a_4 s^4 + a_3 s^3 + a_2 s^2 + a_1 s + a_0 \quad (26)$$

The coefficients in $G(s)$ and $F(s)$ can be calculated by solving (17) with polynomials as given in (19), (20), (24), (25) and (26), i.e. solving the following matrix equation:

$$\begin{bmatrix} a_5 \\ a_4 \\ a_3 \\ a_2 \\ a_1 \\ a_0 \end{bmatrix} = \begin{bmatrix} d_4 & 0 & n_2 & 0 & 0 & 0 \\ 0 & d_4 & 0 & n_2 & 0 & 0 \\ d_2 & 0 & n_0 & 0 & n_2 & 0 \\ 0 & d_2 & 0 & n_0 & 0 & n_2 \\ d_0 & 0 & 0 & 0 & n_0 & 0 \\ 0 & d_0 & 0 & 0 & 0 & n_0 \end{bmatrix} \times \begin{bmatrix} f_1 \\ f_0 \\ g_3 \\ g_2 \\ g_1 \\ g_0 \end{bmatrix} \quad (27)$$

$A(s)$ will be chosen as the denominator of a fifth-order Butterworth filter. A Butterworth filter has a flat frequency response in the passband. Therefore, determining the vector of $G(s)$ and $F(s)$ coefficients gives a controller achieving these desired closed-loop poles. A simple simulation test can be done by using the physical configuration parameters of the BBH, as Table 2 shows. Fig. 8 shows the step response with these parameters. With a higher cut-off frequency, the system presents a faster step response (as expected) and acceptable overshoot. However, in SimMechanics®, in order to avoid breaking down the structure, the cut-off frequency of the desired polynomial should be selected appropriately to compromise between the step response time and the overshoot.

Table 2. Physical parameters

Parameters	Symbol	Value	Unit
Mass of the upper body	M_u	7.5	kg
Mass of the lower leg	M_l	0.75	kg
Length of the upper body	l_u	44.4	mm
Length of the lower leg	l_l	95	mm
Gravitational acceleration	g	9.81	m/s ²

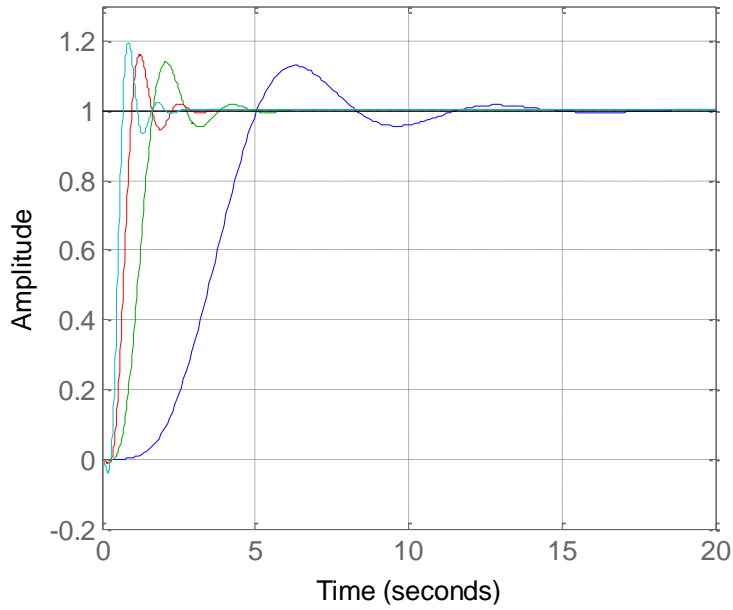


Figure 8. Step response with closed-loop poles for cut-off frequencies of 7 rad/s, 5 rad/s, 3 rad/s and 1 rad/s.

11. Evaluation of the controller

11.1 Minimize the jerk gain

There are four unknowns in $G(s)$, which are the feedback gains related to the output angle, angular velocity, angular acceleration and the derivative of angular acceleration, also named the jerk. It is necessary to minimize the jerk gain, or even make it as zero, because of the noise caused by derivative calculations. By setting the jerk gain as zero, $G(s)$ is going to be a second-order polynomial and $F(s)$ can be a constant value. Such as:

$$F(s) = f_0 \quad (28)$$

$$G(s) = g_2 s^2 + g_1 s + g_0 \quad (29)$$

Additionally, $A(s)$ should be a fourth-order polynomial, which is:

$$A(s) = a_4s^4 + a_3s^3 + a_2s^2 + a_1s + a_0 \quad (30)$$

Then, there will be four unknowns in five equations, which will not give a minimal degree of the solution. In order to solve this set of equations, an extra unknown τ can be introduced by setting the $A(s)$ as:

$$A(s) = (\tau s + 1)(a_{m3}s^3 + a_{m2}s^2 + a_{m1}s + a_{m0}) \quad (31)$$

Combining (17), (19), (20), (28), (29) and (31) gives:

$$\begin{bmatrix} 0 \\ a_{m3} \\ a_{m2} \\ a_{m1} \\ a_{m0} \end{bmatrix} = \begin{bmatrix} d_4 & n_2 & 0 & 0 & -a_{m3} \\ 0 & 0 & n_2 & 0 & -a_{m2} \\ d_2 & n_0 & 0 & n_2 & -a_{m1} \\ 0 & 0 & n_0 & 0 & -a_{m0} \\ d_0 & 0 & 0 & n_0 & 0 \end{bmatrix} \times \begin{bmatrix} f_0 \\ g_2 \\ g_1 \\ g_0 \\ \tau \end{bmatrix} \quad (32)$$

As in the last section, this can be solved for the $G(s)$ and $F(s)$ coefficients and the extra unknown τ . However, τ needs to be evaluated to ensure that it is always a positive value, which means it is a stable pole position. τ can be calculated from (32), which for the plant parameters in Table 2, gives:

$$\tau = -\frac{a_{m1}}{a_{m0} + 0.0095a_{m2}} - \frac{a_{m3}}{105.1349a_{m0} + a_{m2}} \quad (33)$$

$A(s)$ is specified to represent stable poles, as a result, a_{m0} , a_{m1} , a_{m2} and a_{m3} are positive values. According to (33), τ is always negative. In other words, a pole in $A(s)$ is always placed in the right half plane, so the closed-loop system is not stable. Therefore, the jerk feedback cannot be cancelled or avoided in the controller.

11.2 Noise tolerance

Rather than simply attempting to avoid using jerk feedback, a more general approach to reducing the effect of noisy feedback signals on control performance is considered in this section.

As Fig. 9 shows, by including $H(s)$ as a command filter, (34) to (36) indicates that the reciprocal of $H(s)$ can be used as a low pass filter within the closed loop controller to attenuate the noise without altering the response of the whole system.

$$y = \frac{N(s)H(s)}{D(s)F(s) + N(s)G(s)} r + \frac{D(s)F(s)}{D(s)F(s) + N(s)G(s)} e \quad (34)$$

If,

$$D(s)F(s) + N(s)G(s) = A_m(s)H(s) \quad (35)$$

Substituting (35) into (34):

$$y = \frac{N(s)}{A_m(s)} r + \frac{D(s)F(s)}{A_m(s)H(s)} e \quad (36)$$

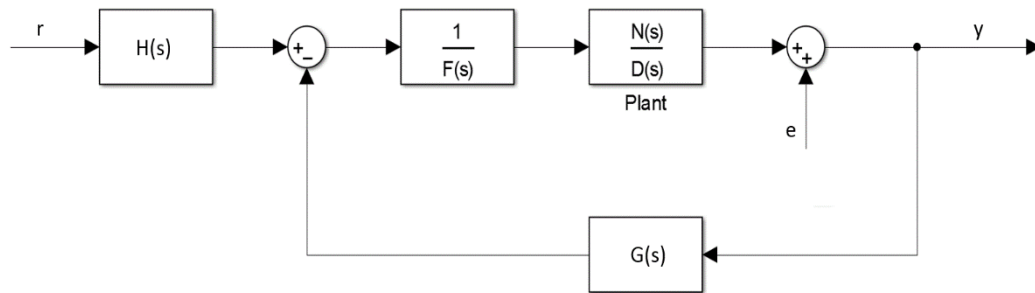


Figure 9. Closed-loop block diagram with $H(s)$ filter.

Here, e is measurement noise. According to the previous discussion, $A_m(s)H(s)$ can be given by a polynomial with desired stable poles, and the steady-state gain is calculated to give unity gain in the closed loop. If $H(s)$ is specified as the denominator of a second-order low-pass filter, which includes two roots of the full characteristic polynomial $A(s)$, it can be used to attenuate the noise without influencing the servo performance of the system. In order to give a unity steady state gain:

$$N(0) = A_m(0) \quad (37)$$

However, it is necessary to evaluate how the noise is affected by using different $H(s)$. Fig. 10 is the noise amplitude against frequency according to different $H(s)$. Here $A_m(s)$ has the poles of a third order Butterworth filter with cut-off frequency. As the cut-off frequency of $H(s)$ reduces, noise above 2Hz is increasingly attenuated, at the expense of low-frequency noise amplification. However, another aspect also needs to be investigated which is the sensitivity of the control signal to noise, as Fig. 11 shows.

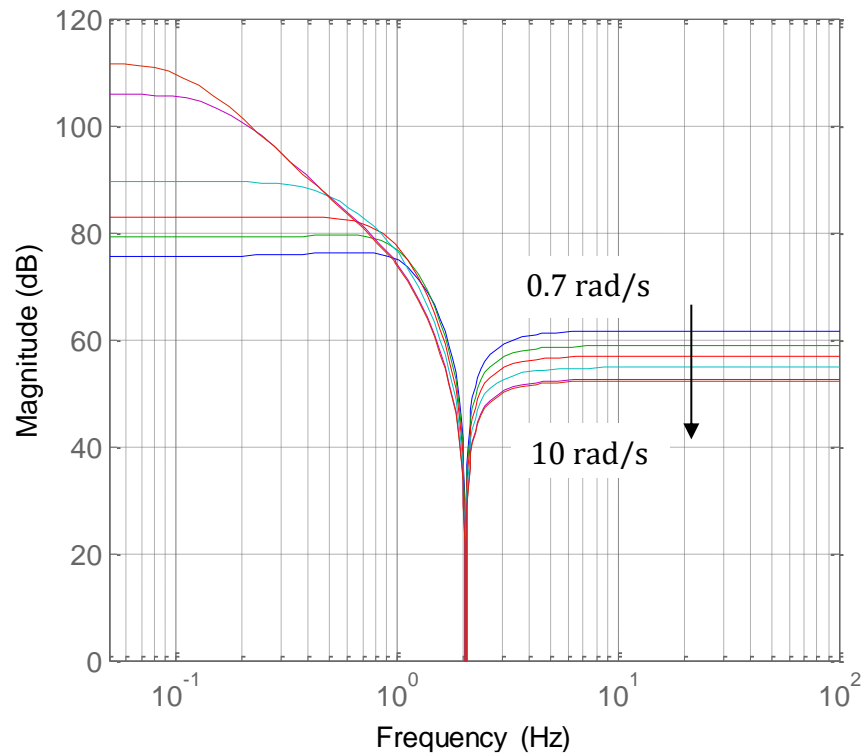


Figure 10. Frequency response of output angle (y) over noise (e) for different cut-off frequency of $H(s)$, as 0.7 rad/s, 1 rad/s, 3 rad/s, 5 rad/s, 7 rad/s and 10 rad/s.

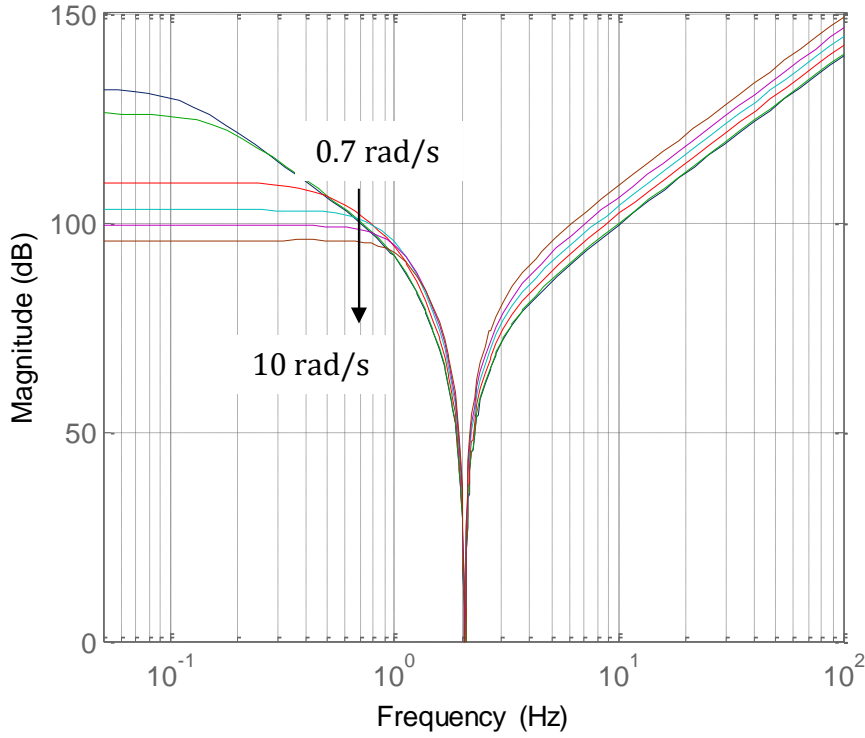


Figure 11. Frequency response of control signal (u) over noise (e) for different cut-off frequency of $H(s)$, as 0.7 rad/s, 1 rad/s, 3 rad/s, 5 rad/s, 7 rad/s and 10 rad/s.

At high frequencies, the noise amplification is increasing dramatically, but it is lower with $H(s)$ which has a lower cut-off frequency. This might be caused by the unstable $D(s)$. These results are influenced by pole selection, which is discussed further in (Chen, 1995).

12. Conclusions

Investigation of the standing balance control of a small size bipedal robot with point foot contact has been undertaken in this paper. A pole placement method is used to develop the controller, based on a double inverted pendulum robot model. According to the calculation, the minimal degree of solution indicates the minimal number of motion feedback states (or position derivatives); in this case, up to the third derivative (jerk) is required. Although the balancing servo-performance appears promising, frequency response analysis shows that measurement noise could be problematic, particularly as it affects the control signal. High-frequency

noise can, however, be reduced to some extent by including lower frequency desired closed loop poles which are cancelled by a command filter.


A state estimator or observer can be built to estimate state variable values without requiring differentiation of measured signals. According to hardware limitations, experimental results will be presented to demonstrate the feasibility of this controller in further research.

References

- [1] Bottaro, A., Casadio, M., Morasso, P. G., & Sanguineti, V. (2005). Body sway during quiet standing: is it the residual chattering of an intermittent stabilization process?. *Human movement science*, 24(4), 588-615.
- [2] Chen, C. T. (1995). *Linear system theory and design*. Oxford University Press, Inc.
- [3] Erbatur, K., Okazaki, A., Obiya, K., Takahashi, T., & Kawamura, A. (2002). A study on the zero moment point measurement for biped walking robots. In *Advanced Motion Control, 2002. 7th International Workshop on* (pp. 431-436). IEEE.
- [4] Hardarson, F. (1970). *Locomotion for difficult terrain*. Dept. mach. des.
- [5] Kajita, S. (1989). *Method and apparatus for dynamic walking control of robot*. US, US4834200.
- [6] Plummer, A. R. (1991). *Digital control techniques for electrohydraulic servosystems* (Doctoral dissertation, University of Bath).
- [7] Raibert, M. (2010, December). *Dynamic legged robots for rough terrain*. In *Humanoid Robots (Humanoids), 2010 10th IEEE-RAS International Conference on* (pp. 1-1). IEEE.
- [8] Sakagami, Y., Watanabe, R., Aoyama, C., Matsunaga, S., Higaki, N., & Fujimura, K. (2002). The intelligent ASIMO: System overview and integration. In *Intelligent Robots and Systems, 2002. IEEE/RSJ International Conference on* (Vol. 3, pp. 2478-2483). IEEE.

Appendix 3

Statement of Authorship

This declaration concerns the article entitled:							
A novel self-excited hopping controller for legged robots							
Publication status (tick one)							
draft manuscript		Submitted	<input checked="" type="checkbox"/>	In review		Accepted	
Publication details (reference)	Submitted to 'IEEE Transactions on Control Systems and Technology'						
Candidate's contribution to the paper (detailed, and also given as a percentage).	<p>Formulation of ideas: Ideas developed by candidate in discussion with supervisors (70%).</p> <p>Design of methodology: Experimental/simulation methodology is solely by the candidate (100%). Results analysis methodology is mainly done by the candidate (80%).</p> <p>Experimental work: Solely the candidate (100%).</p> <p>Presentation of data in journal format: Solely the candidate (100%).</p>						
Statement from Candidate	This paper reports on original research I conducted during the period of my Higher Degree by Research candidature.						
Signed						Date	06/03/2019

PAPER 3: A novel self-excited hopping controller for legged robots

Beichen Ding*, Andrew Plummer*, Pejman Iravani*

*Centre for PTMC, Department of Mechanical Engineering, University of Bath, Bath, UK

Abstract

Legged robots are moving machines that are potentially capable of traversing rough or uneven terrain. Servo-hydraulics is highly suitable for robot leg actuation due to the high power density and quick response. Motion control of hydraulically-actuated mono-legged or bipedal hopping robot is challenging due to highly nonlinear system dynamics. For most hopping height controllers, the transition between flight and stance phases needs to be detected to accomplish different control actions, and the corresponding state variables need to be measured, e.g. the body vertical position, and the corresponding velocity and acceleration. This paper presents a novel hopping height controller that significantly reduces the number of measured variables without the need to explicitly detect the ground contact. The controller is composed of a positive pressure feedback loop and a saturation limit which dictates the hopping height. Moreover, a command velocity feedforward loop is used to improve the system response. A system model, in which all aspects but the saturation limit are linearized is used to analyse the controller performance via the describing function technique. The conditions for self-excited hopping are theoretically derived as well as it is successfully demonstrated experimentally using a small-sized, hydraulically-actuated bipedal hopping robot, which results in the maximum hopping frequency of 2.25 Hz with the height is consistently dictated by the saturation limit. A detailed nonlinear simulation model is developed to explain the main findings from the experiments. It is found that the oil compressibility causes a sustained oscillation of the robot when the pressure feedback signal is zero.

13. Introduction

Inspired by legged animals in the natural world, research on legged locomotion has been going on for decades. Legged moving machines are able to traverse across rough terrain since the foot placement does not require a continuous supporting surface, unlike the wheeled or tracked vehicles. The understanding of mono-legged hopping is useful as it can be expanded and applied to multi-legged

robots. The leg compliance needs to be closely tuned to obtain passive dynamics for effective and efficient running/hopping. From biomechanical studies, the design of legged robots requires careful integration of the actuation approach and leg compliance solutions. Some existing single-legged hopping robots are summarised in [1], which mainly focuses on the mechanical design aspects.

13.1 Control of legged hopping robots

The highly non-linear system dynamics of legged robots bring control challenges. For example, the significant load change between the stance phase and flight phase requires a significant change in controller behaviour. Some control techniques and algorithms for legged robots are reviewed in [2].

Marc Raibert's 'Three-part' control algorithm is widely adapted; it divides the control strategy into control of the hopping height, control of the horizontal velocity and the control of body orientation [3]. The hopping height control can be studied separately by constraining the robot to move in the vertical direction. Raibert illustrated the feasibility of this algorithm using the 3D prototype shown in Fig. 1. The telescopic robot leg uses the air compressibility to provide the system compliance, and the hopping height control is achieved by moving the piston to the desired position to compensate the energy loss during each hop.

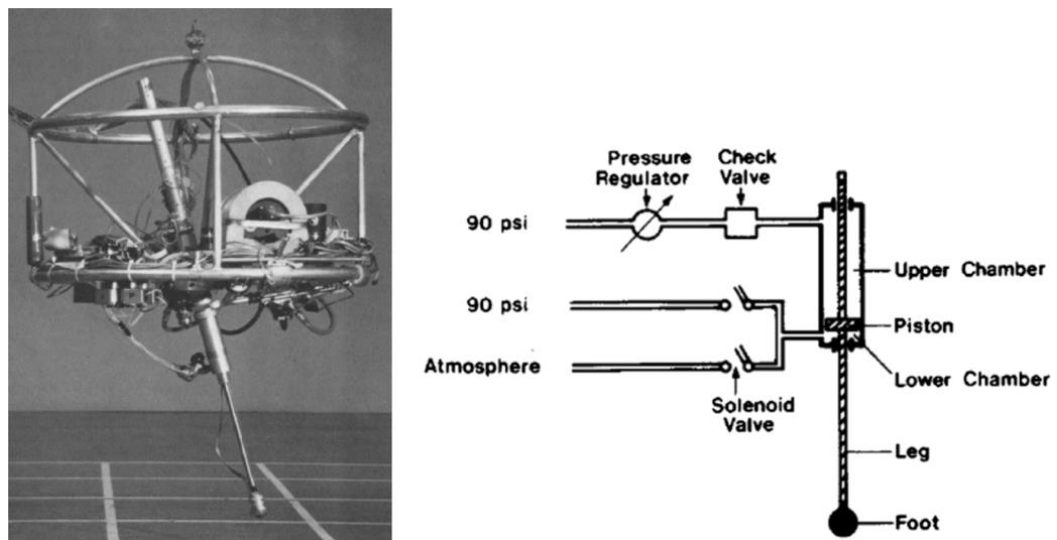


Figure 1. Raibert's 3D hopping robot prototype.

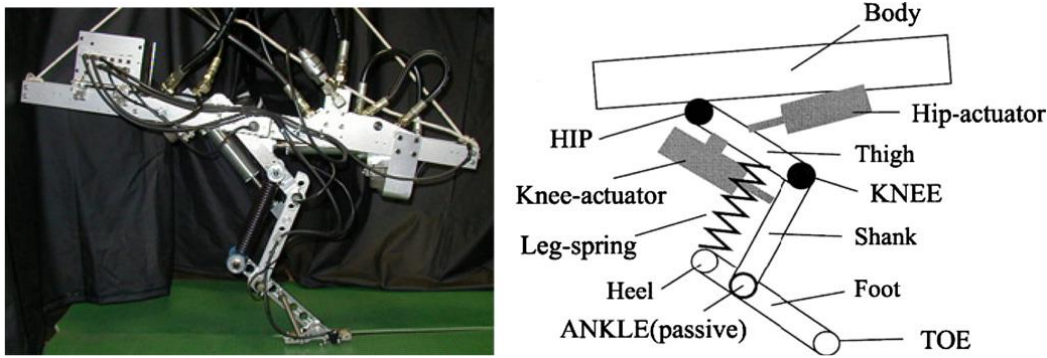


Figure 2. KenKen robot.

Kenken is a hydraulic actuated single leg hopping machine, as shown in Fig. 2, with a multi-link leg mechanism. An empirical hopping controller based on an understanding of the dynamics of a spring-loaded inverted pendulum model is described in [4]. The displacement of the leg actuator is determined by the need for the leg spring to be further deflected to provide the required energy for sustained hopping.

A simple adaptive algorithm for hopping that allows rapid changes of height even when the ground properties change is developed in [5]. An adaptive actuator velocity demand signal is calculated using the previous hopping height and the demand hopping height for the next cycle. It is also found that this adaptive velocity signal has the potential to be replaced by other control parameters, such as the valve's driving voltage. This controller is successfully tested on a two-link robot leg with a springy foot, which is driven by a hydraulic valve-controlled actuator system, as shown in Fig. 3.

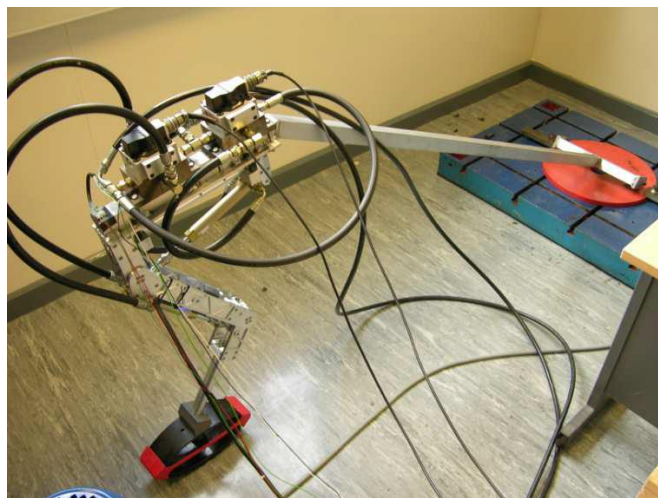


Figure 3. Hopping leg with a springy foot.

Most hopping height controllers require detection of ground contact to enable different control actions to handle the rapid change of system characteristics between the flight and stance phases. This transition can be provided either mechanically or electrically. Moreover, several state variables usually need to be measured, e.g. the actual body position, and the corresponding velocity and acceleration. Therefore, sensor selection and signal processing should be considered carefully to provide sufficiently accurate low-noise measurements.

13.2 Hydraulic actuated legged robots

Servo-hydraulics is highly suitable for robot leg actuation since it significantly increases the payload-to-machine-weight ratio due to its high power density. For example, the first generation of Big Dog as shown in Fig. 4 weighs 109 kg, is hydraulically actuated and powered by a combustion engine [6]. It is designed to be a rough-terrain traveller with a payload of up to 150 kg. Big Dog has a quick response to external disturbances, which also contributes to improving the balancing controller's performance. However, the sound noise issues caused by using a combustion engine compel the military to abandon this platform. The follower of Big Dog, called Spot and Spot mini, choose semi or fully electrical actuation as an improved solution for noise reduction.



Figure 4. The first generation of Big Dog.



Figure 5. HyQ.

HyQ, an electro-hydraulically actuated quadruped robot, which is shown in Fig. 5, stands 1 m tall and weighs 90 kg [7]. For each modular leg, the knee joint is actuated by a hydraulic valve-controlled actuator to handle the requirements of high velocity and high power-to-weight ratio. This actuator is carefully sized using simulations preceded with a series of torque estimation from one-legged hopping tests. Moreover, the electrical motor driven hip joint enables a high bandwidth balancing controller can be implemented.

13.3 Control of hydraulic actuators

A hydraulic valve-controlled actuator system is a simple and reliable way to obtain motion control of a robot leg. Some well-studied closed-loop position control approaches for hydraulic actuators are summarized in [8]. However, the nonlinearities of this actuation system may cause a significant negative effect on the control performance, e.g. the friction effect discussed in [9]. Therefore, some nonlinear adaptive control approaches have been proposed [10].

Closed-loop force control is particularly difficult for hydraulic actuators. Unlike an electrical motor, the actuator output force/torque is not proportional to the control input. For example, a closed-loop error leads to an opening of valve orifice, which allows a certain amount of flow to be delivered into a trapped volume, and taking the fluid compressibility into account, the pressure is an integration of this rate of change of oil volume. Negative force, pressure or acceleration feedback are

well-known methods for increasing damping in servohydraulic position control systems. When driving large inertia loads, the force feedback gain can be adjusted to provide damping to attenuate the system resonance associated with actuator compliance. Positive force feedback performs in the opposite way, tending to reduce or eliminate the stability margins. This is not desirable for common control systems, but a consistent hopping motion can be achieved by creating a marginally stable system. From biomechanical studies, a possible bouncing gait is achievable using positive force feedback approach, which is described in [11]. However, this hasn't been discussed further in depth and demonstrated using legged robots.

With this positive force feedback concept in mind, in this work, a novel self-excited hopping height controller is developed. This controller is tested on a small-sized, hydraulically actuated bipedal hopping robot named Bath Bipedal Hopper (BBH). It is developed with inspiration from kangaroos, which are the largest animals using this mechanism. One advantage of a bipedal hopping robot is that one of the degrees of freedom, which is perpendicular to the moving direction, can be largely neglected. A detailed description of this robot will be provided in the following sections.

14. Control concept

14.1 Simple models

A spring-loaded inverted pendulum (SLIP) model is widely used to analyse the motion of legged robots [12]. Typically, the upper end of a spring-damper is connected to a body mass and the lower end moves freely to simulate the robot foot. In this work, a modified SLIP model is introduced, as shown in Fig. 6, which has the following modifications:

- The foot (bottom of the spring-damper) is tethered to the ground.
- Only the vertical degree of freedom is considered.
- The actuation force between mass and spring-damper comes from a valve-controlled hydraulic actuator.

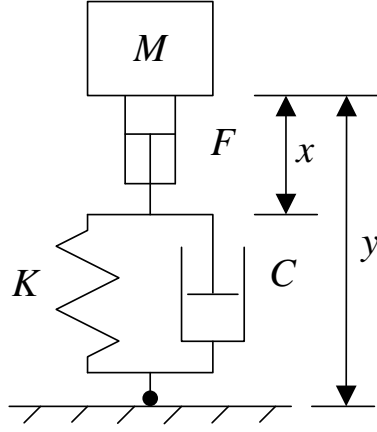


Figure 6. Modified SLIP model.

The equation of motion of the mass is given by:

$$M\ddot{y} = -C(\dot{y} - \dot{x}) - K(y - x) \quad (1)$$

where x is the actuator displacement from mid-stroke, y is the body displacement, K is the spring stiffness, C is damping coefficient and M is the body mass. Displacement y is chosen to be zero with the actuator at mid-stroke in steady state conditions.

A simple linear model of the valve and actuator is useful to understand the proposed control technique, in which a gain is used to represent the valve characteristic relating driving signal to flow rate, and the actuator position is a scaled integral of the valve flow output, which is given by:

$$x = \frac{C_x}{A_p s} u_c \quad (2)$$

where C_x is the valve flow coefficient, A_p is the piston area of the hydraulic actuator and u_c is the valve driving signal.

Thus, a linear model from the valve driving signal to the resultant force is given by:

$$F = \frac{C_x M s (C s + K)}{A_p (M s^2 + C s + K)} u_c \quad (3)$$

where F is the resultant force.

Note that C_x is derived from a linearized valve model that varies due to the actuator's working conditions. It is assumed that the pressure drop across the valve is constant, result in a constant C_x .

14.2 Controller design

A self-excited hopping controller as shown in Fig. 7, is proposed to control the body height, y . It is composed of an outer positive force feedback loop with a saturation limit dictating the hopping height, plus a closed-loop actuator position control loop, for which the demand is generated by the force loop. Additionally, a command velocity feedforward loop is used to improve the system response.

A first-order high pass filter is used to remove the mean value due to the weight component in the force measurement. The resultant force feedback signal can be considered as a command velocity:

$$u_d = \frac{s}{s + \omega_u} a_s \quad (4)$$

where u_v is the command velocity, a_s is the output of the saturation limit relating to the resultant force, and ω_u is the cut-off frequency of the high pass filter. The corresponding command position signal is given by:

$$x_d = \frac{1}{s + \omega_u} a_s \quad (5)$$

where x_d is the command position signal. One interpretation of this arrangement is as an impedance controller, where the impedance model relating force to motion is a damper with negative damping coefficient, thus reducing stability margins.

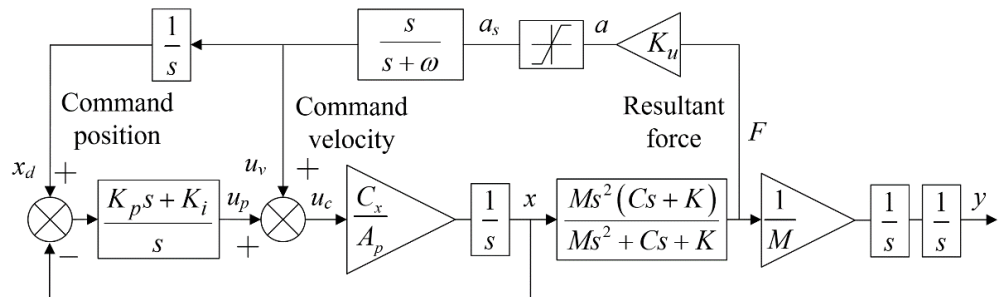


Figure 7. Controller structure.

A PI controller is used to achieve closed-loop position control of the actuator, as is widely used in servohydraulic:

$$u_p = K_p e + K_i \int e dt \quad (6)$$

where u_p is the control signal from the position loop, K_p is the proportional gain, K_i is the integral gain and e is the position error. Therefore, the valve control signal is given by:

$$u_c = u_p + u_v \quad (7)$$

14.3 Describing function analysis

The describing function technique can be used to analyse the controller performance as there is only one non-linear element, i.e. the saturation characteristic in the force feedback loop. Assuming a gradient of 1 in the linear region, define a sinusoid input as:

$$a(t) = A \sin \omega_a t \quad (8)$$

where A is the amplitude and ω_a is the frequency. Thus, the saturation output is:

$$a_s(t) = \begin{cases} -S & a(t) \leq -S \\ a(t) & -S < a(t) < S \\ S & a(t) \geq S \end{cases} \quad (9)$$

where S is the saturation limit.

The describing function of the saturation non-linearity is shown to be [13]:

$$N(A) = \begin{cases} 1 & A < S \\ \frac{2}{\pi} \left[\arcsin \frac{S}{A} + \frac{S}{A} \sqrt{1 - \left(\frac{S}{A} \right)^2} \right] & A \geq S \end{cases} \quad (10)$$

Note that when $A \geq S$, $N(A)$ represents a variable gain which is determined by the saturation limit and is independent of the frequency of the input.

Table 1 Parameter values

Variable	Symbol	Value	Unit
Mass	M	15	kg
Spring stiffness	K	4750	N/m
Damping coefficient	C	8	Ns/m
Piston area	A_p	1.13×10^{-4}	m ²
Valve coefficient	C_x	3.56×10^{-8}	L/min
Supply pressure	P_s	160×10^5	Pa
Return pressure	P_r	0	Pa
Force feedback gain	K_u	5×10^{-3}	m/N
The cut-off frequency of high pass filter	ω_u	1.885	rad/s
Proportional gain	K_p	320	1/m
Integral gain	K_i	120	1/(sm)

$$\frac{N(s)}{D(s)} = \frac{-0.503s^6 - 461s^5 - 9.658 \times 10^4 s^4 - 2.163 \times 10^5 s^3 - 6.761 \times 10^4 s^2}{15s^6 + 4092s^5 + (2.368s^4 + 133.2s^3 + 531.9s^2 + 633.7s + 169.9) \times 10^2} \quad (11)$$

The aim of this controller is to build a self-excited oscillation system, thus, the stability of the non-linear system should be examined. Table 1 presents the parameter values of the linear parts. Note that the control signal u_c is defined as dimensionless. The open-loop transfer function (OLTF) is given as equation (11).

To study the stability of the system, the Nyquist diagram of the linear OLTF is plotted together with the negative reciprocal of the describing function (DF) of the saturation limit, as is shown in Fig. 8.

There is an intersection point, H , of the OLTF and $-1/DF$ curves, which indicates that a limit cycle occurs [13], in other words, the system exhibits an inherent self-

sustaining oscillation. This can be explained from the fact that H separates the $-1/DF$ plot into 2 regions. According to the Nyquist stability criteria:

If $-1/N(A)$ falls in region 1, the closed-loop system is unstable;

If $-1/N(A)$ falls in region 2, the closed-loop system is stable.

Therefore, any disturbance tending to increase the amplitude will move from H to region 2, i.e. stability. Thus, the amplitude will reduce back to H . Vice versa for any disturbance trying to reduce the amplitude. Therefore, H is a stable self-excitation oscillation point.

Fig. 9 shows the relationship between A and $N(A)$ for different saturation limits, S . The value of $N(A)$ at H is 0.02282, which is used to explain the amplitude of y in terms of S .

Fig. 10 shows via simulation that when the system is exhibiting steady oscillation, A is proportional to S , and so the amplitude of body position y is also proportional to S . The oscillation frequency, ω_s , is found from equation (11) to be 17.844 rad/s.

This is very close to the natural frequency, ω_n , given by $\sqrt{K/M}$ to be 17.795 rad/s.

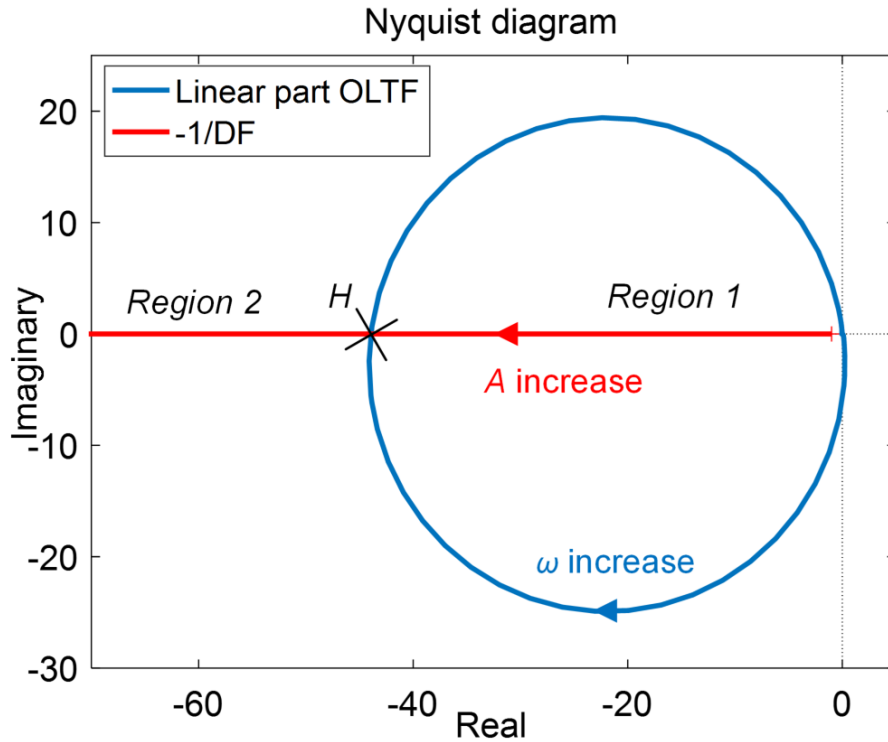


Figure 8. Nyquist diagram of the OPTF and $-1/DF$.

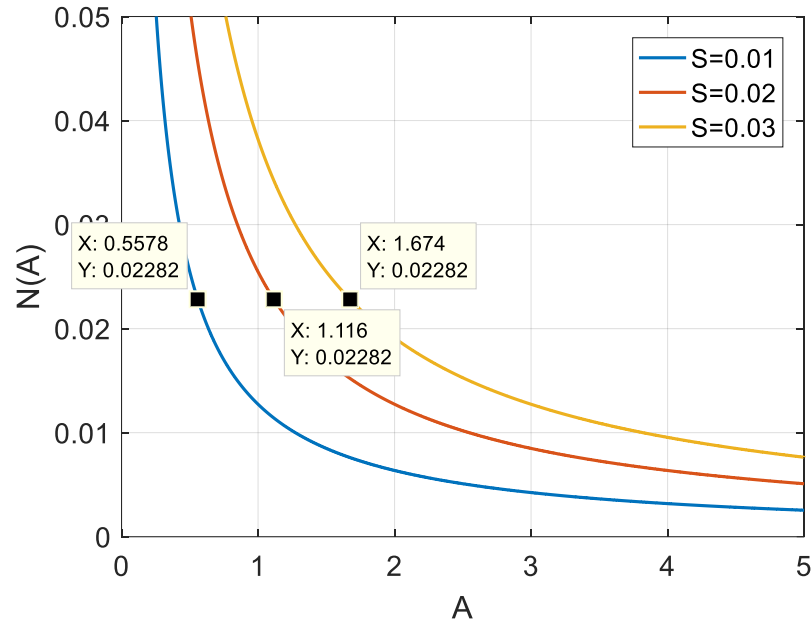


Figure 9. Using DF to predict amplitude A .

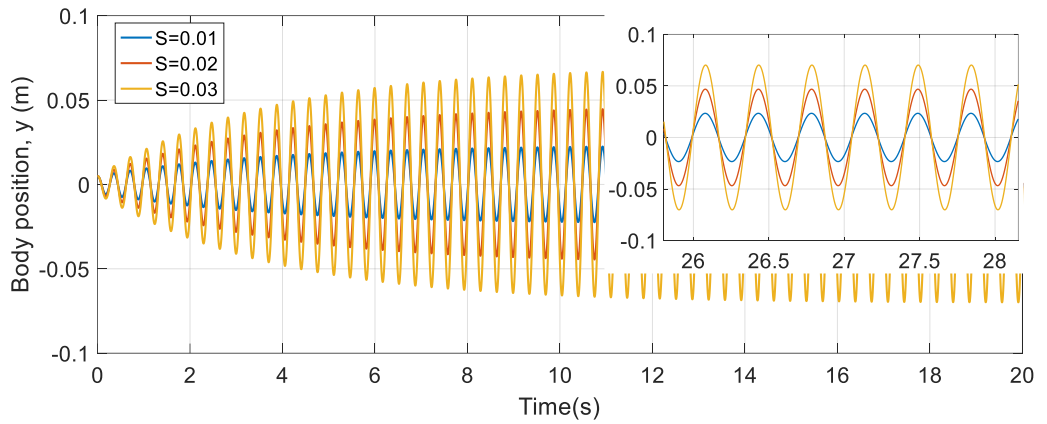


Figure 10. Simulation results of using saturation limit to dictate body position.

14.4 Model with foot free to lift off the ground

A more realistic model allows the foot to lift off the ground. Therefore, the transition between the stance phase and flight phases can occur. Note that during the flight phase, the body vertical motion has a parabolic trajectory due to gravity, and the spring is only functional in the stance phase, as shown in Fig. 11 and explained in equation (12).

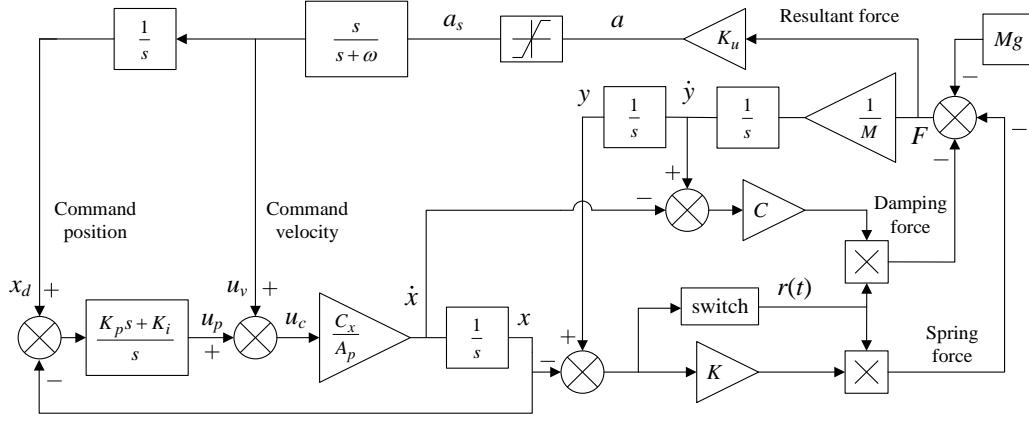


Figure 11. Simulation model considering foot lift off the ground.

A ‘switch’ is used to represent the transition between the flight phase and the stance phase. It is assumed that the natural length of the spring, l_0 , is zero. Therefore, the ‘switch’ outputs 1 if the foot is on the ground and 0 for lift-off, respectively:

$$r(t) = \begin{cases} 1 & y - x \leq 0 \\ 0 & y - x > 0 \end{cases} \quad (12)$$

where $r(t)$ is the output of the switch.

There is a threshold for S that determines if the foot lifts off the ground during the oscillation. In the steady state, the spring displacement, $\Delta \bar{l}$, is given by:

$$\Delta \bar{l} = \left| \frac{Mg}{K} \right| = 0.031 \text{ m} \quad (13)$$

Assuming the damping is small and can be neglected, to have the foot lift off the ground, the spring should return to natural length as shown in Fig. 12.

Defining Y as the amplitude of $y(t)$, from Fig. 7 or Fig. 11, assuming no foot lift-off, the amplitudes Y and A are related by:

$$A = \left| MK_u \omega_s^2 \right| Y \quad (14)$$

where A_t is the amplitude threshold for foot lift off. Therefore, combining equations (10) and (15), the corresponding saturation limit is:

$$S_t = 0.0133 \quad (16)$$

where S_t is the saturation threshold above which hopping (i.e. foot lift off) will occur. This is demonstrated via simulation. Fig. 13 shows that when $S=0.01$, the foot stays on the ground. When S is greater than 0.0133, e.g. for the cases of $S=0.02$ or 0.03, results in a larger hopping height. Thus, the flight phase duration increases and the hopping height is still determined by the saturation limit. Fig. 14 shows that when $S=0.0133$, the foot leaves the ground momentarily in the ‘free foot’ case, which is caused by the approximation when operating the describing function technique.

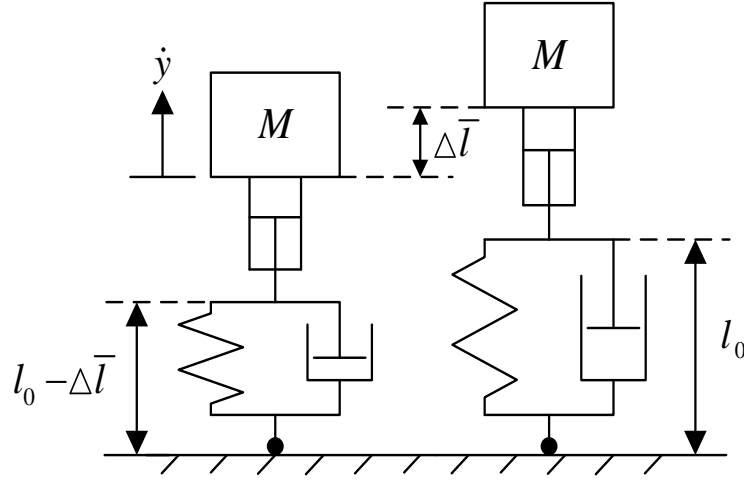


Figure 12. The threshold of spring displacement.

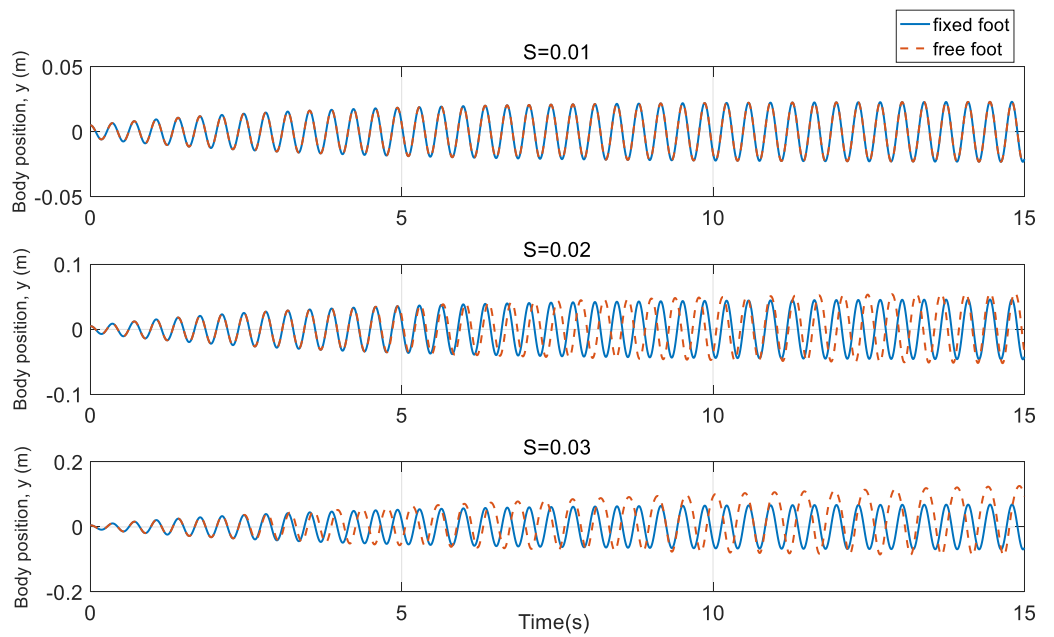


Figure13. Simulation results of $S=0.01$, $S=0.02$ and $S=0.03$.

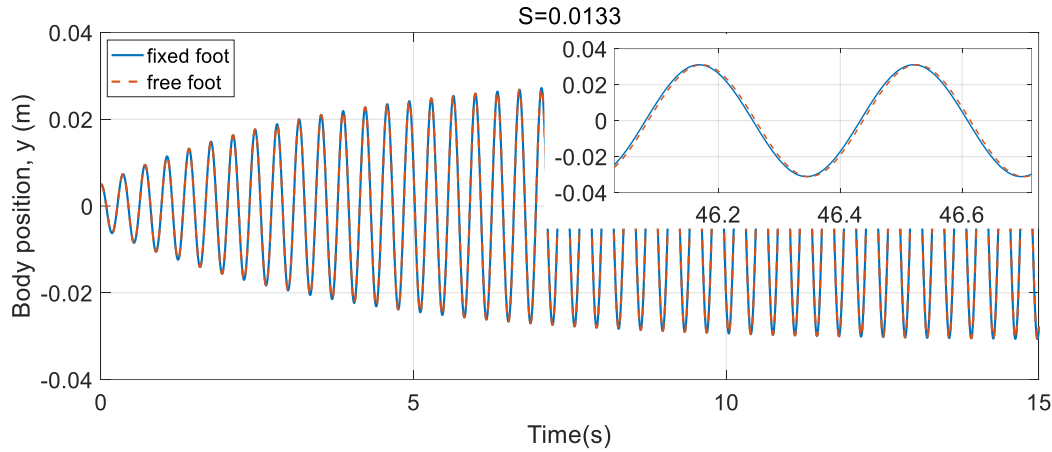


Figure 14. Simulation results of $S=0.0133$. The close-up figure shows a small difference between ‘fixed foot’ and ‘free foot’ cases, which indicate the foot leaves the ground momentarily.

15. Experimental bipedal hopping robot

This controller is experimentally tested on a hydraulically actuated, small-sized bipedal hopping robot, the BBH, which has an articulated type of leg, as shown in Fig. 15. The robot leg is composed of three links:

The 1st link: a hydraulic actuator, named leg actuator, is placed in parallel with the ‘*thigh*’ to actuate the knee joint.

The 2nd link: an extension coil spring is mounted in parallel with the ‘*shank*’ to provide the leg compliance.

The 3rd link: a ‘*foot*’ is used to connect the ankle joint and heel joint.

The length of the ‘*shank*’ is carefully designed so that the ‘*foot*’ is parallel to the ‘*thigh*’ when the spring is in natural length. A 3D printed rubbery foot, which is made of thermoplastic polyurethane (TPU), is attached at the end of the lower leg to generate sufficient horizontal friction to avoid slipping. The robot body is an aluminium frame for mounting the manifold, valves and PC-104 controller, giving a compact size with reasonable mass. This test rig is driven by a hydraulic power pack placed in the adjacent area, which eventually can be replaced by pressurised accumulators to allow untethered operation. Another hip actuator is placed under the body to drive the hip joint. During the test, the hip actuator position is

controlled by a PI controller to give a 45° hip angle, plus the leg actuator is initially controlled to the mid-stroke, resulting in the body's CoM is aligned with the foot contact point, vertically.

The test rig set up is shown in Fig. 16 and Fig. 17. A position transducer is placed in parallel with each leg actuator to measure the piston position. A pressure sensor is used to measure the piston side pressure of the actuator. Additionally, an incremental encoder is added at the heel joint so that the spring displacement can be calculated using a kinematic transformation. The main dimensional specifications of BBH are summarized in Table 2.

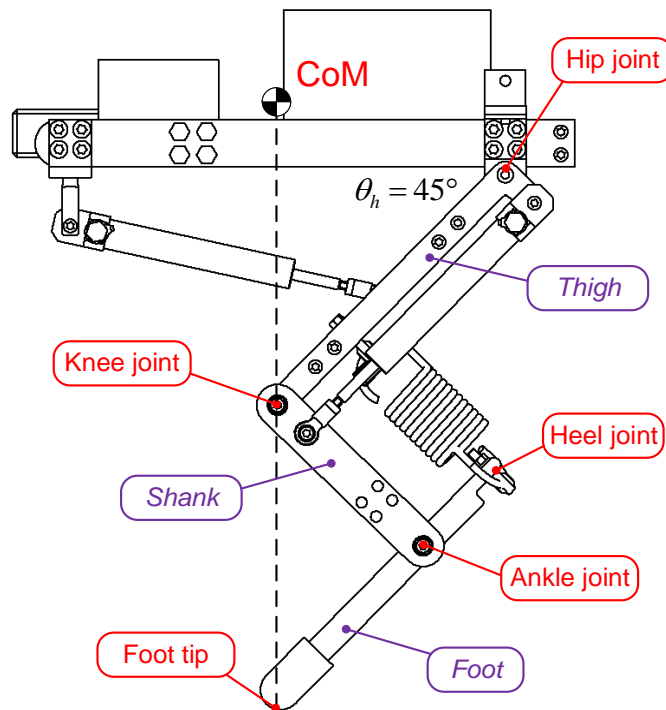


Figure 15. Sketch of the BBH robot.

Table 2 Main dimensional specifications of the BBH robot.

Height:	552 mm
Length:	400 mm
Width:	315 mm
Spring stiffness:	9.62 N/mm
Weight:	14.78 kg

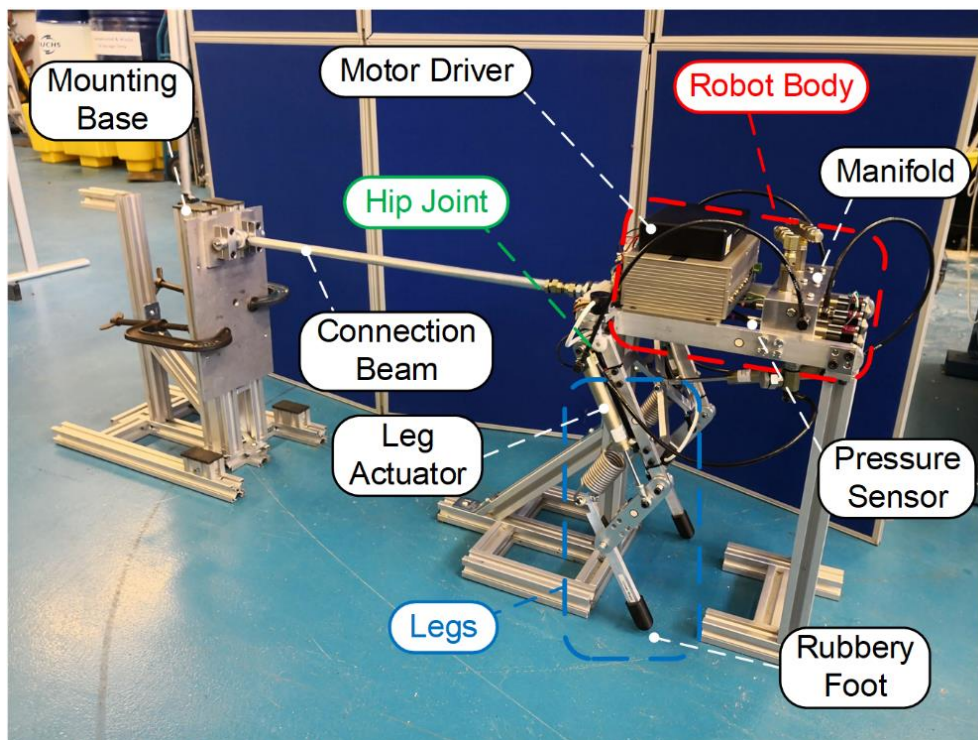


Figure 16. The Bath Bipedal Hopper (BBH) robot.

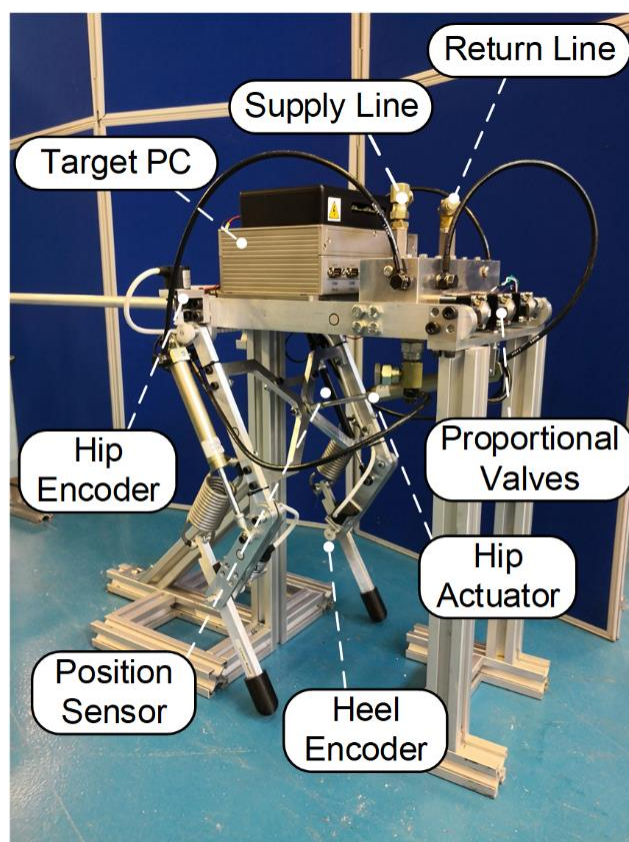


Figure17. The Bath Bipedal Hopper (BBH) robot – close-up.

The practical controller implementation is shown in Fig. 18. The resultant force is calculated using the measurement of fluid pressure. Due to the regenerative hydraulic circuit design, as shown in Fig. 19, the resultant force is:

$$F = P_p A_p - P_s A_a \quad (17)$$

where P_p is the measured piston side pressure.

Additionally, the two leg actuator displacements are synchronised using a ‘Modal Controller’. This controls the mean of the leg actuator positions and the corresponding difference, which are called the average position and roll position, respectively. If the demand roll position is zero, the two leg actuators displacements are synchronised. This average leg actuator position will be considered the output variable from now on.

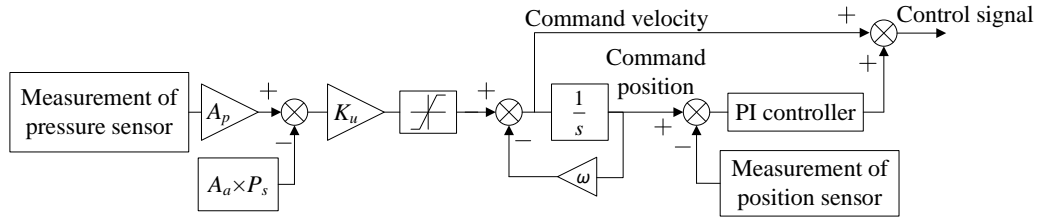


Figure 18. Practical controller implementation.

16. Simulation model

A detailed non-linear simulation model is developed in this section aims to explain the main findings from experiments. The modelling mainly focus on hydraulic and mechanical aspects. The electrical domain, specifically the motor controller is modelled use a simple proportional gain, $K_{mc} = 0.1$ A/V, to convert the control voltage signal into the driving current of the valve.

16.1 Hydraulic models

The dynamic characteristics of the hydraulic actuator, the proportional valve, the hydraulic accumulator and the hose are modelled in this section. The modelling follow well-established procedures [14], with some findings from experiments. The hydraulic circuit is shown in Fig. 19.

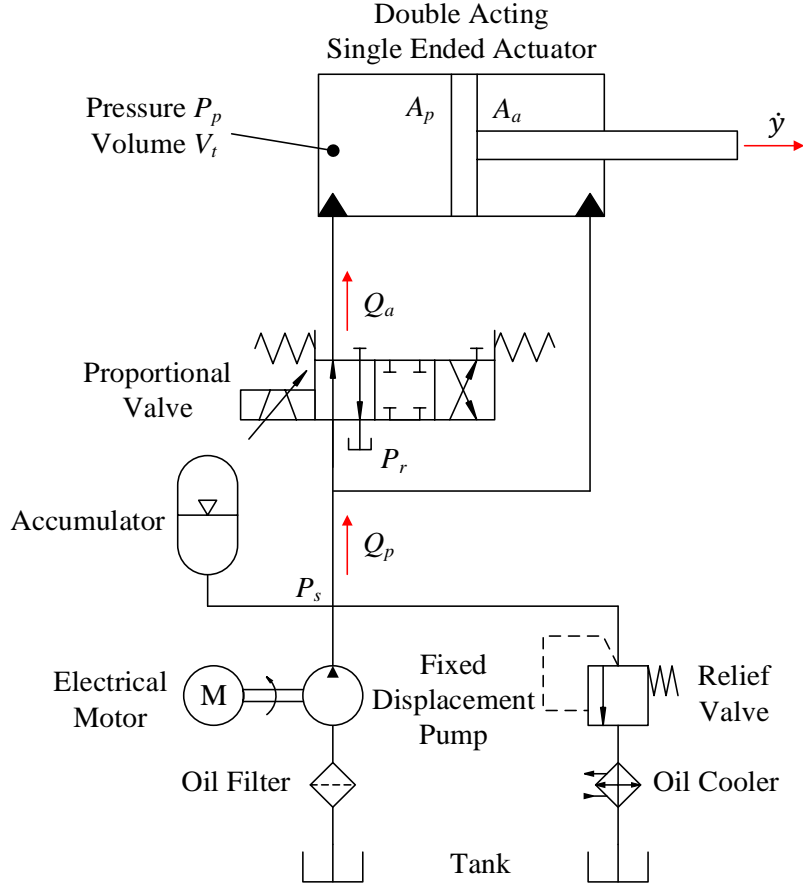


Figure 19. Hydraulic circuit for one leg actuator.

16.1.1 Actuator model

The hydraulic actuator is modelled considering the piston force balance equation and the flow equation. Assuming there is no internal or external leakage:

$$P_p A_p - P_s A_a - F_f = F_h \quad (18)$$

$$Q_a = A_p \dot{y} + \frac{V_t}{B} \dot{P}_p \quad (19)$$

where A_a is the annulus area, F_h is the actuation force, F_f is the friction force, Q_a is the piston side flow rate and V_t is the trapped oil volume and B is the bulk modulus of the oil. Additionally, the friction force is modelled by:

$$F_s = f_v \dot{y} \quad (20)$$

$$F_f = \begin{cases} F_c & \text{for } F_s \geq F_c \\ F_s & \text{for } |F_s| < F_c \\ -F_c & \text{for } F_s \leq -F_c \end{cases} \quad (21)$$

where F_c is the Coulomb friction force, and F_s is velocity-dependent friction at low velocity, introduced to avoid a discontinuity which can cause numerical issues during the simulation; f_v is a friction coefficient which is relatively large.

16.1.2 Valve model

The proportional valve flow is modelled using the orifice equation. Only one orifice equation is needed as the flow is only metered into one side of the actuator. The spool displacement is considered as a dimensionless variable which ranging from -1 to +1 with the closed position corresponding to 0. The valve model is given by:

$$Q_a = K_v X_v \sqrt{P_s - P_v} \quad (22)$$

where P_v is the outlet pressure, K_v is the valve flow coefficient and X_v is the normalised spool displacement.

Additionally, a second-order transfer function is used to represent the valve spool dynamics, which is given by:

$$X_v = \frac{\omega_v^2}{s^2 + 2\zeta_v \omega_v s + \omega_v^2} \tilde{u}_c \quad (23)$$

where \tilde{u}_c is the valve driving signal, ω_v is the spool natural frequency and ζ_v is the spool damping ratio, which are empirical values determined from the manufacturer data sheet or experimental results.

Hysteresis is often a significant non-linearity in valve spool positioning. This is modelled as ‘backlash’, as shown in Fig. 20, which u_w is the dead-band width.

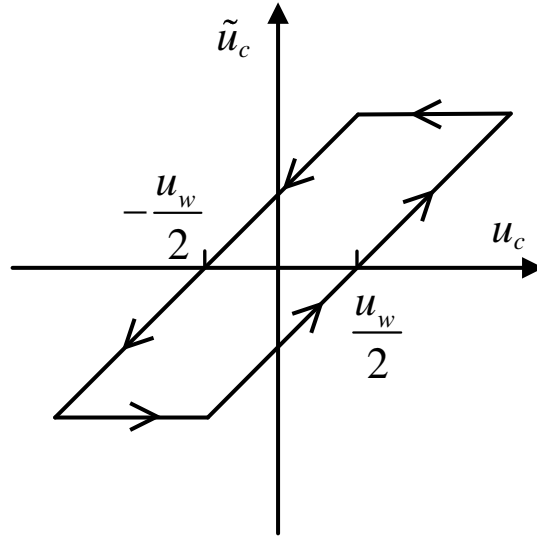


Figure 20. Valve hysteresis.

Table 3 Parameter values of the hydraulic models.

Parameters	Symbol	Value	Unit
Supply pressure	P_s	160×10^5	Pa
Return pressure	P_r	0	Pa
Piston area	A_p	1.13×10^{-4}	m ²
Annulus area	A_a	0.63×10^{-4}	m ²
Valve flow coefficient	K_v	4.89×10^{-8}	m ⁴ /s/N ^{1/2}
Valve spool natural frequency	ω_v	942.48	rad/s
Valve spool damping ratio	ζ_v	0.7	
Backlash deadband width	u_w	0.2	A
Coulomb friction (actuator piston)	F_f	105	N

16.1.3 Hose pressure loss model

The pressure loss between the valve and the cylinder is modelled. Assuming the flow rate passing through the hose is proportional to the square root of the pressure drop:

$$Q_a = K_h \sqrt{P_p - P_v} \quad (24)$$

where K_h is the hose pressure loss factor, which is an empirical value. The parameter values of the hydraulic models are provided in Table 3.

16.2 Mechanical model

The mechanical model of the BBH, which effectively is a planar robot, is built using SimMechanics[®], a multi-body mechanical simulation tool in Simulink[®]. The mechanical properties of the rigid bodies are defined in Autodesk Inventor 2017[®], then uploaded to SimMechanics[®] to create a 3D visualisation. The top-level mechanical model is shown in Fig. 21.

Only the prismatic primitive is considered when modelling the motion between the actuator piston and cylinder since the piston revolute degree of freedom is constrained by the rod end mounting to adjacent rigid bodies. Moreover, it is assumed that the hip joint friction can be ignored due to the application of low-friction ball bearings. A ‘spring and damper force’ block is used to represent the spring force between the connections on the *thigh* and *foot*. Modelling ground contact is an important issue. The reaction force from the ground should support the robot vertically (y-axis) and prevent horizontal foot slip (z-axis) during stance. The other horizontal axis (x-axis) is not relevant as we only consider the planar motion. Define the coordinate of the robot foot as $(0, y_n, z_t)$, and the initial contact point on the ground is $(0, 0, 0)$. The ground reaction force is modelled as a spring and damper both vertically and horizontally. The ground stiffness is relatively large so as not significantly reduce the effective robot leg’s stiffness. Thus, the vertical reaction force and the horizontal friction force are given by:

$$F_y = \begin{cases} -k_y y_n - b_y \dot{y}_n & \text{for stance phase} \\ 0 & \text{for flight phase} \end{cases} \quad (25)$$

$$F_z = \begin{cases} -k_z z_t - b_z \dot{z}_t & \text{for stance phase} \\ 0 & \text{for flight phase} \end{cases} \quad (26)$$

where F_y is the vertical reaction force, k_y is the ground normal spring stiffness and b_y is the ground normal damping coefficient. F_z is the horizontal friction force, k_z is the tangential spring stiffness and b_z is the tangential damping coefficient. Note that F_y is constrained to be a positive value to prevent the robot foot from being stuck when lifting off.

The top level of the simulation model is shown in Fig. 22. Numerical implementation is performed by a stiff/Mod. Rosenbrock solver (Simulink's ODE23s) with variable step size, which is a compromise between the computing speed and the simulation accuracy. Additionally, the visualised model is shown in Fig. 23.

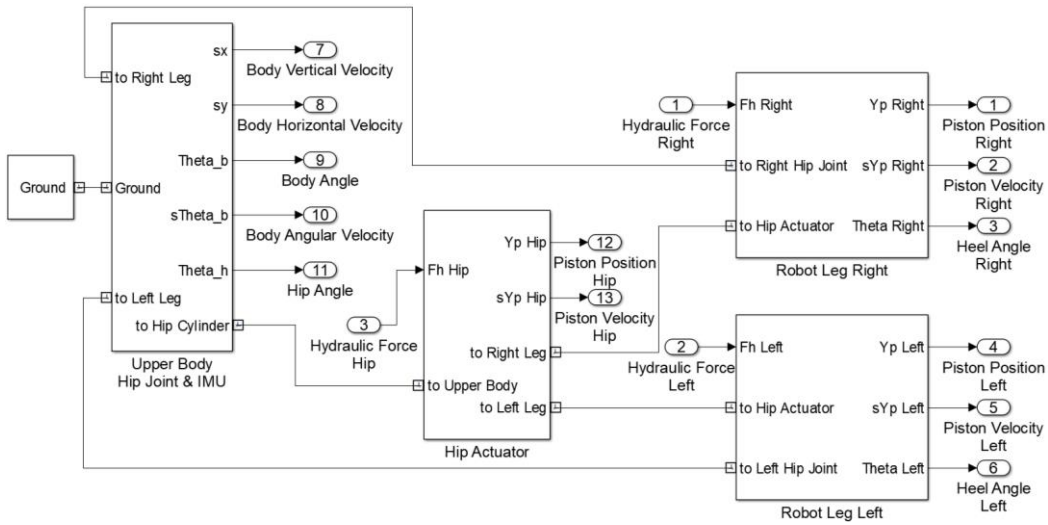


Figure 21. The top level of the mechanical model.

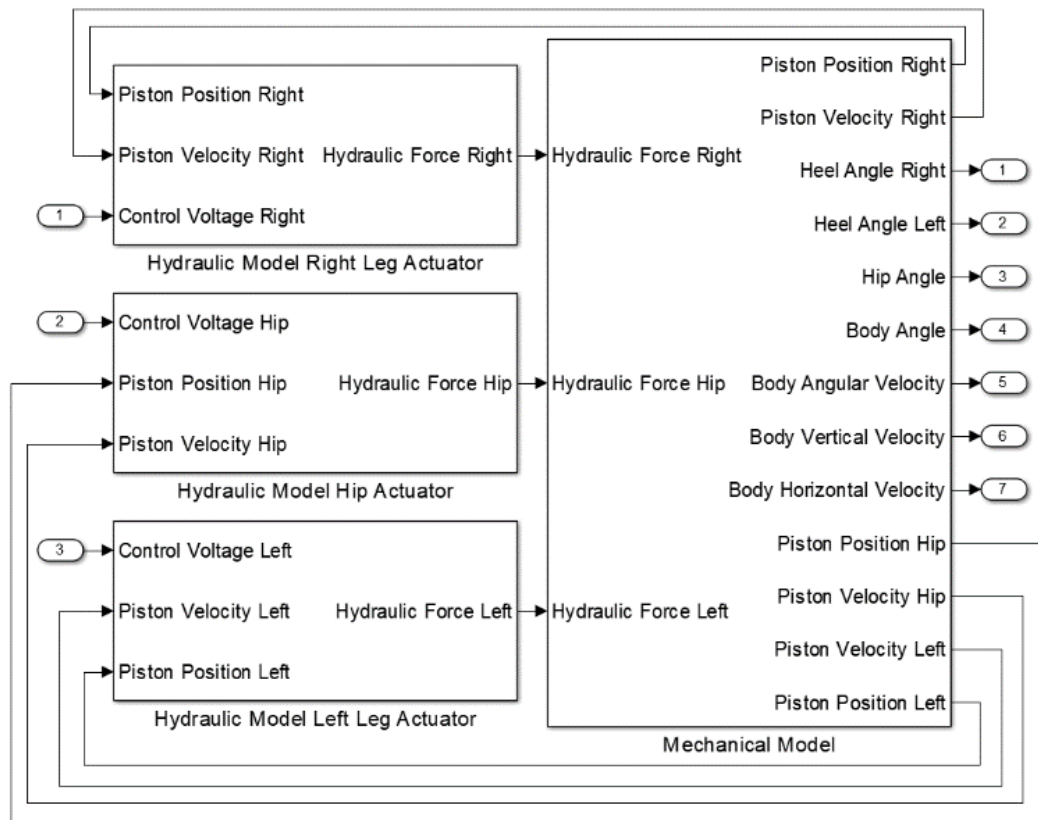


Figure 22. The top level of the simulation model.

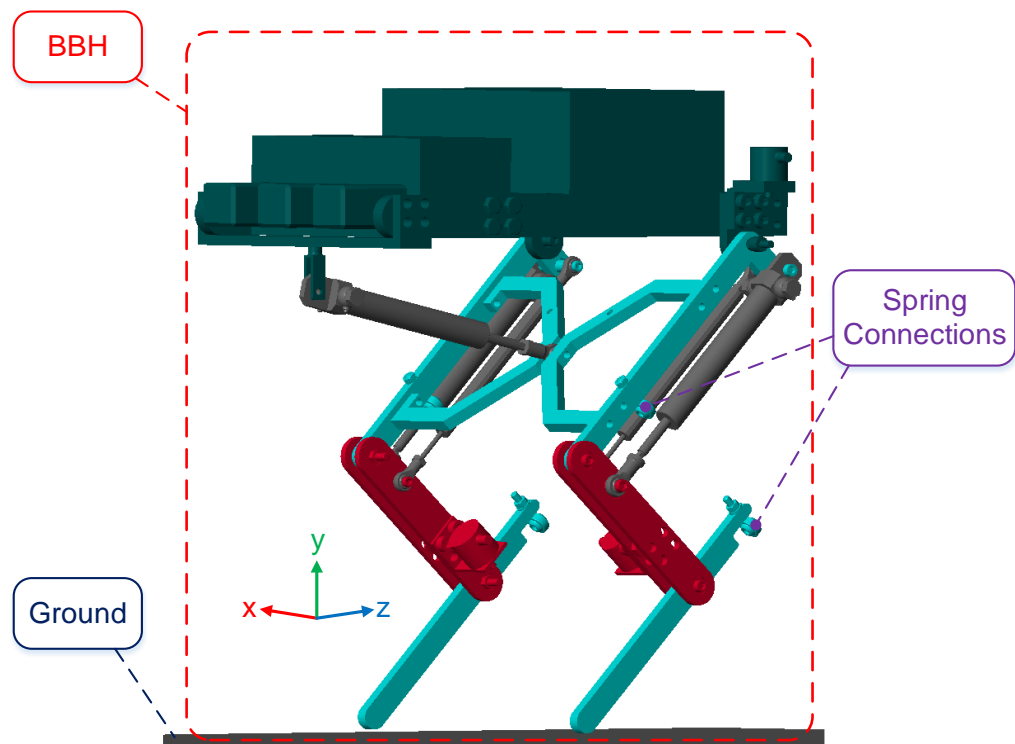


Figure 23. 3D visualisation of the simulated system.

17. Results and discussion

The experimental and simulation results are shown in Fig. 24. As the saturation limit reduces, the spring displacement also reduces. Even though there is no direct measurement of the hopping height, the decrease of spring displacement indicates a decrease in hopping height since less impact energy is stored in the spring. Therefore, the saturation limit does dictate the hopping height. The hopping frequency has a small variation due to the change of saturation limit. When $S=0.02$, the hopping frequency is 2.15 Hz, when $S=0.01$, the hopping frequency is 2.25 Hz. This is consistent with the results of using the simple model in Section 2. The supplementary video provides a visual demonstration.

Note that doubling the saturation limit is not doubling the spring displacement, plus there is a sustained oscillation when $S=0$. Fig. 25 shows that when the robot exhibits sustained oscillation, at each ‘touch-down’, the ground impact force acting on the robot foot results in the actuator piston retracting slightly due to the compressibility of the oil. Then the piston is moved back towards the zero position by the closed-loop position controller. This effect tends to excite the robot into a resonant oscillation. As these oscillations build in amplitude, the foot may leave the ground momentarily. This characteristic is not seen with the simple model, i.e. the simple model gives no sustained oscillation when $S=0$, as it does not include the oil compressibility effect.

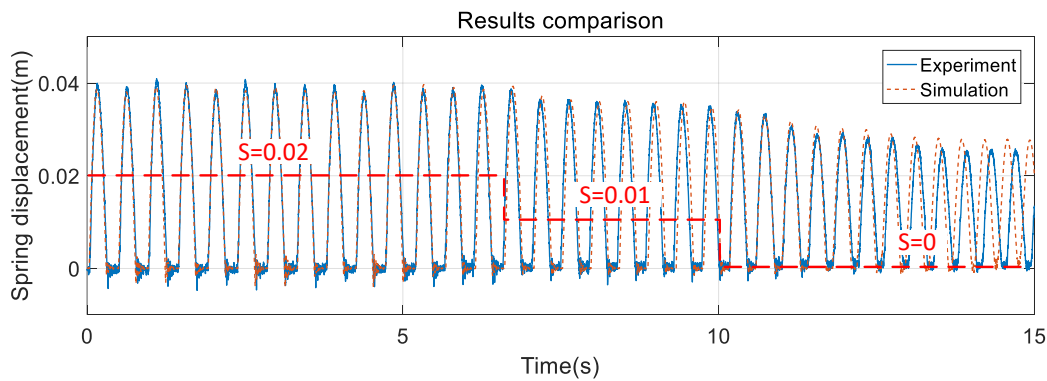


Figure 24. Results comparison.

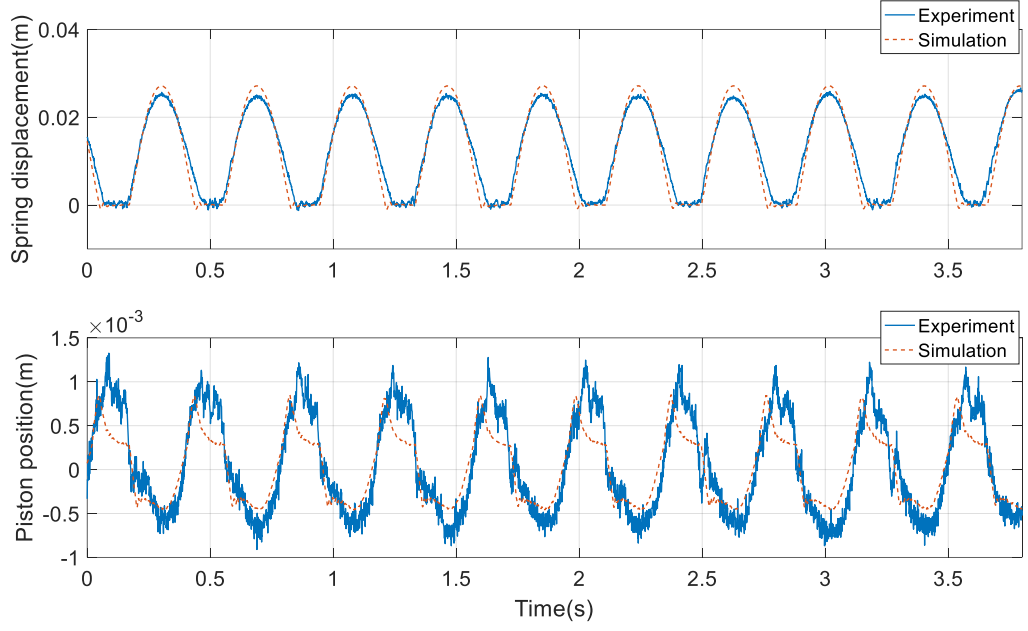


Figure 25. Results comparison.

18. Conclusions

A novel hopping controller for legged robots is investigated in this paper. A self-excited oscillation is achieved using a positive force feedback loop plus a saturation limit, a position feedback loop and a command velocity feedforward loop. The conditions for guaranteed self-excited hopping are theoretically derived using the describing function technique and demonstrated via a simplified simulation model. Experimental results verify the efficacy of the controller. The spring displacement and hopping height are consistently dictated by the saturation limit. A detailed non-linear simulation model is also developed to further explore the main findings from the experiment. In particular, a sustained oscillation occurs when the saturation limit is set to zero, which is related to the compressibility of the oil in the hydraulic actuator. Only two variables need to be measured to implement the controller, the actuator position and the piston side pressure, and no explicit detection of the ground contact is required.

Hopping is the fundamental basis for locomotion by running. The main contributions of this controller are:

- Significantly reduce the difficulty of developing running robots, either in terms of the mechanical design or controller development, in particular, it

is not necessary to distinguish between the flight phase and stance phase, so there is no need to alter the mechanical design or sensor selection to detect the ground contact. Although actuator force measurement is required, as demonstrated here, with hydraulic actuation pressure instead of force can be used, which can be measured reliably without the danger of impact damage sometimes experienced by force sensors.

- Varying the saturation limit provides a simple way of adjusting hopping height and hence flight time.

In this paper, the controller is tested on the BBH robot, a bipedal kangaroo-like robot with multi-jointed legs incorporating hydraulic actuation and coil extension springs to provide compliance. The control approach should be applicable to a range of robot designs and has also been shown to work on a design with a telescopic hydraulic leg with gas-spring compliance using full leg displacement (not just actuator position) feedback [9]. Additional work is underway to study the balancing control of the BBH robot accompanied by the hopping controller developed in this paper.


References

- [1] Zhou, X. and Bi, S., 2012. A survey of bio-inspired compliant legged robot designs. *Bioinspiration & Biomimetics*, 7(4), p.041001.
- [2] Bhatti, J., Plummer, A.R., Iravani, P. and Ding, B., 2015, August. A survey of dynamic robot legged locomotion. In *Fluid Power and Mechatronics (FPM), 2015 International Conference on* (pp. 770-775). IEEE.
- [3] Raibert, M.H. and Sutherland, I.E., 1983. Machines that walk. *Scientific American*, 248(1), pp.44-53.
- [4] Hyon, S.H. and Mita, T., 2002. Development of a biologically inspired hopping robot-" Kenken". In *Robotics and Automation, 2002. Proceedings. ICRA'02. IEEE International Conference on* (Vol. 4, pp. 3984-3991). IEEE.
- [5] Bhatti, J., Plummer, A.R., Sahinkaya, M.N., Iravani, P., Guglielmino, E. and Caldwell, D.G., 2012, July. Fast and adaptive hopping height control of single-legged robot. In *ASME 2012 11th Biennial Conference On Engineering Systems Design And Analysis* (pp. 303-309). American Society of Mechanical Engineers.

- [6] Raibert, M., Blankespoor, K., Nelson, G. and Playter, R., 2008. Bigdog, the rough-terrain quadruped robot. *IFAC Proceedings Volumes*, 41(2), pp.10822-10825.
- [7] Semini, C., Tsagarakis, N.G., Guglielmino, E. and Caldwell, D.G., 2010, October. Design and experimental evaluation of the hydraulically actuated prototype leg of the HyQ robot. In *Intelligent Robots and Systems (IROS), 2010 IEEE/RSJ International Conference on* (pp. 3640-3645). IEEE.
- [8] Jelali, M. and Kroll, A., 2012. *Hydraulic servo-systems: modelling, identification and control*. Springer Science & Business Media.
- [9] Ding, B., Plummer, A. and Iravani, P., 2018, July. A Study of a Compliant Hydraulic Actuator for Running Robots. In *2018 Global Fluid Power Society PhD Symposium (GFPS)* (pp. 1-6). IEEE.
- [10] Yao, B., Bu, F., Reedy, J. and Chiu, G.C., 2000. Adaptive robust motion control of single-rod hydraulic actuators: theory and experiments. *IEEE/ASME Transactions on Mechatronics*, 5(1), pp.79-91.
- [11] Geyer, H., Seyfarth, A. and Blickhan, R., 2003. Positive force feedback in bouncing gaits?. *Proceedings of the Royal Society of London B: Biological Sciences*, 270(1529), pp.2173-2183.
- [12] Ding, B., Plummer, A. and Iravani, P., 2016. Investigating Balancing Control of a Standing Bipedal Robot with Point Foot Contact. *IFAC-PapersOnLine*, 49(21), pp.403-408.
- [13] Schwarzenbach, J. and Gill, K.F., 1978. System modelling and control. J. Wiley.
- [14] Plummer, A.R., 2008. A detailed dynamic model of a six-axis shaking table. *Journal of earthquake engineering*, 12(4), pp.631-662.

Appendix 4

Statement of Authorship

This declaration concerns the article entitled:									
Investigating balance control of a hopping bipedal robot									
Publication status (tick one)									
draft manuscript		Submitted		In review		Accepted	<input checked="" type="checkbox"/>	Published	
Publication details (reference)	Accepted by 'the 20 th Towards Autonomous Robotic Systems Conference' (TAROS 2019)								
Candidate's contribution to the paper (detailed, and also given as a percentage).	<p>Formulation of ideas: Solely the candidate (100%).</p> <p>Design of methodology: Mostly by the candidate (70%).</p> <p>Simulation work: Solely the candidate (100%).</p> <p>Presentation of data in conference format: Solely the candidate (100%).</p>								
Statement from Candidate	This paper reports on original research I conducted during the period of my Higher Degree by Research candidature.								
Signed						Date	06/03/2019		

This is a post-peer-review, pre-copyedit version of an article published in TAROS 2019: Towards Autonomous Robotic Systems. The final authenticated version is available online at: https://doi.org/10.1007/978-3-030-23807-0_15

PAPER 4: Investigating balance control of a hopping bipedal robot

Beichen Ding*, Andrew Plummer*, Pejman Iravani*

*Centre for PTMC, Department of Mechanical Engineering, University of Bath, Bath, UK

Abstract

Legged robots are dynamic moving machines that are potentially able to traverse through rough terrain which is inaccessible for wheeled or tracked vehicles. For bipedal robots, balancing control while hopping/running is challenging, especially when the foot contact area is small. Servo hydraulics is highly suitable for robot leg actuation due to its high power density and good power-to-weight ratio. This paper presents a controller for a hydraulically actuated bipedal robot, the Bath Bipedal Hopper (BBH). The controller follows the well-established structure of the ‘Three-part’ control algorithm. The three parts are: hopping height control; longitudinal velocity control by changing the leg angle during the flight phase to place the foot in the desired position; and body attitude correction during the stance phase. Simulation results from a detailed non-linear model indicate that this controller can successfully balance the hydraulic robot while hopping with different longitudinal velocities.

19. Introduction

Legged animals can be widely found in the natural world, and many are highly effective at traversing rough terrain. Similarly, legged robots present themselves with potential advantages for easily travelling through rough terrain comparing with wheeled or tracked vehicles [1]. Some successfully developed legged moving machines are summarized in [2].

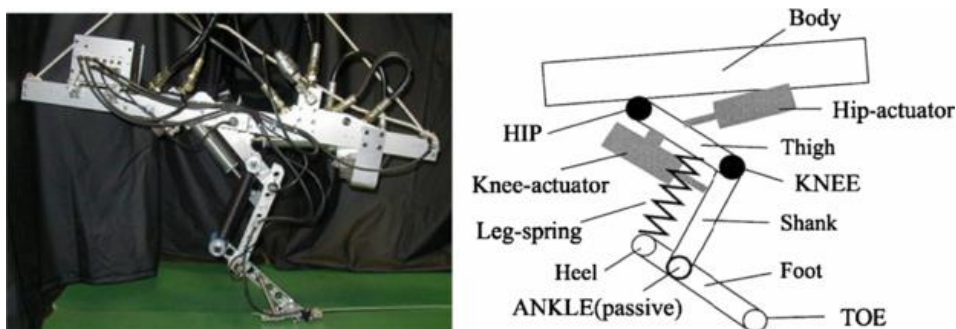


Figure 1. Kenken: one-legged hopping robot.

The study of mono-legged or bipedal hopping robot is a sustained interest that is motivated by human's desire to have a comprehensive understanding of this locomotion, which can also be expanded and applied to multi-legged robots. A springy leg interacting with a body mass is able to give a natural running/hopping frequency. Coil springs and compressed air are widely used to provide the required leg compliance. Servo hydraulics is highly suitable for robot leg actuation due to the high power density and quick system response. KenKen is a famous hopping robot with an articulated type of leg, which takes advantage of coil spring accompanied by hydraulic actuation [3], which is shown in Fig. 1.

Maintaining balance is an important objective for dynamic robots while walking or running. For pseudo-static multi-legged robots, balance can be achieved by keeping the body CoG above the support region created by the feet, which is called 'Zero Moment Point' (ZMP) control [4]. The SILO4 robot and Asimo, as shown in Fig. 2, are successfully balanced using this method while walking.

However, balancing control becomes challenging for bipedal robots when the foot contact area is small. In 1986, Raibert developed a 'Three-part' control algorithm to explain the basic locomotion mechanism of a one-legged case [5], for which there is only one type of gait, namely hopping. The three controlled variables are: the hopping height, the horizontal velocity and the body attitude. In order to accomplish different control actions, a distinction between the flight phase and the stance phase is necessary. During the stance phase, the one-legged behaves as a spring-loaded inverted pendulum (SLIP) with the foot pivoted on the ground. During stance, the robot can be balanced by controlling the body rotation angle, and the leg actuator is required to accomplish the hopping height control tasks. During the flight phase, the horizontal velocity control can be achieved by controlling the leg angle with respect to the CoG to place the foot at the required position for the next touchdown.

Several dynamic running robots were built to test this control algorithm during the 1980s and 1990s, which are introduced in [6]. This controller is also extended for multi-legged robots to control body pitching and rolling [7].



Figure 2. SILO4: a quadruped walking robot; Asimo: a humanoid walking robot.

A hydraulically actuated bipedal hopping robot called the Bath Bipedal Hopper (BBH) has been developed at the University of Bath to study motion control of legged robots. In this paper, the ‘Three-part’ control algorithm is investigated for this robot via simulation. A detailed non-linear simulation model will be developed and the controller implementation is described in the following sections.

20. Description of the Bath Bipedal Hopper robot

A sketch of the BBH is shown in Fig. 3. The BBH is a small-sized, hydraulically actuated bipedal hopping robot. The articulated type robot leg is composed of three links. The 1st link: a hydraulic actuator, named leg actuator, is placed in parallel with the ‘*thigh*’ to actuate the knee joint; The 2nd link: an extension coil spring is mounted in parallel with the ‘*shank*’ to provide the required leg compliance; The 3rd link: a ‘*lower leg*’ is used to connect the ankle joint and the heel joint.

The robot body is an aluminium frame for mounting the manifold, valves and PC-104 controller. A hip actuator is placed under the body to drive the hip joint. For the initial condition, the hip actuator position is controlled by a PI controller to give a 45° hip angle, plus the leg actuator is controlled to the mid-stroke, resulting in the body’s CoM being aligned with the foot contact point, vertically. The main dimensional specifications of BBH are summarized in Table 1.

The test rig setup is shown in Fig. 4. A position transducer is placed in parallel with each leg actuator to measure the piston position. A pressure sensor is used to

measure the piston side pressure of the actuator. Additionally, an incremental encoder is added at the heel joint so that the spring displacement can be calculated using a kinematic transformation.

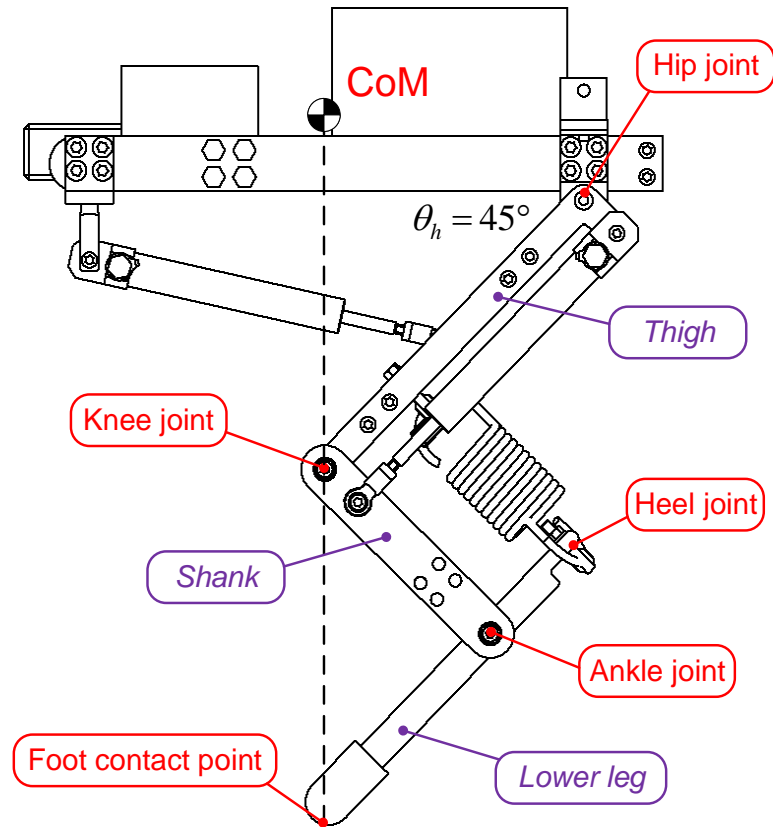


Figure 3. Sketch of the BBH robot.

Table 1. Main dimensional specifications of the BBH

Height:	552 mm
Length:	400 mm
Width:	315 mm
Spring stiffness:	9.62 N/mm
Weight:	14.78 kg

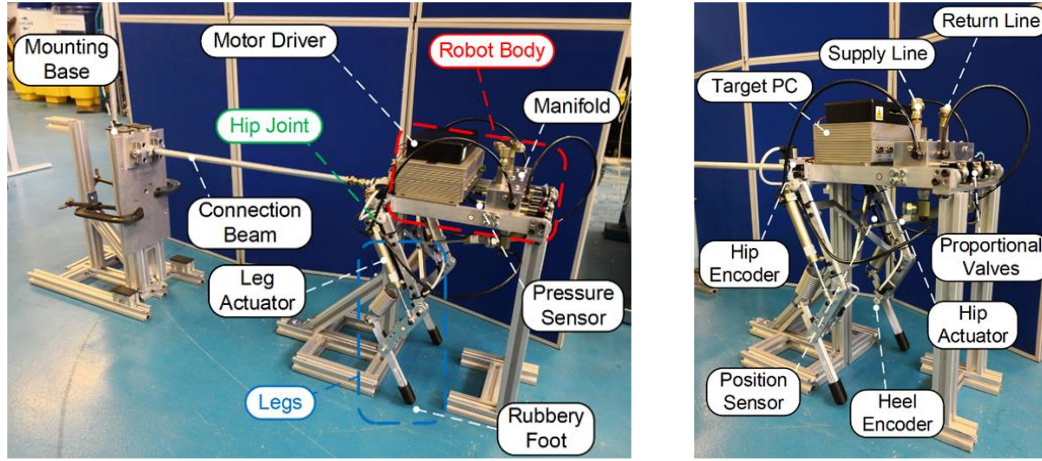


Figure 4. The BBH robot (shown with mechanical constraint, left picture).

A primary bench test has been taken to validate the efficacy of the mechanical design of the robot. A sinusoid position signal (2 mm of the amplitude at a 3Hz frequency) is used to excite the leg actuator to achieve an open loop hopping. Additionally, the two leg actuator displacements are synchronized using a ‘Modal Controller’. This controls the mean of the leg actuator positions and the corresponding difference, which are called the average position (y_a) and roll position (y_r), respectively. If the demand roll position is zero, the two leg actuators are synchronized. The consistent spring displacement in Fig. 5 indicates that the robot is hopping, plus the roll position error is mainly caused by different friction applied at each foot, left and right.

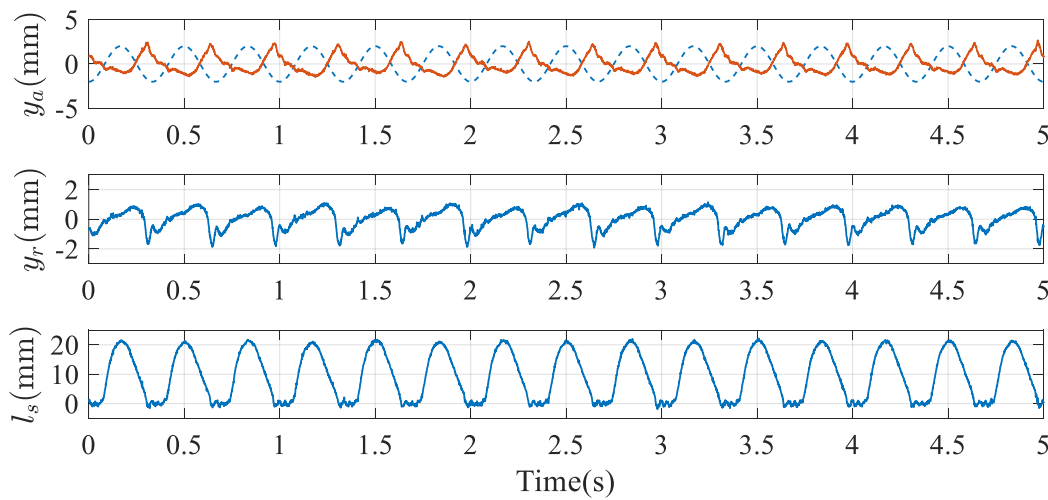


Figure 5. Experimental results of using 3 Hz sinusoid signal to excite the leg actuator.

21. Modelling

21.1 Hydraulic models

The modelling follows well-established procedures [8] accompanied by some findings from experiments. The hydraulic circuit is shown in Fig. 6.

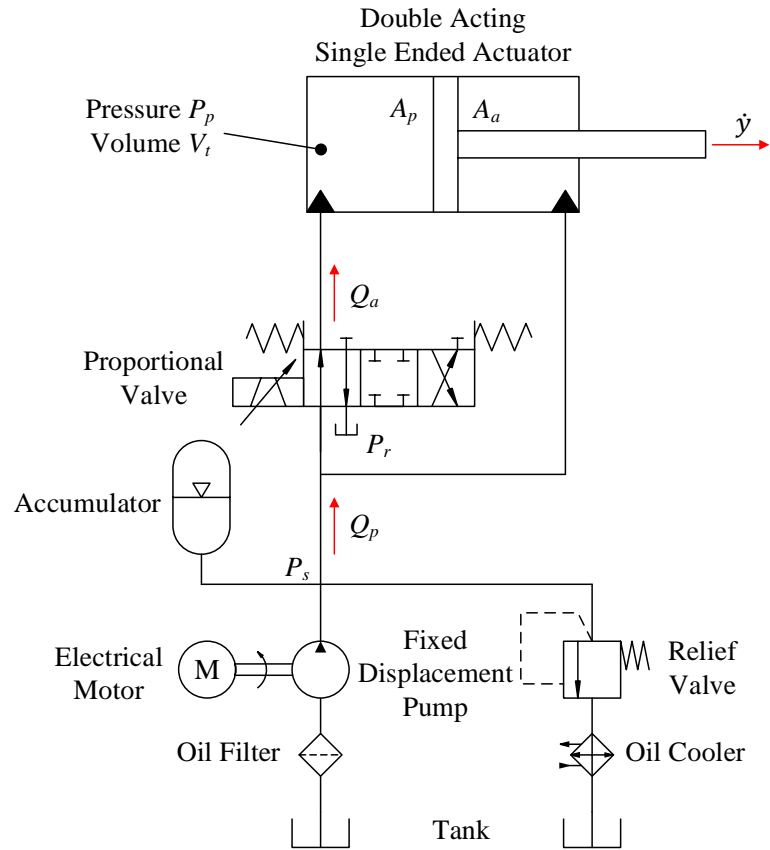


Figure 6. Hydraulic circuit for one leg actuator

21.1.1 Actuator model

Assuming there is no internal or external leakage, the hydraulic actuator is modelled by:

$$P_p A_p - P_s A_a - F_f = F_h \quad (1)$$

$$Q_a = A_p \dot{y} + \frac{V_t}{B} \dot{P}_p \quad (2)$$

where A_p is the piston area, A_a is the annulus area, F_h is the actuation force, F_f is the friction, Q_a is the piston side flow rate, V_t is the trapped oil volume and B is the bulk modulus of the oil. Additionally, the friction force is modelled by:

$$F_f = f_v \dot{y} \quad (3)$$

$$F_f = \begin{cases} F_c & \text{for } F_s \geq F_c \\ F_s & \text{for } |F_s| < F_c \\ -F_c & \text{for } F_s \leq -F_c \end{cases} \quad (4)$$

where F_c is the Coulomb friction force, and F_s is velocity-dependent friction at low velocity, introduced to avoid a discontinuity which can cause numerical issues during the simulation; f_v is a friction coefficient which is relatively large.

21.1.2 Valve model

The proportional valve flow is modelled using the orifice equation. Only one orifice equation is needed as the flow is only metered into one side of the actuator. The spool displacement is considered as a dimensionless variable which ranging from -1 to +1 with the closed position corresponding to 0. The valve model is given by:

$$Q_a = K_v X_v \sqrt{P_s - P_v} \quad (5)$$

where P_v is the outlet pressure, K_v is the valve flow coefficient and X_v is the normalized spool displacement. Additionally, a second-order transfer function is used to represent the valve spool dynamics, which is given by:

$$X_v = \frac{\omega_v^2}{s^2 + 2\xi_v \omega_v s + \omega_v^2} \tilde{u}_c \quad (6)$$

where \tilde{u}_c is the valve driving signal, ω_v is the spool natural frequency and ξ_v is the spool damping ratio, which are empirical values determined from the manufacturer data sheet or experimental results. The hysteresis of the valve is modelled as ‘backlash’, as shown in Fig. 7, in which u_w is the dead-band width.

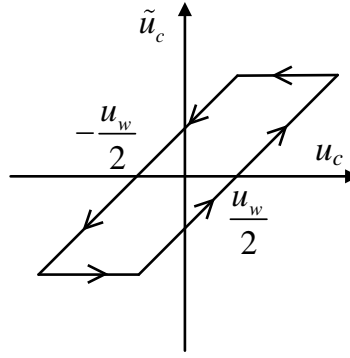


Figure 7. Valve hysteresis.

21.1.3Hose pressure loss model

The model of the pressure loss between the valve and the cylinder is given by:

$$Q_a = K_h \sqrt{P_p - P_v} \quad (7)$$

where K_h is the hose pressure loss factor, which is an empirical value.

The parameter values of the hydraulic models are provided in Table 2.

Table 2. Parameter values of the hydraulic models

Parameters	Symbol	Value	Unit
Supply pressure	P_s	160×10^5	Pa
Return pressure	P_r	0	Pa
Piston area	A_p	1.13×10^{-4}	m ²
Annulus area	A_a	0.63×10^{-4}	m ²
Valve flow coefficient	K_v	4.89×10^{-8}	m ⁴ /s/N ^{1/2}
Valve spool natural frequency	ω_v	942.48	rad/s
Valve spool damping ratio	ζ_v	0.7	
Backlash deadband width	u_w	0.2	A
Coulomb friction (actuator piston)	F_f	105	N

21.2 Mechanical model

The mechanical model of the BBH, which effectively is a planar robot, is built using SimMechanics[®], a multi-body mechanical simulation tool in Simulink[®]. The mechanical properties of the rigid bodies are defined in Autodesk Inventor 2017[®], then uploaded to SimMechanics[®] to create a 3D visualization.

A ‘spring and damper force’ block is used to represent the spring force between the connections on the *thigh* and *foot*. Modelling ground contact is an important issue. The reaction force from the ground should support the robot vertically (y-axis) and prevent horizontal foot slip (z-axis) during the stance phase. Define the coordinate of the robot foot contact point is $(0, y_n, z_t)$ and the corresponding projection to the ground is $(0, 0, 0)$. The ground reaction force is modelled as a spring and damper both vertically and horizontally. The ground stiffness is relatively large so as not to significantly reduce the effective robot leg's stiffness. Thus, the vertical reaction force and the horizontal friction force are given by:

$$F_y = \begin{cases} -k_y y_n - b_y \dot{y}_n & \text{for stance phase} \\ 0 & \text{for flight phase} \end{cases} \quad (8)$$

$$F_z = \begin{cases} -k_z z_t - b_z \dot{z}_t & \text{for stance phase} \\ 0 & \text{for flight phase} \end{cases} \quad (9)$$

where F_y is the vertical reaction force, k_y is the ground normal spring stiffness and b_y is the ground normal damping coefficient. F_z is the horizontal friction force, k_z is the tangential spring stiffness and b_z is the tangential damping coefficient.

Combining with the hydraulic models implemented in Simulink[®], the top level of the simulation model and the 3D visualization is shown in Fig. 8. Numerical implementation is performed by a stiff/Mod. Rosenbrock solver (Simulink's ODE23s) with variable step size, which is a compromise between the computing speed and the simulation accuracy.

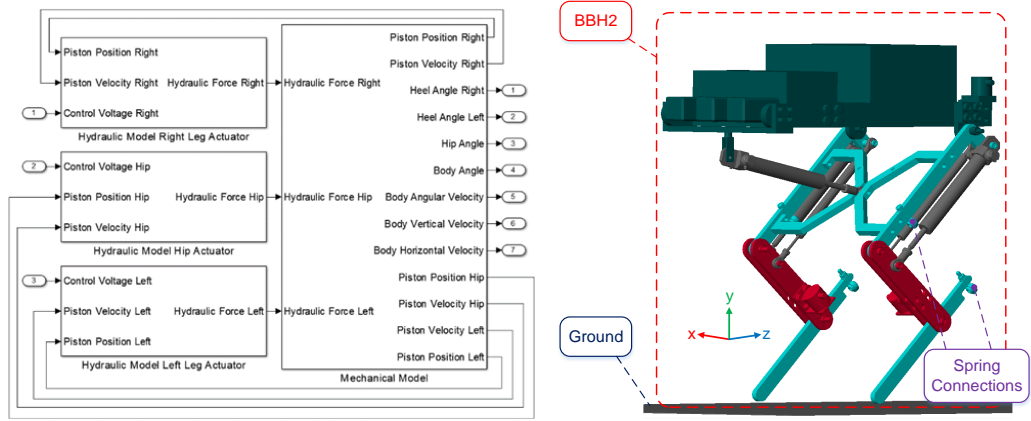


Figure 8. The top level of the simulation model and 3D visualization.

22. Controller implementation

To simplify the controller implementation, the distance between the body CoG and the foot is introduced as a ‘*virtual leg*’. The leg displacement is calculated using a kinematics transformation. Fig. 9 is a simplified diagram of one hopping cycle.

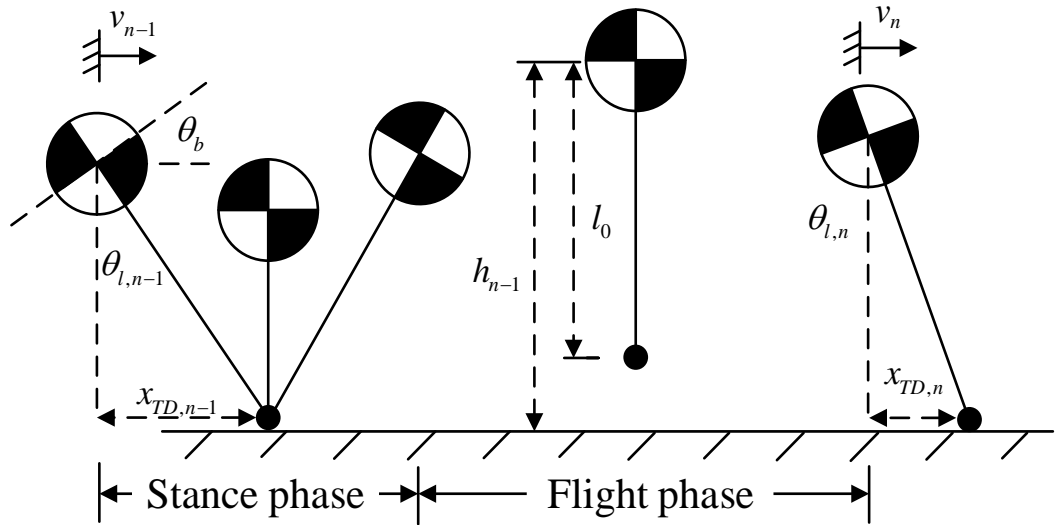


Figure 9. Simplified diagram of one hopping cycle.

22.1 Control of the hopping height

Bhatti et al. developed a simple hopping height control technique for a planar robot travelling over discontinuous surfaces in [9]. The leg actuator demand velocity

during the stance phase is derived using the achieved height of the previous hop, denoted $h_{n-1,a}$, and the desired height for the next hop, $h_{n,d}$, and is given by:

$$q_{n,d} = K_{h1}\sqrt{h_{n,d}} + K_{h2}\left(\sqrt{h_{n,d}} - \sqrt{h_{n-1,a}}\right) \quad (10)$$

where $q_{n,d}$ is the desired extension velocity of the leg, K_{h1} and K_{h2} are the controller gains. Integrating this desired velocity gives the demand position, which is common for a servo-hydraulics system. Additionally, the virtual leg is controlled to return to mid-length during the flight phase to be ready for the next touchdown, plus the demand hopping height remains constant in this simulation, i.e. $h_{n,d}=0.43$ m. The closed-loop leg length control is achieved using a PI controller:

$$u_c = K_p e + K_i \int e dt \quad (11)$$

where K_p is the proportional gain, K_i is the integral gain and e is the leg position error.

22.2 Control of the longitudinal velocity

During the flight phase, the robot has a parabolic trajectory, thus moving the hip actuator results in different rotation angle for the body and legs due to the moment of inertia. The leg angle, θ_l , is controlled to place the foot on the ground at a horizontal position, x_{TD} , relative to the body CoG, to achieve the required longitudinal velocity.

An appropriate leg angle for the next touch-down can be calculated from the previous hop. Thus, the foot placement at the previous touch-down, $x_{TD,n-1,a}$, is given by:

$$x_{TD,n-1,a} = \frac{1}{2} v_{n-1,a} T_{s,n-1,a} \quad (12)$$

where $v_{n-1,a}$ is the achieved body longitudinal velocity at previous touch-down and $T_{s,n-1,a}$ is the corresponding stance duration.

Thus the leg angle is given by:

$$\theta_{l,n-1,a} = \sin^{-1} \frac{x_{n-1,TD,a}}{l_0} \quad (13)$$

where $\theta_{l,n-1,a}$ is the achieved leg angle of the previous hop, and l_0 is the nominal length of the virtual leg, which is 0.4 m.

According to small perturbation approximation, define:

$$\Delta\theta_l = K_l(v_{n,d} - v_{n-1,a}) \quad (14)$$

where $v_{n,d}$ is the desired body longitudinal velocity for the next touchdown, $\Delta\theta_l$ is the corresponding leg angle change and K_l is the feedback gain. Thus, the desired leg angle for the next touch-down, $\theta_{l,n,d}$, is given by:

$$\theta_{l,n,d} = \theta_{l,n-1} + \Delta\theta_l \quad (15)$$

If hip torque is the control variable, leg angle can be controlled in a closed loop.

$$\tau_l = K_{l1}(\theta_{l,n} - \theta_{l,n,d}) + K_{l2}(\dot{\theta}_{l,n}) \quad (16)$$

where τ_l is the control torque for the hip during flight phase, K_{l1} and K_{l2} are feedback gains, and $\theta_{l,n}$ is the actual leg angle.

22.3 Control of the body attitude

Controlling the leg angle during flight phase changes the body pitch angle, which can be corrected during the stance phase. It is assumed there is sufficient friction at the ground to avoid the robot foot slipping. The body angle, θ_b , is controlled towards a horizontal position, i.e. $\theta_{b,d}=0^\circ$, using a simple servo given by:

$$\tau_b = K_{b1}(\theta_b - \theta_{b,d}) + K_{b2}(\dot{\theta}_b) \quad (17)$$

where τ_b is the control torque for the hip during stance phase, K_{b1} and K_{b2} are feedback gains, and $\theta_{b,d}$ is the desired body angle. Table 3 shows the values of the controller gains and feedback gains used in this simulation.

Table 3. Controller and feedback gains.

Parameters	Value	Unit
K_{h1}	0.02	$\text{m}^{1/2}/\text{s}$
K_{h2}	1	$\text{m}^{1/2}/\text{s}$
K_{l1}	100	Nm/rad
K_{l2}	0.02	Nms/rad
K_{b1}	1×10^5	Nm/rad
K_{b2}	9×10^3	Nms/rad
K_p	320	1/m
K_i	100	1/(sm)

23. Simulation results

Fig. 10. shows the simulation results. The simulation starts with a free drop of the robot from a small initial body height. The achieved hopping frequency is approximately 3 Hz, and the hopping height controller is able to correct the robot motion within several hops when the longitudinal velocity is changing. The leg angle is adjusted by the controller to achieve different velocity demands. At $t=6$, a sudden movement of the hip actuator is found due to a large step change of the velocity demand, so more hops are needed to allow the robot to gradually achieve the demand velocity. Between $t=5$ and 10, the forward travelling speed is 0.24 m/s; between $t=15$ and 20, the backward speed is 0.08 m/s; between $t=20$ and 25, the backward speed is 0.15 m/s. The body angle is successfully controlled to maintain balance, not only when hopping on a spot, i.e. $\dot{x}(t)=0$, but also to be balanced with different moving speed.

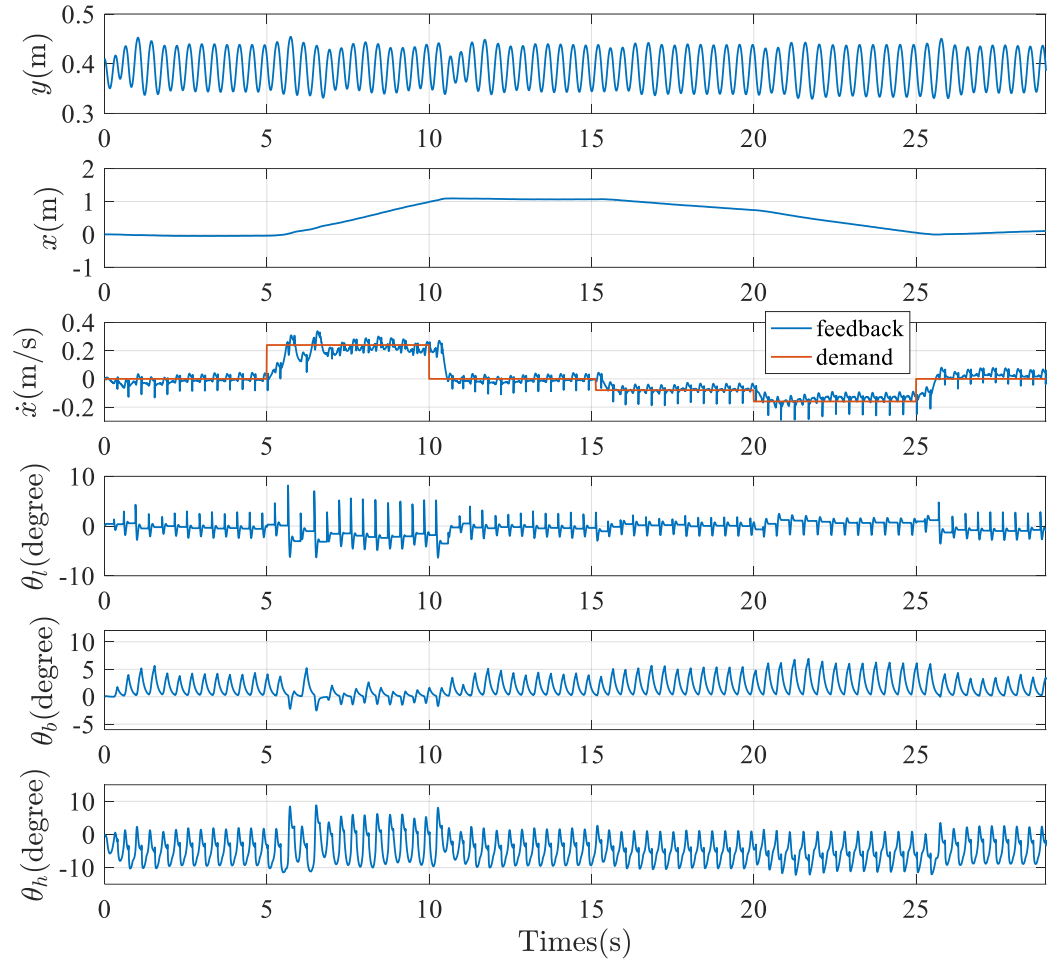


Fig. 10. Simulation results.

24. Conclusion

The investigation of the control of a bipedal robot while hopping is undertaken in this paper. The bench test results indicate the efficacy of the mechanical design of the BBH robot. A detailed non-linear simulation model accompanied by physical empirical data is developed. The implemented controller is built according to the well-established ‘Three-part’ control algorithm. The hopping height is controlled using an adaptive controller; changing the leg angle during the flight phase to place the foot in the desired position is able to achieve longitudinal velocity control; the body attitude is controlled during the stance phase to maintain balance. The simulation results demonstrate that the controller can successfully balance the robot while hopping with different longitudinal velocities, e.g. travelling forward at 0.24 m/s, backward at 0.08 m/s or 0.15 m/s.

The practical implementation of this controller is challenging, mainly due to the performance of the sensors and signal processing, e.g. the direct measurement of the robot hopping height and longitudinal velocity requires sufficiently quick response and high measurement accuracy of the sensors. If necessary, state estimators or observers can be built, i.e. derive the hopping height or longitudinal velocity from the estimated state variables.

References

- [1] Sayyad, A., Seth, B., Seshu, P.: Single-legged hopping robotics research—A review. *Robotica*, 25(5), pp.587-613 (2007).
- [2] Bhatti, J., Plummer, A.R., Iravani, P., Ding, B.: A survey of dynamic robot legged locomotion. In: *Fluid Power and Mechatronics (FPM)*, 2015 International Conference on IEEE, pp. 770-775, July 2015.
- [3] Hyon, S.H., Mita, T.: Development of a biologically inspired hopping robot-" Kenken". In: *Robotics and Automation*, 2002. Proceedings. ICRA'02. IEEE International Conference on IEEE, Vol. 4, pp. 3984-3991, May 2002.
- [4] Al-Shuka, H.F., Corves, B., Zhu, W.H., Vanderborght, B.: Multi-level control of zero-moment point-based humanoid biped robots: a review. *Robotica*, 34(11), pp.2440-2466, (2016).
- [5] Raibert, M.H.: Hopping in legged systems—modelling and simulation for the two-dimensional one-legged case. *IEEE Transactions on Systems, Man, and Cybernetics*, (3), pp.451-463, (1984).
- [6] MIT Leg Laboratory. <http://www.ai.mit.edu/projects/leglab/>
- [7] Raibert, M., Chepponis, M., Brown, H.B.J.R.: Running on four legs as though they were one. *IEEE Journal on Robotics and Automation*, 2(2), pp.70-82, (1986).
- [8] Plummer, A.R.: A detailed dynamic model of a six-axis shaking table. *Journal of earthquake engineering*, 12(4), pp.631-662, (2008).
- [9] Bhatti, J., Plummer, A.R., Sahinkaya, M.N., Iravani, P., Guglielmino, E., Caldwell, D.G.: Fast and adaptive hopping height control of single-legged robot. In: *the 11th Biennial Conference on Engineering Systems Design and Analysis*. American Society of Mechanical Engineers, pp. 303-309, July 2012.